CHARACTERIZATION OF THERMOSENSITIVE HYBRID ARCHAEOSOMES AND DPA-CY3[22,22]/POPC LIPOSOMES AND *IN VITRO* EVALUATION OF THEIR POTENTIAL USEFULNESS IN TARGETED DELIVERY AND CONTROLLED RELEASE

A Dissertation
Submitted to
the Temple University Graduate Board

In Partial Fulfillment
of the Requirements for the Degree
DOCTOR OF PHILOSOPHY

By:

Umme Ayesa

May 2016

Examining Committee Members:

Parkson Lee-Gau Chong, PhD, Medical Genetics and Molecular Biochemistry
Brad Rothberg, PhD, Medical Genetics and Molecular Biochemistry
Ana Gamero, PhD, Medical Genetics and Molecular Biochemistry & FELS
Charles Grubmeyer, PhD, Medical Genetics and Molecular Biochemistry & FELS
Servio H. Ramirez, PhD, External Examiner, Pathology and Laboratory Medicine

ABSTRACT

One of earlier challenges in treating cancer was utilizing drugs that are powerful yet cause severe toxicity to patients. Although the use of liposomal drugs has somewhat met that challenge, our objective now is to create liposomal drugs with an even better drug efficacy and further reduced toxicity. Doxorubicin hydrochloride (DXO), for example, is an anticancer drug used to treat many types of cancers, but it is toxic to the gastrointestinal tract and the heart. Encapsulating DXO into liposomes as done in the first FDA-approved liposomal DXO, Doxil, minimizes toxicity and improves the half-life, allows more opportunities for the drug to reach the tumor. While liposomal DXO is in the market with an annual sale of approximately 450 million dollars, the addition of cholesterol and lipids with polyethylene glycol (PEG) in the formulation to increase liposome stability and circulation time can give rise to other concerns such as potential harm to the patient and reduction in drug loading/release. In addition, in hopes of increasing drug accumulation at the diseased tissue, the use of active or targeted nanoparticles has been explored for selective drug delivery. However, despite ongoing efforts to design and test targeted nanocarriers for drug delivery, there is no known targeted liposome commercially available at this time. This illustrates that there is still room to improve the formulation of the liposomal carriers in the areas of stability, specificity to the cancer sites, and maximum drug at diseased sites.

The main focus of our research is to develop novel liposomal carriers that have a higher therapeutic index and lower cytotoxicity than currently used liposomal drugs. In this research, we were able to construct two stable liposomal systems. First, we constructed a liposomal system having the ability to specifically target phosphatidylserine

(PS) exposed tissues. This liposomal system contains 1-palmitoyl-2-oleoyl-*sn*-glycero-3-phosphocholine (POPC) and hydrophobic PS-targeting molecule bis-dipicolylamine-Zn-Cy3[C22,22] (abbreviated DPA-Cy3[22,22]). We have tested stability and PS binding ability of DPA-Cy3[22,22]/POPC liposomal carriers using light scattering and ion-exchange chromatography, respectively. In addition, with confocal microscopy and flow cytometry, we have tested DPA-Cy3[22,22]/POPC liposomes' affinity to cancer cells. Furthermore, cell viability assay was used to determine the cytotoxic effect of DPA-Cy3[22,22]/POPC liposomes on cancer cells and non-cancer cells. In short, we found that DPA-Cy3[22,22]/POPC liposomes were stable, displayed binding to PS-exposed cells, and were taken up by PS-exposed cells inducing considerable cytoxicity.

Second, we have developed and characterized the physical properties of thermosensitive liposomes made of archaeal bipolar tetraether lipids (BTL) and "conventional" monopolar diester lipids. These liposomes are also termed hybrid archaeosomes. Specifically, we used the polar lipid fraction E (PLFE) isolated from the thermoacidophilic archaeon *Sulfolobus acidocaldarius* as the BTL component of the hybrid archaeosomes. Dynamic light scattering and zeta potential measurements showed that the presence of PLFE greatly stabilizes liposomes. The most striking result is that at 25-30 mol% PLFE in DPPC liposomes, there is a dramatic change in zeta potential with temperature. The most abrupt change was detected in 30 mol% PLFE in DPPC, where the zeta potential changes from ~45mV at 37˚C to ~5mV at 42˚C. This drastic change in liposome zeta potential by temperature is unprecedented and could be used to develop new thermosensitive liposomes. This dramatic change in zeta potential is likely to result from gross changes in membrane structure by temperature at particular PLFE mole

fractions. To further characterize PLFE/DPPC hybrid archaeosomes, we have used steady state nano-second fluorometry. The fluorescent data show that from 37˚C to 43˚C, the probe diphenylhexatrine (DPH) in the PLFE/DPPC mixtures experience a decrease in order parameter and an increase in rotational motion. With entrapped DXO we found that below 37˚C, the drug release from hybrid archaeosomes is slow. However, when the temperature was raised to above 39˚C, the initial drug release rate constant was increased by a factor of 2. Taken together, the findings suggest that a mild temperature jump changes the membrane packing and dynamics of the PLFE/DPPC mixture, making the membrane more permeable for small molecules. Additionally, confocal fluorescence microscopy showed that these hybrid archaeosomes can be taken up by live cells (e.g., MCF-7 breast cancer cells) and deliver entrapped drug molecules to the cell's nucleus, with a rate significantly lower than that obtained from conventional diester liposomes.

Our results indicate that both of these two novel liposomal systems have great potential to be used for delivery of therapeutic agents such as small drug molecules (e.g., DXO), siRNA, DNA, or peptides/proteins for cancer treatment and various other purposes. Unlike currently available liposomal drugs, DPA-Cy3[22,22] containing liposomes could be useful for targeting PS-exposed diseased tissues. 30 mol% PLFE/DPPC archeosomes are a unique thermosensitive liposome system with extraordinary stability at the body temperature and able to release entrapped drugs molecules when the local temperature of the diseased tissue is subject to hyperthermic treatment.

ACKNOWLEDGMENTS

First and foremost, my sincerest appreciation goes to my advisor Dr. Parkson Lee-Gau Chong for giving me the opportunity to do my thesis work in his lab. I am thankful to have gained tremendous knowledge from him. And, I will continue to strive for his level of patience and work ethic. Next, I would like to thank the current and former members of my advisory committee, Dr. Collins, Dr. Merali, Dr. Gamero, Dr. Rothberg, and Dr. Grubmeyer, for giving me insightful comments and guiding me throughout the years. Thank you to my external reader, Dr. Ramirez, for taking the time to help me during this process. I would also like to thank Dr. Giangiacomo for giving me her words of advice and motivation exactly when I needed them. Thank you to Dr. Gallucci for taking me into her lab as an undergrad, showing me how horrifyingly exhilarating research can be, and giving me access to resources for my thesis work. I have made it this far because of all of your support.

I would also like to acknowledge my grad school colleagues in the Department of Medical Genetic and Molecular Biochemistry, Maria Barton and Danielle Feather, for being great classmates and friends. A very special thanks goes to Elsie Samakai Moore for being the best confidante anyone can ask for. I am very grateful to have met her and have her in my life. Thank you to all the members of the Chong lab. Varsha Daswani, thank you for being a great friend and making so many good lab memories with me. Thank you, Zhan Jiang and Alex Bananno, for joining me in all the ups and downs of research in the lab. Many thanks go to all the undergraduate students for making my time in the lab so enjoyable and fulfilling. Regrettably, because there are so many, I cannot acknowledge them by name.

Last but not least, I would like to thank my family. I would like to acknowledge my mother and father for being the best parents in the world, for being the best role models, and for giving me unconditional love and support. I thank God each and every day for having them in my life. I want to thank my sister who has been my best friend and my motivator throughout my life. A warm and heartfelt thank you goes out to my husband for always being there for me, caring for me and for making me laugh in good times and in bad. I would also like to thank my grandmother, my late gradfather, mother-in-law and father-in-law, brothers-in-law and sisters-in-law, aunts, uncles, and cousins for their outpouring prayers, support and encouragement. I cannot image my life without each and every one of you.

The work reported in this dissertation was supported by grant DMR1105277 from NSF to my research sponsor, Dr. Parkson Lee-Gau Chong.

TABLE OF CONTENTS

LIST OF ABBREVIATIONS

7AAD	7-aminoactinomycin D
AC	alternating current
BTL	bipolar tetraether lipids
Comp 1	compound 1
Comp 2	compound 2
Comp 3	compound 3
Camp	camptothecin
Cy3	cyanine 3
DC	direct current
DPA-Cy3[22,22]	bis- dipicolylamine zinc-cyanine 3 C[22,22]
DPA-Cy3[22,22]/POPC	bis- dipicolylamine zinc-cyanine 3 C[22,22] and POPC containing liposomes
DPH	1,6-diphenyl-1,3,5-hexatriene
DPPC	dipalmitoyl-L-α-phosphatidylcholine
DPPC/PLFE	DPPC and PLFE containing hybrid archeosomes
DXO	doxorubicin
FBS	fetal bovine serum
FITC	fluorescein isothiocyanate
GDGT	glycerol dialkyglycerol tetraether
GDNT	glycerol dialkylcalditol tetraether
GP_{em}	emission generalized polarization

LUV	large unilamellar vesicles
MLV	multilamellar vesicles
mol %	mole percent
mV	megavolt
nmol	nanomole
ns	nanosecond
PDI	polydispersity index
PLFE	polar lipid fraction E
POPC	1-palmitoyl-2-oleoyl-sn-glycero-3-phosphocholine
POPS	1-palmitoyl-2-oleoyl-sn-glycero-3-phospho-L-serine
PS	phosphatidylserine
Rad	radius
RXN	reaction
TES	2-[[1,3-dihydroxy-2-(hydroxymethyl)propan-2-yl]amino]ethanesulfonic acid
T_m	phase transition temperature
Tris	2-Amino-2-hydroxymethyl-propane-1,3-diol
TSL	thermossensitive liposome
ZP	zeta potential
+/-	positive/negative
τ	lifetime
θ	rotational correlation time
r_∞	residual/limiting anisotropy

R	rotation rate
S	order parameter
ζ	zeta potential
µL	micro liter
µM	milcro molar
mM	mili molar

LIST OF TABLES

Table **Page**

LIST OF FIGURES

Figure **Page**

LIST OF DIAGRAMS

Diagram **Page**

CHAPTER 1: INTRODUCTION

Overview

The overall goal of our study can be divided into two parts. **First, we focus on developing a targeted liposomal drug delivery system that is able to selectively bind diseased or cancer cell surfaces in order to improve efficacy of drug delivery and avoid toxicity to healthy cells.** We achieve this by utilizing a molecule that is able to recognize and bind anionic phospholipids that are found on the cell surface during stressed conditions. Using this molecule, we develop and characterize various liposome formulations, test the ability to bind cells, and determine the liposomes' effect on cancer cells. **Second, we explore archaea lipid as a stabilizing agent and a key component in the formulation of thermosensitive liposomes.** Here, we look at the unique properties of a hybrid membrane prepared with conventional diester lipids and archaeal bipolar tetraether lipids, particularly the polar lipid fraction E (PLFE) isolated from the archaeon *Sulfolobus acidocaldarius*. Specifically, we examine membrane order parameter, probe rotational rate, zeta potential, and the rate constant of drug release as well as their temperature dependencies. Because liposomal drugs continue to be a powerful and useful way to treat numerous diseases, our research has a potential therapeutic use. With the possibility of creating two new and potentially useful liposomal drug carriers, we hope to enhance drug efficacy and improve patient's survival.

Part I: Phosphatidylserine Targeted Liposomal Drug Carriers

1.1 Passive and Targeted Liposomal Nanocarriers

Liposomes are widely used for drug delivery to improve efficacy of free drugs, decrease toxicity and increase drug loading at diseased sites (Lim, Banerjee, & Onyuksel, 2012; Mufamadi et al., 2011; Vaage, Working, & Uster, 1998). Liposomal nanocarriers with various lipid compositions can carry both hydrophobic and hydrophilic drugs and passively deliver powerful drugs which accumulate at neoplastic tissues due to the enhanced permeability and retention (EPR) effect (Iyer, Khaled, Fang, & Maeda, 2006) (Diagram 1). FDA approved liposomal drugs are commonly used for cancer treatment and reduce life threatening side-effects to patients (Iwamoto, 2013). However, without much modification to the liposome surface, passive liposomal delivery systems have a short half-life and the EPR phenomenon may not be sufficient to direct nanoparticles to the targeted tissue (Amselem, Gabizon, & Barenholz, 1990; Dreher et al., 2006; Gabizon & Papahadjopoulos, 1992). To overcome the challenges of passive drug delivery systems, active targeting drug delivery systems with longer circulation time and the ability to selectively bind to the cell surface markers of diseased cells are being investigated (Madni et al., 2014; Tila et al., 2015). Selective binding is possible due to incorporation of proteins, peptides and molecules that can interact with certain cell surface markers only present in diseased cells (Guo at al., 2012; Mamot et al., 2006; Mamot et al., 2012). By increasing affinity to diseased cells, liposomal delivery systems can increase drug efficacy, decrease loss of liposomes in blood circulation, and increase the opportunity for the liposomes to accumulate at the diseased sites without relying on diffusion and chance (Diagram 1).

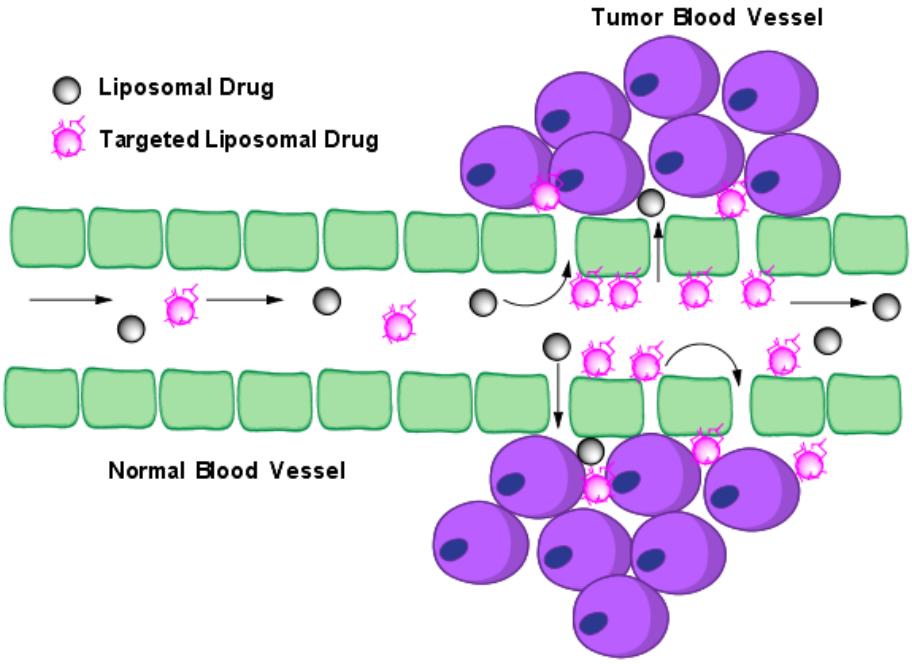

Diagram 1: Conventional and targeted liposomal nanoparticles used to deliver drug molecules to tumor sites.

Conventional liposomes accumulate at tumor sites due to high permeability and retention of tumor blood vessels. Targeted liposomal nanocarriers have high affinity to tumor cells and endothelial cells of tumor blood vessels, which results in higher liposomal accumulation near the tumor site than conventional liposomes.

1.2 Cell Membrane Phospholipid Distribution

Biomarkers have been studied extensively for the purpose of designing targeted drug delivery systems. Cell surface makers are identified by studying the cell membrane abnormalities that differentiate healthy cells from unhealthy cells. The cell membrane lipid bilayer consists of two leaflets. The outer leaflet is composed of two major lipid components: sphingomyelin and phosphatidylcholine, both of which are zwitterionic lipids at physiological pH. The inner leaflet consists of zwitterionic and negatively charged lipids such as phosphatidylinositol (PI) and phosphatidylserine (PS) (Figure 1) (Belhocine & Prato, 2011; Marquardt, Geier, & Pabst, 2015). These negatively charged lipids interact with various membrane and cytosolic proteins and take part in the cellular signaling processes. The lipid bilayer asymmetry is regulated by several types of membrane protein families, including flippase, floppase, scramblase and ATP cassette transporters (Borst & Elferink, 2002; Frasch et al., 2000). In normal physiological conditions, these proteins maintain negatively charged lipids, such as PS, within the inner leaflet of the bilayer through bidirectional or unidirectional movement of lipids across the cell membrane. ATP-dependent membrane transporters, such as flippase, utilize ATP hydrolysis to bind and to translocate negatively charged lipids from one leaflet to the other (Borst & Elferink, 2002).

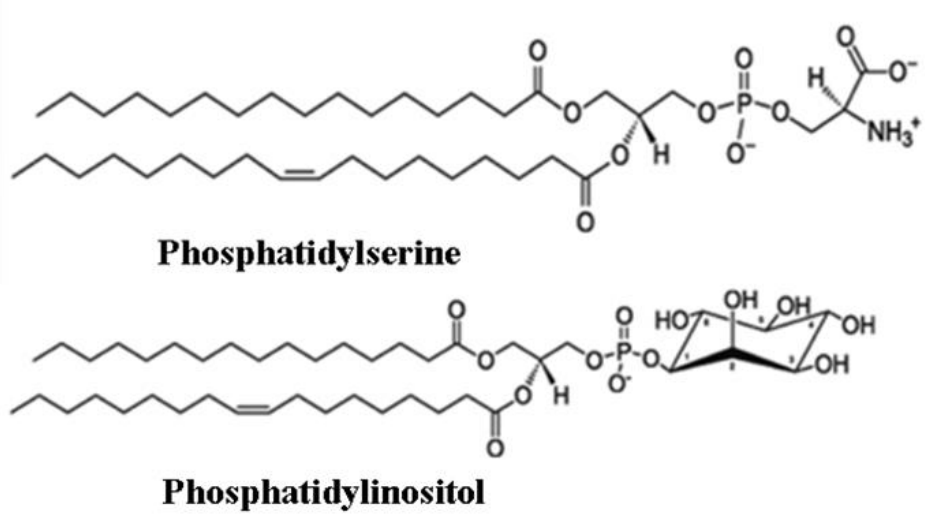

Figure 1: Structure of anionic phospholipids: phosphatidylserine (PS) and phosphatidylinositol (PI) present in cell membrane.

During certain normal cellular events, the asymmetrical distribution of phospholipids can be disrupted. Some of these events include programmed cell death, platelet activation, and T-cell activation etc. (Zwaal, Comfurius, & Bevers, 2005). These processes require negatively charged lipids to be translocated to the outer leaflet in order to fulfill different cellular functions. For example, during cell death, PS translocation to the outer leaflet of the bilayer is necessary for recruiting macrophages to apoptotic cells for clearance (Zwaal et al., 2005). In these events, the asymmetry of the lipids can be disrupted by the activation of membrane protein families of phospholipases and scramblases (van Meer, 2011; van Meer, 2011), which promote movement of negatively charged lipids to the outer leaflet in order to perform biological function.

1.3 Mechanism of PS Exposure in Diseased Cells

In abnormal and cancer cells, various environmental stressors such as hypoxia, low pH, generation of reactive oxygen species (ROS), and increased intracellular Ca^{2+} concentration contribute to deregulation of the membrane proteins that maintain the asymmetrical distribution of PS in the bilayer (Schutters & Reutelingsperger, 2010; Woehlecke et al., 2003). Injured and tumor tissues generate inflammatory cytokines TNFα and IL4, which promote leukocyte and macrophage adhesion as well as ROS generation. Sequentially, ROS production cause the membrane proteins to be oxidized and stimulate cells to influx calcium in the cytosolic compartment (Ran, Downes, & Thorpe, 2002; Ran et al., 2005). In the event of cellular stress, flippase is deactivated and phospholipase and scramblase is activated, resulting in PS to be exposed to the outer leaflet of the bilayer. The detailed pathway that leads to PS exposure in diseased cells is still unclear, but recently, Nagata's group identified Xk-Related Protein 8 (Xkr8) as the enzyme that activates apoptosis-induced lipid scrambling (Suzuki, Denning, Imanishi, Horvitz, & Nagata, 2013). Xkr8 is deregulated in cancer, resulting in exposure of PS and suppression of the “eat me” signal allowing cells to escape being engulfed by macrophages (Mariño & Kroemer, 2013). Moreover, many types of tumor cells and diseased cells bear PS on the outside (Ran & Thorpe, 2002; Riedl, Zweytick, & Lohner, 2011; Zwaal et al., 2005), which provides opportunity to use PS as a target for diagnosis and treatment.

1.4 PS is a Biomarker for Diagnosis and Treatment of Diseases

The use of PS as a biomarker for diagnosis of disease and injury sites has become more common since studies show that significantly high level of PS exposure occurs outside of tumors, cancer cells, infected cells and injured tissues. An increasing number of studies suggest PS externalization is a common occurrence in tumors including prostate, colon, breast, ovarian (Ran & Thorpe, 2002; Riedl, Zweytick et al., 2011; Zwaal et al., 2005), and blood vessels of their tumor microenvironment(Ran & Thorpe, 2002; Ran et al., 2002; Thorpe, 2010). In addition, PS externalization also occurs in autoimmune disease, rheumatoid arthritis, Crohn's disease and during cardiac ischemia/reperfusion as well as spinal injuries (Post et al., 2002; Schutters & Reutelingsperger, 2010; Zhu et al., 2008). Since PS externalization is a commonly occurring phenomenon in diseases, the use of fluorescently tagged PS binding proteins, antibodies, and molecules (Ran & Thorpe, 2002; Riedl et al., 2011; Schutters & Reutelingsperger, 2010; Stafford & Thorpe, 2011; Utsugi, Schroit, Connor, Bucana, & Fidler, 1991; Zwaal et al., 2005) with high affinity for anionic phospholipids on cell surfaces has become a popular tool for diagnosis, imaging, and, potentially, treatment.

1.5 Anionic Phospholipid Binding Proteins, Peptides and Molecules

To visualize and image different physiological and pathophysiological cellular events, anionic phospholipid binding proteins and molecules linked to fluorophores have been synthesized and used. One of the most commonly used proteins for imaging cell death is annexin V (Schutters & Reutelingsperger, 2010). Annexin V is a 36 kD anti-coagulating protein found in all types of cells, although its function is still unclear. Annexin V can bind anionic phospholipids PS and PI in the presence of high Ca^{2+} concentration (Faiß, Kastl, Janshoff, & Steinem, 2008; Niu & Chen, 2010). Other proteins such as synaptotagmin I and lactadherin can also bind anionic phospholipids in a calcium-dependent manner. Synaptotagmin I and lactadherin have a C2A domain which binds two Ca^{2+} ions to interact with the negatively charged head group of phospholipids (Schutters & Reutelingsperger, 2010). However, all of these proteins require high levels of Ca^{2+} and long incubation for lipid association, which could result in more anionic lipid exposure and cellular stress (Engeland, Nieland, Ramaekers, Schutte, & Reutelingsperger, 1998; Schutters & Reutelingsperger, 2010). Use of peptides and small molecules is more advantageous for imaging because they are efficient, easily penetrated into tissues, and have fast clearance from blood circulation resulting in little or no toxicity. Negatively charged lipid targeting fluorescently labeled peptides such as CLSYYPSYC and ApoScence molecules have been used to image tumor bearing mice (Niu & Chen, 2010) with high efficiency. These peptides and molecules can accumulate at dead or diseased tissue, avoiding healthy cells, but have a short half-life and are easily degraded by the body.

1.6 Family of Zinc Dimetallic Coordinating Complex

The family of dimetallic zinc(II) coordinating complex, zinc(II)-dipicolylamine (Zn-DPA), synthesized and reported by Bradley Smith's group (University of Notre Dame), can bind anionic phospholipids with high affinity. Similar to annexin V, DPA binds negatively charged lipid, PS, strongly using dimetallic ions (O'Neil & Smith, 2006). Many metal coordinating complexes can form in water with the use of an organic scaffold. The organic scaffold, in this case nitrogen, holds the Zn^{2+} metal ions at a distance. The presence of an anion induces three-component assembly with scaffold and metal ions (Figure 2) (O'Neil & Smith, 2006). The three nitrogen, part of the DPA ligand, can coordinate strongly with Zn^{2+} cations with an association constant of ~10^7 M^{-1} in water (O'Neil & Smith, 2006) (Diagram 1). Dipicolylamine Zn (II) (Zn-DPA), a positively charged moiety that can be linked to a range of fluorescent dyes, interacts with negatively charged PS containing liposomes, resulting in increased fluorescence intensity (DiVittorio et al., 2008; A. V. Koulov et al., 2003; O'Neil & Smith, 2006; O'Neil & Smith, 2006; Smith et al., 2010). Unlike annexin V, DPA can bind to PS instantaneously without Ca^{2+} dependency, can be easily manipulated for a variety of use, and is more cost effective (Hanshaw & Smith, 2005; A. V. Koulov, & Smith, 2005).

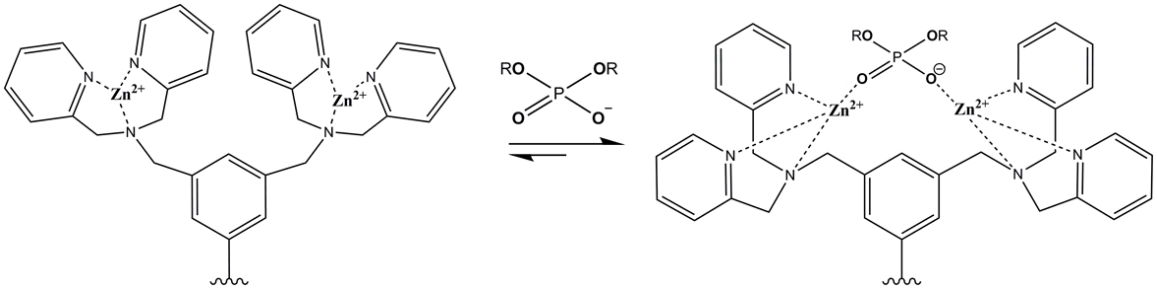

Figure 2: Mechanism of zinc (II) dipicolylamine binding to anionic phospholipids

Zinc (II) dipicolylamine binds to negatively charged phosphate of anionic phospholipid using two zinc ions forming complex with phosphate oxygen of lipid headgroupds (O'Neil & Smith, 2006).

1.7 Use of water soluble Zn-DPA for non-invasive optical imaging in live cells and animals

Earlier in his work, Smith et al. synthesized DPA analogue, PSS 380, to detect apoptotic cells. PSS 380 contains the DPA moiety linked to the fluorophore anthracene (Figure 3). Although PSS 380 shows high affinity for PS exposed apoptotic cells, since anthracene is excited with UV light, PSS 380 cannot be used for live cell imaging (A. V. Koulov et al., 2005). Later, for the purposes of live cell imaging, DPA linked to either 7-nitrobenz-2-oxa-1,3-diaza-4-yl (NBD) fluorophore, called Probe 1, or 5-carboxyfluorescein, called PSS-480 was synthesized (Figure 3). Since these fluorophores are excited by near infrared light, imaging can be done without harming cells or animals (DiVittorio et al., 2008; A. V. Koulov et al., 2003; Lakshmi, Hanshaw, & Smith, 2004; O'Neil & Smith, 2006; Smith et al., 2010). Synthesis of membrane sensors such as PSS-480 and similar DPA analogues allows for imaging anionic lipids PS on the surface of cells, tissues with bacteria (Leevy et al., 2006) or viral infections, (Ran & Thorpe, 2002) and tumors in mice (O'Neil & Smith, 2006; Smith et al., 2010). All of the fluorescently labeled DPA molecules mentioned are water soluble molecules that are injected intravenously into patients for diagnosis and imaging in biological conditions.

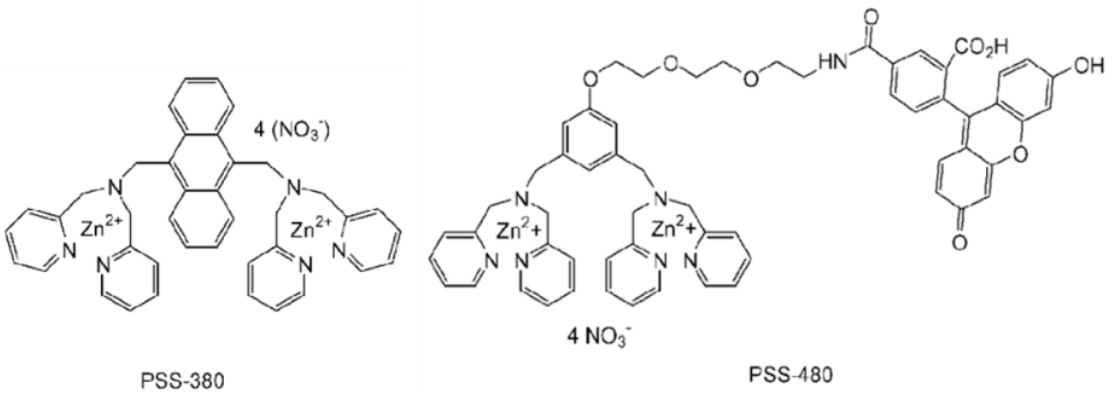

Figure 3: Chemical structure of DPA analogue PSS-380 and PSS-480

1.8 Nanoparticles Targeting PS for the Purposes of Diagnosis and Drug Delivery

The use of PS binding molecules has been extended to the development of nano carriers for imaging and delivery (Chu et al., 2013; Tila et al., 2015). PS binding proteins and antibody conjugated liposomes generated using annexin V, saposin C and anti-PS antibodies (Garnier, Bouter, Gounou, Petry, & Brisson, 2009; Kaimal et al., 2011; Zhang, Zhou, Belzile, Thorpe, & Zhao, 2014) are usually large and aggregate easily due to protein-lipid interaction (Loughrey, Wong, Choi, Cullis, & Bally, 1990), which can affect liposome biodistribution and penetration into tissues. Non-lipid based nanoparticles were also synthesized using PS binding molecules and detected using magnetic resonance imaging (MRI), but these nanoparticles have not been used to deliver drugs (Zhou et al., 2014).

Very recently, the first Zn-DPA based liposomes were created by conjugating Zn-DPA to nanoparticles showing binding to PS exposed cells (Turkyilmaz, Rice, Palumbo, & Smith, 2014). Turkyilmaz et al., first synthesized bis-dipicolylamine carboxylic acid using series of reduction and coupling reactions. To generate lipid conjugates, an amine bond is formed between commercially available H_2N-PEG_{2000}-DSPE lipid and bis-dipicolylamine carboxylic acid, and subsequently the product is purified using TLC (Turkyilmaz et al., 2014). The Zn-DPA lipid conjugate construction process is lengthy and inefficient. Until now, few attempts have been made to generate liposomes using hydrophobic Zn-DPA. Hydrophobic Zn-DPA along with commercially available lipids can form liposomes spontaneously, which makes liposome preparation more feasible and efficient. Using hydrophobic Zn-DPA, Zn-DPA-Cy3[22,22], we have the potential to create more stable PS specific liposomes for drug delivery to target a wide range of diseases.

1.9 Use of Hydrophobic Bis-Dipicolylamine Zinc Cyanine 3 C[22,22] in Liposomes for Targeted Drug Delivery

Our study utilizes the novel DPA analogue bis-dipicolylamine zinc (II) cyanine 3 C[22,22] (abbreviated as DPA-Cy3 [22,22]), a lipid-soluble Zn-DPA derivative provided by Molecular Targeting Technology. Unlike water soluble and lipid-conjugated DPA analogues, this compound contains two 22-carbon hydrocarbon chains and a fluorophore cyanine 3 (Cy3) linked covalently to the DPA moiety (Figure 4). The two hydrocarbon chains allow DPA-Cy3 [22,22] to be easily incorporated into liposomes for drug delivery. The presence of cyanine 3 fluorophore will allow detection and imaging of DPA-Cy3 [22,22] containing liposomes in *in vitro* and *in vivo* studies. By mixing DPA-Cy3 [22,22] with a conventional unsaturated zwitterionic lipid 1-palmitoyl-2-oleoyl-*sn*-glycero-3-phosphocholine (POPC), we are able to create stable liposomes with DPA which has affinity for PS and can potentially carry free drugs to the target site.

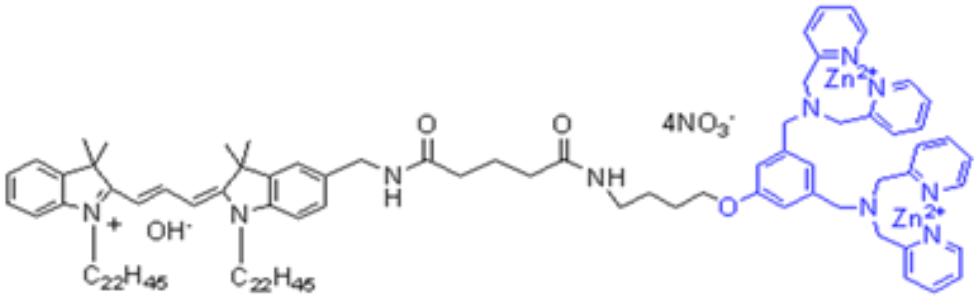

Figure 4: The structure of bis-dipicolylamine-zinc(II) cyanine 3 (DPA-Cy3[22,22])

DPA-Cy3[22,22] contains a dipicolylamine moiety (blue) linked to the fluorophore cyanine 3 with two long hydrocarbon chains ($C_{22}H_{45}$).

Part II: Hybrid Thermosensitive Liposomes for Drug Delivery

2.1 Anti-cancer Drug Doxorubicin

Doxorubicin hydrochloride (DXO) is an anthracycline anti-cancer drug that is widely used to treat various diseases including, bladder, breast, lung, stomach, and ovarian cancer, Hodgkin's lymphoma, leukemia and others(Gabizon et al., 1989; Vaage et al., 1998). DXO causes cellular toxicity by entering the cell nucleus and intercalating inside the DNA strands between the base pairs. This prevents the movement of the replication fork inhibiting proliferation and translation, resulting in cell death (Tacar, Sriamornsak, & Dass, 2013). DXO also inhibits the activity of enzyme topoisomerase II which is needed for DNA repair (Thorn et al., 2011). However, because free DXO has no specificity to tumors or cancer cells, it can cause severe toxicity to healthy cells and organs. Major side effects after DXO administration include toxicity of the gastrointestinal tract and the heart (Batist et al., 2001). To overcome the issues with toxicity and specificity, liposomal DXO was developed to increase the chance of delivering drugs to the site of the tumor, preventing the free drug from entering healthy organs. For this part my thesis, I will utilize DXO entrapped thermosensitive hybrid archaeosome formulation to study drug release and cytotoxicy *in vitro*.

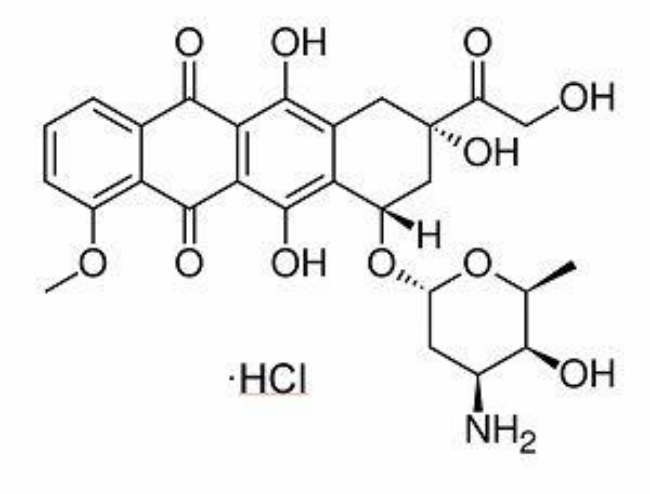

Figure 5: Structure of doxorubicin hydrochloride

Table 1: FDA Approved Liposomal Doxorubicin in clinical trials

Drug product	Active ingredient	Manufacturer	Indications	FDA approved date/clinical trial status
Doxil (Caelyx)	Pegylated doxorubicin	Orthobiotech, Schering-Plough	Ovarian/breast cancer	November 1995
Abraxane	Albumin-bound Paclitaxel nanospheres. Nab paclitaxel in combination with gemcitabine	Abraxis Bioscience, Astra Zenica Celgene	Various cancers Metastatic pancreatic cancer	Jan-05 September 2013
Myocet	Liposome-encapsulated Doxorubicin	Elan/Sopherion therapeutics	Breast cancer	2000, Approved in Europe and Canada
DaunoXome	Liposome-encapsulated Daunorubicin	Gilead Science	HIV-related Kaposi sarcoma	Apr-96
DepoCyt	Liposomal Cytarabine	Skye Pharma, Enzon	Lymphomatous meningitis	Apr-99
Oncaspar	PEGasparaginase	Enzon	Acute Lymphocytic Leukemia	Feb-94
Onco-TCS	Liposomal Vincristine	Inex	Non-Hodgkin Lymphoma	In clinical phase I/II
LEP-ETU	Liposomal Paclitaxel	Neopharma	Ovarian/breast/lung cancers	In clinical phase I/II
Aroplatin	Liposomal Cisplatin analog	Antigenics Inc.,	Colorectal cancer	In clinical phase I/II
OSI-211	Liposomal Lurtotecan	OSI	Lung cancer/recurrent ovarian	In clinical phase II
SPI-77	Stealth liposomal Cisplatin	Alza	Head & Neck cancer/Lung cancer	In clinical Phase III
EndoTAG-I	Paclitaxel	Medigene/SynCore Biotechnology	Breast cancer/Pancreatic cancer	In clinical phase II
Marqibo	Vincristine	Talon Therapeutics	Philadelphia chromosome-negative lymphoblastic leukemia	Aug-12
Thermodox	Doxorubicin	Celsion	Hepatocellular carcinoma	In clinical phase III
Atragen	Liposomal all trans-retinoic acid	Aronex Pharmaceuticals	Acute promyelocytic leukemia	In clinical phase II
Lipoplatin	Liposomal Cisplatin	Regulon	Pacreatic/ Head and Neck/breast cancer	In clinical phase III
Aurimmune (CYT-6091)	TNF-α bound to colloidal Gold nanoparticles	Cytimmune Sciences	Head and Neck cancer	In clinical phase II
Auroshell	Gold nanoshells	Nanospectra Biosciences	Aurolace therapy of cancer	In clinical Phase 1
Genexal-PM	Paclitaxel-loaded polymeric micelle	Samyang	Breast cancer/small cell lung cancer	Marketed in Europe, Korea
Paclical	Paclitaxel micelles	Oasmia Pharmaceutical AB	Ovarian cancer	Phase III
Nektar -102	Irinotecan, PEGylated liposome	Nektar therapeutics	Breast /colorectal cancer	In clinical Phase 3
NKTR-105	PEG-Docetaxel	Nektar therapeutics	Solid tumors	Phase 1
Ontak	Diphtheria toxin and	Seragen, Inc	Cutaneous T-cell	1999

2.2 Liposomal DXO for Cancer Therapy

Liposomes are biocompatible and have been used clinically for drug delivery to reduce non-specific toxicity of free drugs (Al-Jamal, Al-Ahmady, & Kostarelos, 2012; H. L. Chang & Yeh, 2012; Davis, Chen, & Shin, 2008; Goyal et al., 2005). The liposomal form of DXO, known as Doxil or Caelyx, was the first liposomal drug approved by the FDA (Barenholz, 2012). Liposomal DXO is currently being used to treat metastatic breast cancer, ovarian cancer, multiple myelomas, and AIDS-related Kaposi's sarcoma (Duggan & Keating, 2011; Sheela, 2005). Other formulations of liposomal DXO have been produced and have demonstrated reduction in systemic toxicity, increase in circulation time, and increase in accumulation at the tumor sites (Batist et al., 2001; Harashima, Iida, Urakami, Tsuchihashi, & Kiwada, 1999; Lyass, Hubert, & Gabizon, 2001; Uster, Working, & Vaage, 1998). However, some major drawbacks of currently used conventional liposomal DXO include very low stability and slow drug release at physiological conditions (Al-Jamal et al., 2012; Immordino, Dosio, & Cattel, 2006). Additionally, liposomes that accumulate at the tumor site fail to penetrate into deep tumor tissue, which in turn lowers the therapeutic index of the liposomal drug (Kong, Braun, & Dewhirst, 2001; Manzoor et al., 2012). For these reasons, it is essential to create a more controllable liposomal formulation that is able to increase drug efficacy without compromising stability and safety.

2.3 Thermosensitive Liposomes

One way to improve drug efficacy is using controlled drug release, in which drug exposure at the tumor site can be maximized by inducing drug release from liposomes via local hyperthermia. Hyperthermia increases blood flow near tumor vessels, thereby increasing nanoparticle extravasation and permeability into deep tissues (Dreher et al., 2006; Kong et al., 2001). Hyperthermia treatment in concert with conventional liposomes such as Doxil and Caelyx shows little change in drug accumulation within the tumor, whereas a combination of hyperthermia and thermosensitive liposomes (TSL) allow free drugs to enter the tumor once drug release is induced by locally heating the tumor site (Li et al., 2013; Manzoor et al., 2012). TSL are currently being formulated to attain maximum drug release in response to temperature change from 37°C to 39-43°C. This treatment is usually performed below 45°C to avoid vascular hemorrhage (Chen et al., 2014; Kneidl et al., 2014; Ta & Porter, 2013). Table 1 lists some conventional liposomes and TSL that are currently used for therapeutic purposes and in clinical trials. Most of the TSL formulations show successful drug release at hyperthermic temperature; however, a more stable and temperature-sensitive formulation will increase the efficacy of drug even further. If successful, the liposomal formulations will achieve higher drug accumulation at diseased sites, as opposed to healthy tissues and organs, and release more drug molecules at the site of local hyperthermia treatment.

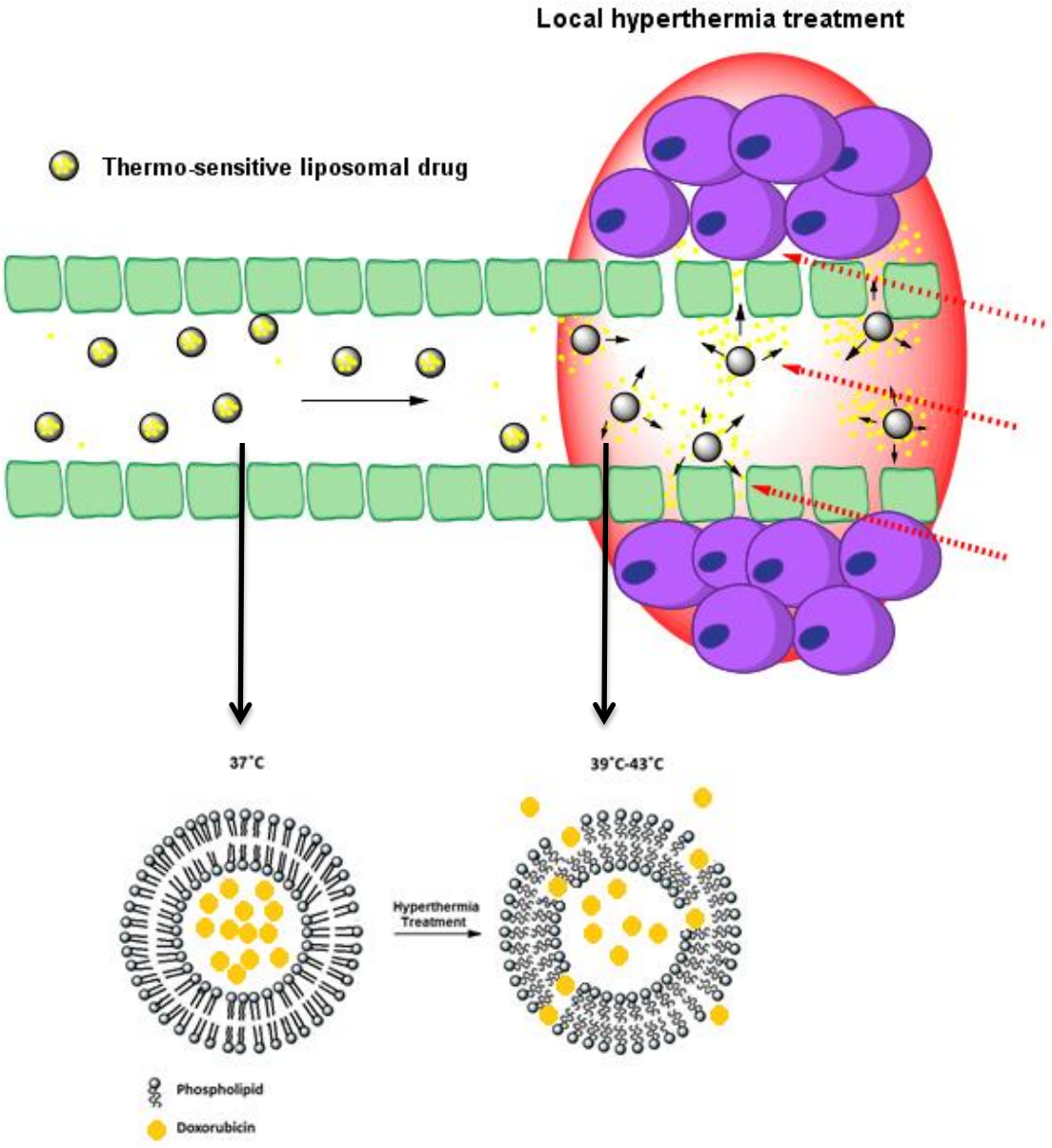

Diagram 2: Thermosensitive liposomal drugs

Thermosensitive liposomes releases entrapped drug molecules when temperature is increased from 37 ˚C to 39 ˚C-43 ˚C using local hyperthermia treatment.

2.4 Thermosensitive Liposome Compositions

For temperature-sensitive liposomes, the phase transition temperature (T_m) of the phospholipid is an important factor in determining liposome composition. In liposomes, phospholipids are tightly packed when below T_m, a temperature region known as the gel state, and loosely packed when above T_m (Ohline et al., 2001). Lipids that have T_m slightly higher than body temperature are commonly used in thermosensitive liposomal formulations. For most current thermosensitive liposomes, lipids with a T_m between 39°C and 43°C is used. For example, one thermosensitive liposome currently in phase III of clinical trials, Thermodox, employs the commonly used lipid 1,2-palmitoyl-*sn*-glycero-3-phosphocholine (DPPC) with a T_m of approximately 41.6 °C, as its major lipid component in its liposome composition. The Thermodox formulation also includes single chain lysolipid monostearoylphosphatidylcholine (MSPC) and poly(ethylene glycol) (H. L. Chang & Yeh, 2012; Chen et al., 2014). MSPC is used to slightly lower the transition temperature (T_m) of DPPC, allowing drug release to occur with mild hyperthermia (Al-Jamal et al., 2012; Anyarambhatla & Needham, 1999). Although successful at reducing the T_m, the addition of MSPC to liposomal formulation makes the liposomal system very unstable at physiological temperatures (Banno et al., 2010).

To increase liposomal stability, Thermodox and many other liposomal delivery systems contain cholesterol and polyethylene glycol. However, cholesterol has been shown to resist thermal shock by stabilizing the gel-state of the lipid membrane, compromising thermal sensitivity, (Beck, Mathieu, Loudet, Buchoux, & Dufourc, 2007; Gaber, Hong, Huang, & Papahadjopoulos, 1995), and polyethylene glycol can lower drug loading at higher concentrations, reducing overall drug exposure at the tumor site (Banno

et al., 2010; May & Li, 2012; Sandstrom, Ickenstein, Mayer, & Edwards, 2005). In order to use TSL for targeted delivery of therapeutic agents, attaining both vesicle stability and thermal sensitivity is highly desirable but difficult to achieve. This is the issue to be addressed in Part II of my thesis research. .

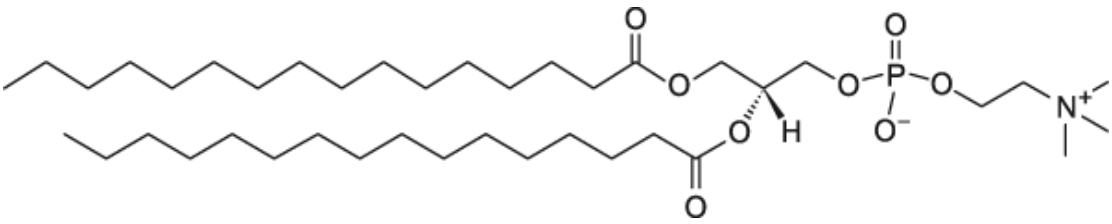

Figure 6: Chemical structure of dipalmitoyl-L-α-phosphatidylcholine (DPPC) saturated phospholipid.

2.5 Polar Lipid Fraction E (PLFE) from Thermoacidophilic Archaea

One crucial aspect of developing thermosensitive formulation is selecting lipids that are stable at physiological conditions. Archaeal bipolar tetraether lipids (BTL) are all saturated, containing varying numbers of cyclopentane rings and branched methyl groups. The polar lipid fraction E(PLFE) extracted from *Sulfolobus acidocaldarius* contains a mixture of GDNT (glycerol dialkylcalditol tetraether) and GDGT (glycerol dialkyglycerol tetraether) (Figure 8) (E. L. Chang & Lo, 1991; Lo, Montague, & Chang, 1989; Lo & Chang, 1990). The GDNT component (~90% of total PLFE) contains phospho-*myo*-inositol on the glycerol end and β-glucose on the calditol end, whereas the GDGT component (~10% of total PLFE) has phospho-*myo*-inositol attached to one glycerol and β-D-galactosyl-D-glucose to the other glycerol skeleton (Figure 8). The hydrophobic region of PLFE contains a pair of 40-carbon biphytanyl chains with isoprene units. Each biphytanyl chain includes up to four cyclopentane rings. PLFE lipids have incredible stability against high temperature, pressure, low pH, and auto-oxidation, fusogenic compounds, and lipases (Bagatolli, Gratton, Khan, & Chong, 2000; Chong, Ravindra, Khurana, English, & Winter, 2005).Also, PLFE lipids containing liposomes are not toxic which makes PLFE lipids suitable for biological research (Daswani, 2015). These characteristics demonstrate the usefulness of PLFE lipids especially in liposomal formulation.

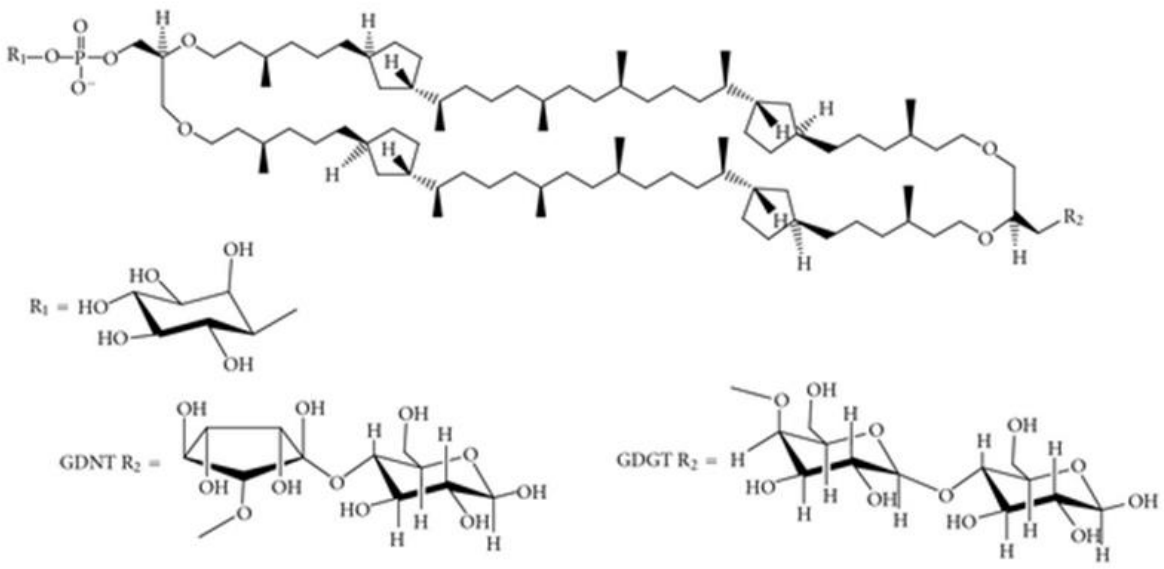

Figure 7: Structure of polar lipid fraction E (PLFE) extracted from *Sulfolobus acidocaldarius*.

PLFE is macrocyclic with four tetraether linkages at either end of the structure with two head groups. PLFE also contains varying numbers of cyclopentene rings (0-4) and branched methyl groups.

2.6 PLFE Liposomes

PLFE lipids can form stable multilamellar, unilamellar, giant unilamellar vesicles as well as planer membranes (Bagatolli et al., 2000; Kanichay, Boni, Cooke, Khan, & Chong, 2003; Ren et al., 2014). In liposomes, PLFE lipids form a monomolecular structure spanning the entire membrane. PLFE liposomes have the ability to withstand high temperatures in the autoclaving cycles compared to conventional liposomes (Brown, Venegas, Cooke, English, & Chong, 2009). In addition, PLFE liposomes exhibit much lower volume fluctuations compared to diester liposomes (Chong, Sulc, & Winter, 2010). Previous studies from our lab also demonstrated that proton permeability and dye leakage in PLFE liposomes are lower and less temperature sensitive than those in liposomes composed of monopolar diester lipids (Komatsu & Chong, 1998). In the present study, we studied the physical properties of hybrid liposomes made of diester and tetraether lipids. Such mixtures have already been shown to be non-toxic in mammalian systems (Daswani, 2015; Z. Li, Chen, Sun, & Xu, 2010; Patel, Agnew, Deschatelets, Fleming, & Sprott, 2000). However, the physical properties of such hybrid mixtures have not been explored to a great extent. Here, we studied DPPC/PLFE hybrid liposomes' physical characteristics and revealed surprising results, which can be utilized to develop a new TSL formulation. We demonstrated that these hybrid liposomes possess great vesicle stability at and below the physiological temperature. Upon mild hyperthermia (~42 ˚C) treatment, these vesicles exhibited sudden release of entrapped drug molecules.

Statement of Goals

PART I: PS targeting liposomes DPA-Cy3[22,22]/POPC

The objective of this project is to design and test a novel drug delivery system that is stable and able to target phosphatidylserine (PS) on the surface of diseased cells/tissues. We used lipophilic DPA-Cy3[22,22] (obtained through collaboration with Molecular Imaging Technology Inc.), which contains a PS recognizing moiety and two hydrocarbon chains, to develop liposomal carriers. Together, DPA-Cy3[22,22] and POPC can make vesicles that have the ability to recognize and bind PS exposed cells guiding the liposome to the cancer sites.

I. Determine size stability and size homogeneity of various molar ratios of DPA-Cy3[22,22] and POPC liposomes using dynamic light scattering (DLS).

II. Test binding and specificity of DPA-Cy3[22,22]/POPC liposome to PS
    a. Use anion exchange chromatography to demonstrate the ability of DPA-Cy3[22,22]/POPC liposomes to bind PS containing liposomes.
    b. Use flow cytometry to determine if and to what extent DPA-Cy3[22,22]/POPC liposomes can bind PS exposed and non-PS exposed cells.

III. Visualize DPA-Cy3[22,22]/POPC liposome-cell interaction using confocal microscopy
    a. Demonstrate that liposome bind to cells only when DPA moiety is present.

IV. Test the cytotoxicity of DPA-Cy3 [22,22]/POPC liposomes on cancer cells (MCF-7) and non-cancer cells (MCF-12A) in a dose dependent and molar ratio dependent manner.

V. Explore the mechanism of DPA-Cy3[22,22]/POPC liposome internalization by cells and localizing in cellular compartment using confocal microscopy.

PART II: Thermosensitive liposome hybrid DPPC/PLFE

The goal of this project is to develop archaeal tetraether lipid based liposomal anti-cancer drugs that would have considerable liposome stability and the ability to conduct controlled drug release when using hyperthermia treatment. We will use bipolar tetraether archeal lipids PLFE isolated from thermoacidophilic archaea in the lab and commercially available diester lipid DPPC for making liposomal DXO. In order to demonstrate that PLFE lipids have an impact on DPPC/PLFE hybrid liposome stability and temperature sensitivity, we explore the biophysical properties of the hybrid system and how PLFE lipids affect the formulation of thermosensitive drug carrier.

I. Conduct characterization of DPPC(diester)/PLFE(tetraether) hybrid liposomes
   a. Determine the size, polydispersity and zeta potential of liposomes with various molar ratios.
   b. Study DPPC/PLFE liposome membrane packing and dynamics using steady state and nano-second probe fluorometry and polarization.

II. Demonstrate that DPPC/PLFE hybrid liposomes, at certain molar ratios, have unique temperature sensitive properties

a. Show change in zeta potential of DPPC/PLFE liposomes from the physiological temperature (37°C) to the hyperthermic treatment temperature (41-42°C).
b. Show a significant increase in drug release rate constant from DPPC/PLFE liposomes due to a change from the physiological temperature (37°C) to the hyperthermic treatment temperature (41-42°C)

III. Assess the effects of DPPC/PLFE liposomal DOX on cell viability at physiological temperature (37°C) and at hyperthermic treatment temperature (41-42 °C)

IV. Conduct confocal microscopy studies to observe the differences in cellular uptake and localization of DOX when cells are treated with DPPC/PLFE liposomal DXO at physiological temperature (37°C) and at hyperthermic treatment temperature (42 °C).

CHAPTER 2: MATERIALS AND METHODS

Materials

1.1 Diester Lipids and Fluorescence Probes

1-Palmitoyl-2-oleoyl-*sn*-glycero-3-phosphocholine (POPC), 1,2-dipalmitoyl-*sn*-glycero-3-phosphocholine (DPPC), and 1-palmitoyl-2-oleoyl-*sn*-glycero-3-phospho-L-serine (POPS) were purchased from Avanti Polar Lipids (Alabaster, AL). Bis-dipicolylamine zinc cyanine 3 [C22,22] (DPA-Cy3[22,22]) and $DiIC_{22}H_{45}$ (Compound 1, 2, and 3) were obtained from Molecular Targeting Technologies (MTT, West Chester, PA).

6-Lauroyl-1,2-dimethylamino naphthalene (Laurdan) and 1,6-diphenyl-1,3,5-hexatriene (DPH) were purchased from Molecular Probes (Eugene, OR) and *p*-bis[2-(5-phenyloxazolyl)]benzene (POPOP) was purchased from Eastman Kodak Co. (Rochester, NY). PS binding protein annexin V tagged with fluorescein isothiocyanate (FITC), cell nucleus dye Hoechet 33342 and cytosolic dye calcein were all obtained from Life Technologies (Carlsbad, CA). For cell death staining, the fluorescent dye 7-aminoactinomycin D (7AAD) was purchased from BD Biosciences (San Jose, CA).

1.2 Archaeal Cells and Lipids

Sulfolobus acidocaldarius cells (strain DSM639; American Type Culture Collection, Rockville, MD) were grown aerobically and heterotrophically at 69–70°C and pH 2.5–3.0. Polar lipid fraction E or PLFE lipids were isolated from *S. acidocaldarius* dry cells

by soxhlet extraction with chloroform/methanol (1:1, v/v) for 48 h, as previously described (E. L. Chang & Lo, 1991; Lo et al., 1989; Lo & Chang, 1990).

1.3 Mammalian Cell Cultures

The cell lines used for this study were MCF-7 and MCF-12A grown at 37°C and 5% CO_2. MCF-7 (ATCC, Manassas, VA) cells were cultured in Hyclone Dulbecco's modified Eagle's medium (DMEM) which contained high calcium, 4.5 g/L glucose, L-glutamine and sodium pyruvate, 10% FBS and 1% Penstrap (Fischer, Waltham, MA). MCF-12A (obtained from Fox Chase Cancer Center, FCCC) cell culture was supplemented with 1:1 mixture of Dulbecco's modified Eagle's medium and Ham's F12 medium, 20 ng/ml human epidermal growth factor, 100 ng/ml cholera toxin, 0.01 mg/ml bovine insulin and 500 ng/ml hydrocortisone, and 5% (v/v) horse serum. All the supplements were obtained from FCCC. Cells were subcultured every 3 days or when ~80% confluency was reached. Cells were detached from culture dish with 0.25% trypsin-EDTA and counted using a hemocytometer.

1.4 Human Serum

Human serum donated from a healthy Caucasian male 27 years of age was processed by removing the coagulating factors and obtained from Dr. Rao's lab in Sol Sherry Thrombosis Research Center, Temple University School of Medicine (Philadelphia, PA).

Methods

2.1 Liposome Preparation

2.1.1 DPPC/PLFE hybrid archeosomes

DPPC stock solution was prepared in chloroform, and PLFE stock solution was made in chloroform/methanol/water (118:67:15, v/v/v). After pipetting appropriate amounts of DPPC and PLFE lipid stock solution into a screw capped Pyrex test tube, the lipids were first dried under a stream of N_2 gas and then placed under high vacuum (Labconco Freezone 4.5, Kansas City, MO) overnight to remove residual organic solvents. Dried lipids were hydrated with pre-heated 50 mM Tris (tris(hydroxymethyl)aminomethane) buffer (pH 7.2) (Sigma, St. Louis, MO) containing 10 mM EDTA and 0.02% NaN_3, and the lipid dispersion was vortexed at ~69°C for ~3 min to generate multilamellar vesicles (MLVs). MLVs were subject to 3 heating/cooling cycles at 4°C for 30 min and 69°C for 30 min per cycle. Samples were then incubated for 1-2 days at room temperature. Unilamellar vesicles (LUVs) were prepared from MLVs via extrusion (Lipex Biomembranes, Vancouver, British Columbia, Canada) at 69°C using 200 nm polycarbonate membranes at 120 atm N_2 pressure followed by 1-2 days of incubation at room temperature. Total lipid concentration was determined using Bartlett phosphate assay (Tejera-Garcia, Connell, Shaw, & Kinnunen, 2012).

2.1.2 DPA-Cy3[22,22]/POPC liposomes

POPC and DPA-Cy3[22,22] stock solutions were made in chloroform and ethanol, respectively. To determine the DPA-Cy3[22,22] to POPC molar ratio in liposomes, the amount of DPA-Cy3[22,22] was determined spectroscopically by

measuring the absorbance at 481 nm in ethanol using the extinction coefficient 72,100 $M^{-1}cm^{-1}$ (provided by MTT) and the POPC concentration was determined using the Bartlett phosphate assays previously described (Tejera-Garcia et al., 2012).

To prepare DPA-Cy3[22,22]/POPC liposomes at the desired molar ratio, appropriate amounts of POPC and DPA-Cy3[22,22] were pipetted into a Pyrex screw capped test tube and dried first with nitrogen gas and subsequently under high vacuum overnight as described earlier. Dried lipids were hydrated with 10 mM TES buffer (pH 7.4) containing 145 mM NaCl. The buffer was pre-warmed to ~50˚C, and the hydrated lipid dispersion was vortexed at 50˚C for ~3 min to make DPA-Cy3[22,22]/POPC MLVs. The MLVs were subject to 3 cycles of heating at 45˚C for 30 min and cooling at 4˚C for 30 min. Annealed MLVs were incubated for at least 2 days at 24˚C in the dark under argon. MLVs were then extruded at 50˚C through two polycarbonate membranes with 200 nm pore size at elevated nitrogen pressure (~200 psi) to create unilamellar vesicles (LUVs). LUVs were then flushed with argon and stored in a desiccating chamber for > 2 days at 24˚C before use.

2.2 Liposome Size Measurement

Liposome size was determined by the dynamic light scattering (DLS) technique on a Malvern Zetasizer HS or a Malvern Zetasizer Nano ZS (Worcestershire, UK). For these measurements, liposomes were suspended in Tris-HCl buffer in a disposable cuvette and the scattered light was measured at 25˚C. The Z_{ave} value (hydrodynamic radius) was determined by the instrument using the Stokes-Einstein equation:

$$d(H) = kT/3\pi\eta D$$

where, d(H) is the hydrodynamic diameter (nm), D the translation diffusion coefficient, *k* Boltzmann's constant, T the absolute temperature (kelvin), and η is the viscosity of the medium, which in our case is the water viscosity at the measured temperature.

2.3 Zeta Potential

Zeta potential (ζ) was determined using the electrophoretic mobility method through laser doppler velocimetry (LDV). The zeta potential values were calculated using Henry's equation:

$$U_E = \frac{2\,\varepsilon\zeta\,f(ka)}{3\eta}$$

Where, U_E is the electrophoretic mobility, ζ zeta potential (mV), η viscosity, ε the dielectric constant of the medium and f(ka) is Henry's function. For samples, in aqueous solution, the most commonly used theory for calculating zeta potential was developed by Marian Smoluchowski (Smoluchowski, 1903). For dispersed particles of various shape and concentration, Smoluchowski's theory uses f(ka) of 1.5 and was applied to all our zeta potential measurements. The temperature dependence of zeta potential was measured at a rate of ~3°C/15 min and measurements were taken in triplicates at each temperature. The temperature dependent zeta potential experiment was repeated at least 3 times for each sample. Before zeta potential measurements, the instrument was calibrated using zeta potential transfer standard DTS1235, a polystyrene latex, in aqueous buffer at pH 9 with expected zeta potential of -42 ± 4.2 mV (Malvern, Worcestershire, UK).

2.4 Doxorubicin Entrapment

Doxorubicin (DXO) was encapsulated into liposomes using either passive or active entrapment methods. For passive drug entrapment, the MLVs were prepared by hydrating dried lipids with 50 mM Tris buffer (pH 7.2), containing 10 mM EDTA and 0.02% NaN_3) and DXO, followed by vortexing at 69°C and multiple heating/cooling cycles. The MLVs were then extruded, followed by 3 additional heating/cooling cycles.

Liposomal doxorubicin was also prepared using active entrapment method. In this case, dried lipids were hydrated with 250 mM ammonium sulfate (pH 4). An ammonium sulfate gradient was formed by removing the ammonium sulfate from the external liposome medium by dialysis using a Slide-A-Lyzer dialysis cassette (10,000 MWCO; Pierce, Carlsbad, CA). Specifically, liposome sample (1 mL) was injected into the dialysis cassette and dialyzed against 300 mL of 50 mM Tris buffer (pH 7.2 containing 140 mM NaCl) for 3 hours with buffer exchanged every hour.

Afterwards, DXO HCl was added to the liposome dispersion at a temperature above the phase transition of the liposomal lipids (65°C) and incubated for 30 minutes. Ammonium sulfate gradient is used for loading of amphipathic weak bases, such as DXO, into liposomes. DXO, a cationic amphiphile, has a primary amino group in its sugar moiety, in an ionized and non-ionized form. The amino group of DXO has a pKa value of 8.46 (Haran, Cohen, Bar, & Barenholz, 1993; Toxnet, 2010). At pH 7.2, ~95% of DXO molecules are in the non-ionized form, according to the calculation using the Henderson-Hasselbalch equation. The non-ionized form of DXO enters the liposome and is ionized inside the liposome due to the proton rich environment. The protonated DXO

becomes impermeable across the liposome bilayer (Gabizon, Shmeeda, & Barenholz, 2003; Xingong et al., 1998) (Diagram 2).

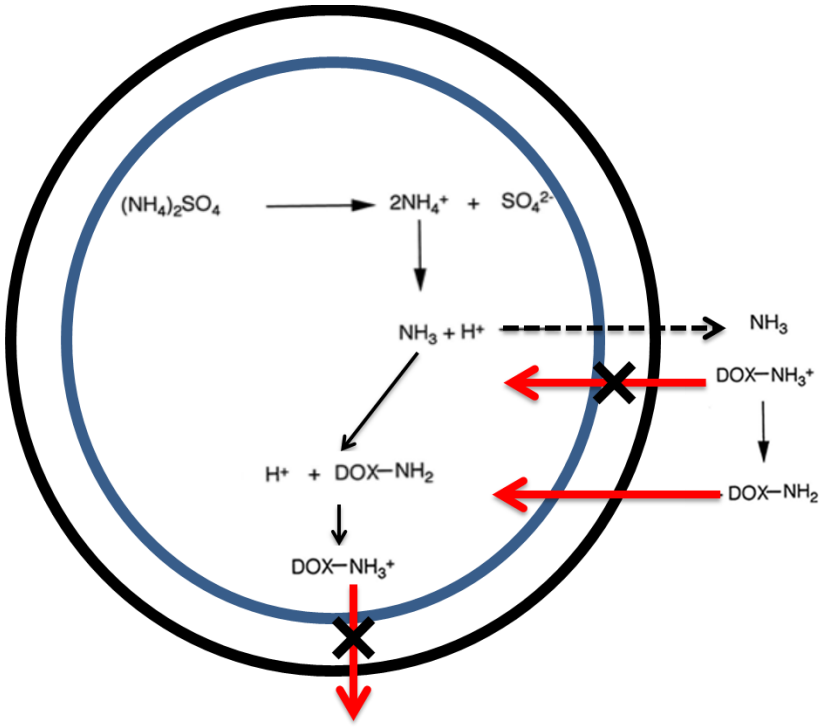

Diagram 3: Drug entrapment using ammonium sulfate gradient method.

Inside the liposomes, ammonium sulfate dissociates into sulfate anions and ammonium cations. Ammonium cations can further dissociate to neutral ammonia and proton (H^+). When neutral form of DXO permeates into the liposomes, the free proton will attach to it resulting in protonation of DXO and impermeability out of the liposomes.

Un-encapsulated drug was removed using Sephadex G-50 or dialysis using a Slide-A-Lyzer dialysis cassette (10,000 MWCO, Pierce, Carlsbad, CA) at room temperature against 50 mM Tris buffer (pH 7.2) containing 200 µM NaCl for at least 5 hours. Drug entrapment was determined after addition of 0.02% Triton X-100 to lyse the

liposome. The absorbance of lysed liposome with DXO was measured spectroscopically at 481 nm using the extinction coefficient of 11,500 $M^{-1}cm^{-1}$ (Etrych 2008).The percent entrapment was calculated using the equation:

% efficiency = [Liposomal DXO/(Free DXO + Liposomal DXO)] x 100

DXO entrapment efficiency using passive entrapment was <60% whereas active loading method yielded > 90% DXO entrapment in liposomes.

2.5 Ion-Exchange Chromatography

DEAE-Sephadex A25 anion exchange resin was hydrated in buffer and packed in a column (18 cm x 1 cm). Two buffer systems were used for either equilibrating the column or eluting materials bound to the column. Equilibrating buffer (buffer 1: 50 mM TES buffer (pH 7.4) containing 150 mM NaCl) was used to wash the column and collect the flow through. In the first reaction, DPA-Cy3[22,22]/POPC liposomes (30 nmol lipids) (Reactant A) was reacted with POPS/POPC liposomes (90 nmol) (Reactant B) for 3 hrs at room temperature. The second reaction included DPA-Cy3[22,22]/POPC liposomes (Reactant A) and POPC (Reactant B) liposomes with the same reaction condition as the first reaction. The reaction mixture was loaded onto the column and eluted with buffer 1. The bound material was then eluted out of the column by using buffer 2 (50 mM TES (pH 4) containing 1M NaCl).

2.6 Generalized Polarization of Laurdan Fluorescence

Laurdan fluorescence emission was monitored with an SLM-8000 fluorometer. Laurdan dissolved in ethanol was added to aliquot of DPPC and PLFE containing

liposomes. In the cuvette, each liposome sample contained 40 nmol of lipids in a final volume of 1.8 mL with a probe-to-lipid molar ratio of 1/600. The vesicles were incubated with Laurdan at 24°C for 1 hr. Then, the emission spectra of Laurdan fluorescence were taken at different temperatures (in the range 17-50°C) under gentle stirring. The background readings from vesicles without the probe were subtracted from the sample readings. Change in polarity of a fluorescent probe is detected by shifts in the Laurdan emission spectrum, and the Generalized Polarization function (GP) was defined as a way of measuring wavelength displacements. The excitation generalized polarization (GP_{ex}) of Laurdan fluorescence was calculated from the spectral readings.

$$GP_{ex} = (I_{435} - I_{500}) / (I_{435} + I_{500})$$

Here I_{435} and I_{500} were the fluorescence intensities measured at 435 and 500 nm, respectively, when the sample was excited at 340 nm (T. Parasassi, De Stasio, d'Ubaldo, & Gratton, 1990; T. Parasassi, De Stasio, Ravagnan, Rusch, & Gratton, 1991).

2.7 DPH Fluorescence Polarization

In measuring the fluorescence polarization, a fluorophore is excited with light that passes through a polarizer. The polarized fluorescence is measured after passing through an emission polarizer either parallel or perpendicular to the exciting light's plane of polarization. Two intensity measurements are obtained ($I_{\perp}$ and $I_{\parallel}$) and polarization (P) is calculated using the equation (Lakowicz, 1999):

$$P = \frac{I_{\parallel} - I_{\perp}}{I_{\parallel} + I_{\perp}}$$

$I_{\parallel}$ is the fluorescence intensity parallel to the excitation plane, and $I_{\perp}$ is the fluorescence intensity perpendicular to the excitation plane.

The stock solution of the fluorescent probe, DPH, was prepared in methanol and the concentration was determined spectroscopically at 354 nm using the extinction coefficient of 91,000 $M^{-1}cm^{-1}$ (Repakova et al., 2005). Liposomes were mixed with aliquots of DPH/ethanol, with a probe-to-lipid ratio of 1/400, for 1 hr. at room temperature. To measure DPH polarization, the DPH labeled liposomes (~60 nmol of lipids) were excited at 350 nm (slitwidth =1nm). The emission was detected at 420 nm through a monochromator (slitwidth = 2nm) as a function of temperature (17-60°C) on an ISS K2 fluorometer (Champaign, IL). Blank readings were used to subtract the background from sample readings.

2.8 DPH Fluorescence Lifetime and Differential Polarized Phase and Modulation Fluorometry

2.8.1 Theory

Fluorescence lifetime is the average time a fluorophore spends in its excited state in a particular environment. There are two methods of measuring lifetime, the time-domain and frequency domain (Jameson, 2014; Lakowicz, 1999). Here, frequency domain or phase-modulation method is used to determine DPH lifetime. In this method, sample is excited with modulated light described by:

$$E(t) = E(0)\,[1 + M_E sin\ \omega t]$$

$$M_E = \left(\frac{AC}{DC}\right)_{Ex}$$

E(t) and E(0) are intensities at time t and 0, ω is the angular modulation frequency, and M_E is the modulations of excited light related to AC (alternating current) and DC (direct current) (Jameson, 2014; Lakowicz, 1999). Samples excited with such modulated light also emits at the same modulation frequency. The emission, delayed in time relative to the excitation, is measured as phase delay (ϕ). The emission F(t) and modulation of emission (M_F) is described as:

$$F(t) = F(0)\,[1 + M_F sin\,(\omega t + \phi)]$$

$$M_F = \left(\frac{AC}{DC}\right)_{Em}$$

The phase and modulation lifetime τ_p and τ_m respectively can be determined using the following equations (Jameson, 2014; Lakowicz, 1999):

$$\tau_p = \omega^{-1}\, tan\phi \qquad\qquad \tau_m = \sqrt{\frac{1}{\omega}\left[\frac{1}{M^2} - 1\right]}$$

, which includes the phase delay (ϕ), relative modulation (M), and angular frequency (ω) in megahertz.

2.8.2 Sample preparation and measurement procedure

To measure lifetime, first, DPH in ethanol was added into liposome dispersions with the DPH-to-lipid ratio of 1/500. In the cuvette, for the lifetime and anisotropy decay measurements, 0.10-0.15 mM lipids and the total volume of 1.8 mL were used. After adding DPH into DPPC/PLFE and PLFE liposomes, samples were incubated at 65˚C for 30 min and DPPC liposomes were incubated at 50˚C for 1 hr. in the ISS K2 fluorometer sample compartment under magnetic stirring. Samples were allowed to cool to room

temperature for 30 min before beginning measurements. DPH lifetimes and anisotropy decays were measured as a function of temperature in the range 25-50˚C on the ISS K2 fluorometer using a LED at 370 nm (ISS Inc. Champaign, IL) as the light source. Fluorescence emission was detected through a KV480 cut off filter. Phase and modulation values were determined relative to the reference (POPOP in ethanol, with the fluorescence lifetime of 1.35 ns). Phase and modulation values were determined using modulation frequencies ranging from 2 to 100 MHz.

2.8.3 Data analysis

The data were analyzed and fit into multiple exponential decay functions using non-linear least squares methods in which the phase and modulation ratio data are fitted to different models on the ISS Vinci software. The quality of the fit is then judged by the chi-square value (χ^2):

$$\chi^2 = \left[\left(\sum_{i=1}^{n} \frac{(P_i c - P_i m)^2}{\sigma^2_{P_i m}}\right) + \left(\sum_{i=1}^{n} \frac{(M_i c - M_i m)^2}{\sigma^2_{M_i m}}\right)\right]$$

, where P and M are phase and modulation data, respectively, c and m refer to calculated and measured values , and σ_P and σ_M are the standard deviations of phase and modulation measurement, respectively.

2.9 Drug Leakage

Drug release from liposomes was performed after column separation of free drug from liposomal drug. Slow kinetics of the drug release from liposomes was monitored in 50 mM Tris buffer (pH 7.2) containing 10 mM EDTA and 200 µM NaCl (equivalent to

drug concentration) or in human serum. For the drug release experiment in human serum, liposomes were pipetted in the cuvette with 50% plasma (v/v) and 50% (v/v) HEPES buffered saline (pH 7.5) containing 145 mM NaCl, 5 mM KCl, 0.1 g/L glucose, and 0.1g/L BSA. For the studies of temperature dependence of drug release, both the water-jacketed Sephadex column and the fluorometer sample compartment were set to the desired temperature, and buffer was preheated to the right temperature before use.

Leakage of entrapped DXO from liposomes was monitored by measuring the increasing DXO fluorescence intensity due to un-quenching. Liposomal DXO dispersions were collected from Sephadex G-50 column and excited at 480 nm, and the fluorescence intensity at 590 nm (F_t) was recorded as a function of time on the ISS K2 fluorometer. At the end of each experiment, the sample was mixed with 0.2% Triton X-100 to release all the entrapped DXO, providing the maximal fluorescence intensity (F_{max}). The rate constant *k* was determined by fitting the normalized fluorescence intensity ($F = F_t/F_{max}$) into the equation:

$$F = A + B(1 - e^{-kt}),$$

where t is time, and A and B are constants..

2.10 Cell Cytotoxicity Assay

2.10.1 Thermosensitive liposomes: 70 mol% DPPC/ 30 mol% PLFE

Mild hyperthermia treatment is a clinical approach to raise the local body temperature from 37˚C to 41-42˚C. To test the effects of mild hyperthermia on the cytotoxicity of DPPC/PLFE liposomal DXO on MCF-7 cells, we used the Invitrogen

CyQuant Kit (Invitrogen, Carlsbad, CA). Approximately 1,000 cells/well in a 96-well plate were plated with 100 µL of cell medium (DMEM with 10% FBS and 1% penicillin-streptavidin) and left to adhere overnight. Cells were then incubated with various concentrations of 100 mol% DPPC, 100 mol% PLFE, and DPPC/PLFE (molar ratio: 7:3) liposomal DXO at 42˚C for 15 minutes or at 37˚C for 15 minutes (control). Subsequently, cells were incubated at 37˚C for additional 24 hours. After treatment, cells were washed with PBS two times and stored at -70˚C for at least 12 hrs. Remaining live cells were then quantified using the fluorescence intensity of a dye embedded in the CyQuant assay kit using a Spectra Max M5 microplate reader (Molecular Devices, Sunnyvale, CA) with the excitation wavelength set at 480 nm and the emission detected at 530 nm. A standard curve was constructed for each sample set using known amounts of MCF-7 and then the fluorescence intensities measured were converted to the number of cells.

2.10.2 PS targeting liposomes: DPA-Cy3[22,22]/POPC

Effects of DPA-Cy3[22,22]/POPC liposomes on MCF-7 cell viability is tested using various lipid concentrations and DPA-to-lipid molar ratios. After the MCF-7 cells were plated in a 96-well plate, cells were left to adhere overnight, then, treated with DPA-Cy3[22,22]/POPC liposomes for 4, 8, 24 and 48 hrs. After treatment, the dead cells (floating in the growth medium) were removed. The cell proliferation assay was performed to determine the number of cells remaining alive (i.e. those still attached to the wells). The assay was performed at room temperature using the CyQuant Kit (Invitrogen, Carlsbad, CA) according to the manufacturer's instructions. Fluorescent intensities were measured at 530 nm with excitation at 485 nm. A standard curve was constructed for each sample set using known amounts of MCF-7 cells counted with a hemocytometer.

2.11 Flow Cytometry

MCF-12A or MCF-7 cells plated in 6-well plates (~600,000 cell per well) were trypsinized for ~1 min and then counted using a hemocytometer. Cell viability was determined using trypan blue. Aliquots of 100,000 cells were washed with PBS and resuspended in binding buffer provided in the Cell Death Assay Kit (Life Technologies, Carlsbad, CA). Staining was carried out according to the manufacturer's instructions. Cells were treated with different concentrations of DPA-Cy3 [22,22]/POPC for 15 min. Afterwards, cells were stained with annexin V-FITC for 15 min and 7AAD for 5 min before taking readings.

To increase cell PS exposure, an apoptotic inducer camptothecin (Life Technologies, Carlsbad, CA) was used. Cells were treated with 10 μM camptothecin in 6-well plates for 0, 2, and 4 hrs and then trypsinized and incubated with DPA-Cy3 [22,22]/POPC liposomes, annexin V, and 7AAD. All measurements were completed within 1 hr. of staining. Measurements were taken using a flow cytometer FACS Canto cell analyzer (BD, Franklin Lakes, NJ). All data were analyzed using the software FlowJo version 10 (Ashland, OR) and Flowing Software 2.0 (Turku, Finland).

2.12 Confocal Microscopy

2.12.1 DPA-Cy3[22,22]/POPC liposomes

Cells (600,000 cells/well) were plated in a 6-well plate with coverslips and left to adhere overnight in cell media (DMEM high calcium with 10% FBS and 1% penstrap mixture). Cells treated with DPA-Cy3[22,22]/POPC liposomes (λ_{ex}= 545 nm/ λ_{em}= 575 nm) were visualized using three different dyes: (i) Cy3 fluorescence which was

excited with a HeNe laser at 543nm and detected through an emission filter LP615; (ii) the cytoplasmic fluorescent dye calcein which was excited using an argon laser at 488 nm and the emission ($\lambda_{ex,max}$ = 528 nm) was observed through a BP505-550 filter; (iii) the nuclear dye Hoechst 33342) which was excited with a diode laser at 407 nm and the fluorescence ($\lambda_{em,max}$ = 440 nm) was observed using a LP420 filter. Cells were imaged using a Carl Zeiss Meta 510 confocal microscope (Jena, Germany) with a 40× oil objective with 1.5× digital zoom.

MCF-7 cells treated with camptothecin for 0-6 hrs were washed with 1X PBS and 1X annexin V binding buffer (provided in Live/Dead Imaging Kit, Life technologies) and then incubated with annexin V-FITC and DPA-Cy3C[22,22]/POPC liposomes for 15 min followed by washing with 1X PBS and 1X binding buffer before cell imaging under Zeiss LSM 510 MET (Jena, Germany). Fluorescence signal of FITC was observed through a BP505-550 filter using 488 nm excitation from an argon laser. Cy3 was excited with a HeNe laser at 543 nm and the emission was observed through a LP615 filter. Images and data were analyzed using the Zen software (Zeiss).

2.12.2 DPPC/PLFE liposomes

Approximately 500,000 MCF-7 cells were plated in a Matek dish and left to adhere overnight at 37°C. Then, cells were treated with 10μM free DXO or liposomal DXO and immediately put into incubator set at either 37°C (control) or 41.6°C (hyperthermia treatment) for 15 minutes. Afterwards, dishes containing cells and drug were treated for 15 minutes at 37°C or 41.6°C and were incubated at 37°C for additional 30 or 60 minutes. Nuclear dye Hoechst was added to cells 15 minutes prior to imaging.

Treated and stained cells were washed with 1x PBS and images were taken under Zeiss LSM 510 META (Jena, Germany). DXO fluorescence was observed using argon laser excited at 488 nm and Hoechst was excited with a diode laser at 407 nm. Images were analyzed using Zen software.

CHAPTER 3: RESULTS

Part I: Characterization of DPA-Cy3 [22,22]/POPC Liposomes

1.1 Stability of DPA-Cy3[22,22]/POPC Liposomes as Judged by Particle Size and Polydispersity

Liposomes containing conventional zwitterion lipid POPC and DPA-Cy3[22,22] were prepared with various DPA-Cy3[22,22]-to-POPC molar ratios. The DPA-Cy3[22,22]-to-POPC molar ratios 1/5, 1/10, 1/20, 1/30, and 1/50 will be described as 17, 9.1, 4.8, 3.2, and 2 mole percentage of DPA-Cy3[22,22], respectively. DPA-Cy3[22,22], shown in Figure 8-1, is anticipated to bind the negatively charged lipids, PS. The first experiment was conducted to test the effect of DPA-Cy3[22,22] content on the stability of liposomes. Using dynamic light scattering (Zetasizer 1000HSA), the size (Z_{ave}) and polydispersity of DPA-Cy3 [22,22] liposomes with varying molar ratios of DPA-Cy3[22,22] and POPC was monitored for at least 1 week (Figure 8-2).

The size and polydisersity was measured for DPA-Cy3[22,22]/POPC liposomes containing 17, 9.1, 4.8 and 3.2 mol% DPA-Cy3[22,22] (Figure 8-2). After extrusion using 200-nm polycarbonate membranes, the liposome size was ~150 nm and polydispersity was between 0.15-0.20.Thereafter, liposomes were measured for 9 consecutive days to observe changes in size and polydispersity. The data in Figure 8-2 show that, at 4.8 and 3.2 mol% DPA-Cy3[22,22], POPC liposome size (~150 nm) stayed constant (Figure 8-2A), and polydispersity remained at ~0.2 for 1 week. On the other hand, for 17 and 9.1 mol% DPA-Cy3[22,22] in POPC liposomes, a gradual increase in size (Figure 8-2A) and polydispersity (Figure 8-2B) was observed over time. Although

the size change was less dramatic, polydispersity for 17 and 9.1 mol% DPA-Cy3[22,22] containing liposomes increased from ~0.2 to ~0.8 which indicates that these liposomes in solution became highly heterogeneous over time.

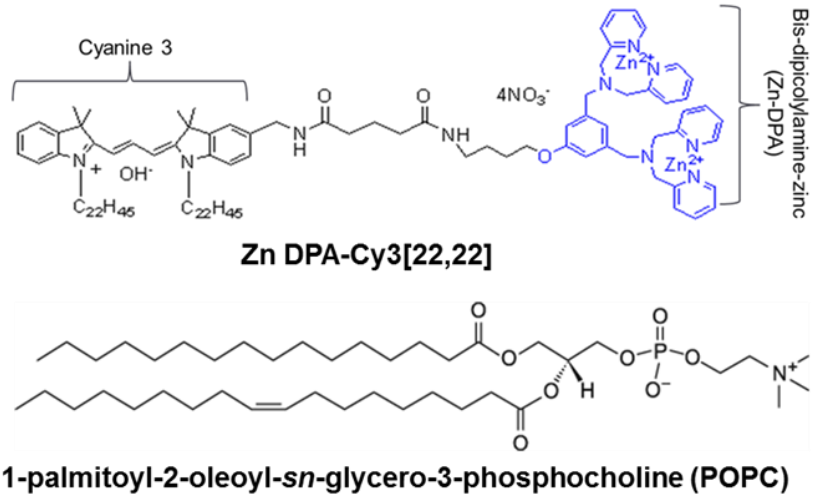

Figure 8-1 Structure of PS recognizing hydrophobic molecule Zn DPA-Cy3[22,22] and zwitterionic lipid POPC in DPA-Cy3[22,22]/POPC liposomes.

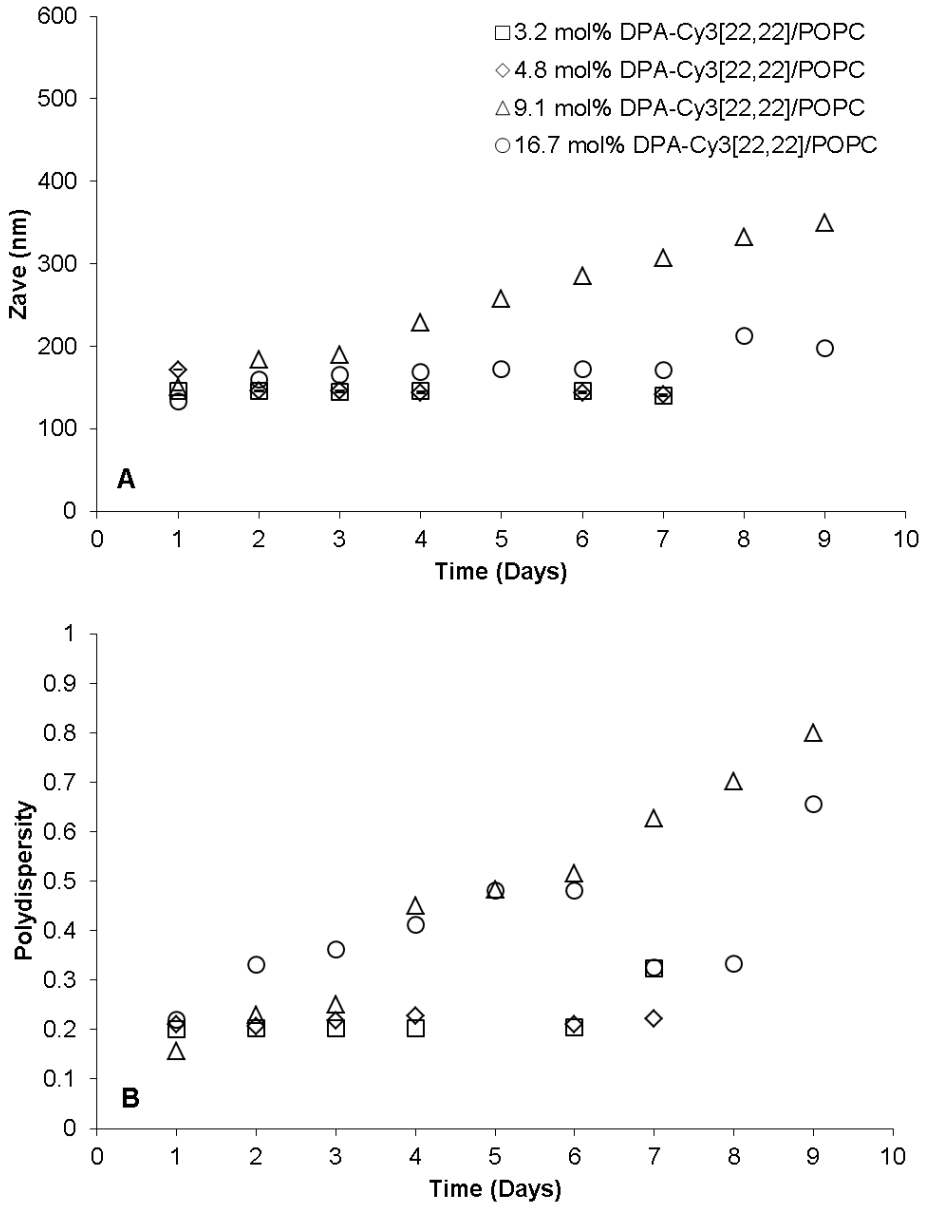

Figure 8-2: Size (A) and polydispersity (B) of DPA-Cy3[22,22]/POPC liposomes measured using dynamic light scattering (DLS).

Measurements were collected from 17, 9.1, 4.8, and 3.2 mol% DPA-Cy3[22,22] in POPC liposomes. Standard deviations were calculated from 3 measurements.

.

1.2 Affinity of DPA-Cy3[22,22]/POPC Liposomes to PS Liposomes

To test whether liposomes containing DPA-Cy3[22,22] have the ability to bind PS containing liposomes, I used anion exchange chromatography. The binding of 4.8 mol% DPA-Cy3[22,22]/POPC liposomes to POPS/POPC and POPC liposomes was tested. In Figure 9, elution profiles of three conditions are presented. First, 4.8 mol% DPA-Cy3[22,22]/POPC liposomes alone were able to flow through the column (Sephadex A-25), as did POPC liposomes. However, POPS/POPC (50/50) liposomes interacted with the anion exchange resin Sephadex A-25. As a result, POPS/POPC liposomes were retained inside the column (Figure 9-I). Second, when DPA-Cy3[22,22]/POPC liposomes were mixed with POPS/POPC liposomes and the mixture was loaded onto the column, 4.8 mol% DPA-Cy3[22,22]/POPC liposomes were not observed in the flow through and remained inside the column until the elution buffer containing low pH (pH=3) and high NaCl concentration ([NaCl] = 1 M) was used to elute bound materials (Figure 9-II). After applying the elution buffer, two peaks were detected (Figure 9II). One peak was detected using Cy3 fluorescence, incorporated in DPA-Cy3[22,22]/POPC liposomes, and the second peak, due to the presence of POPS/POPC liposomes, was detected by light scattering (excitation 500 nm/emission 505 nm). Third, as a control, the previous condition was repeated with POPC liposomes mixed with DPA-Cy3[22,22]/POPC liposomes to show that DPA-Cy3[22,22]/POPC liposomes were not retained in the column without PS. As predicted, all the liposomes in the POPC and DPA-Cy3[22,22]/POPC mixture came out in the flow through (Figure 9-III). One major finding from this data is that DPA-Cy3[22,22]/POPC liposomes were able to bind the anion exchange resin in the presence of PS containing liposomes as a result of high

affinity to PS. This was the first evidence for DPA-Cy3[22,22]/POPC liposome binding to PS.

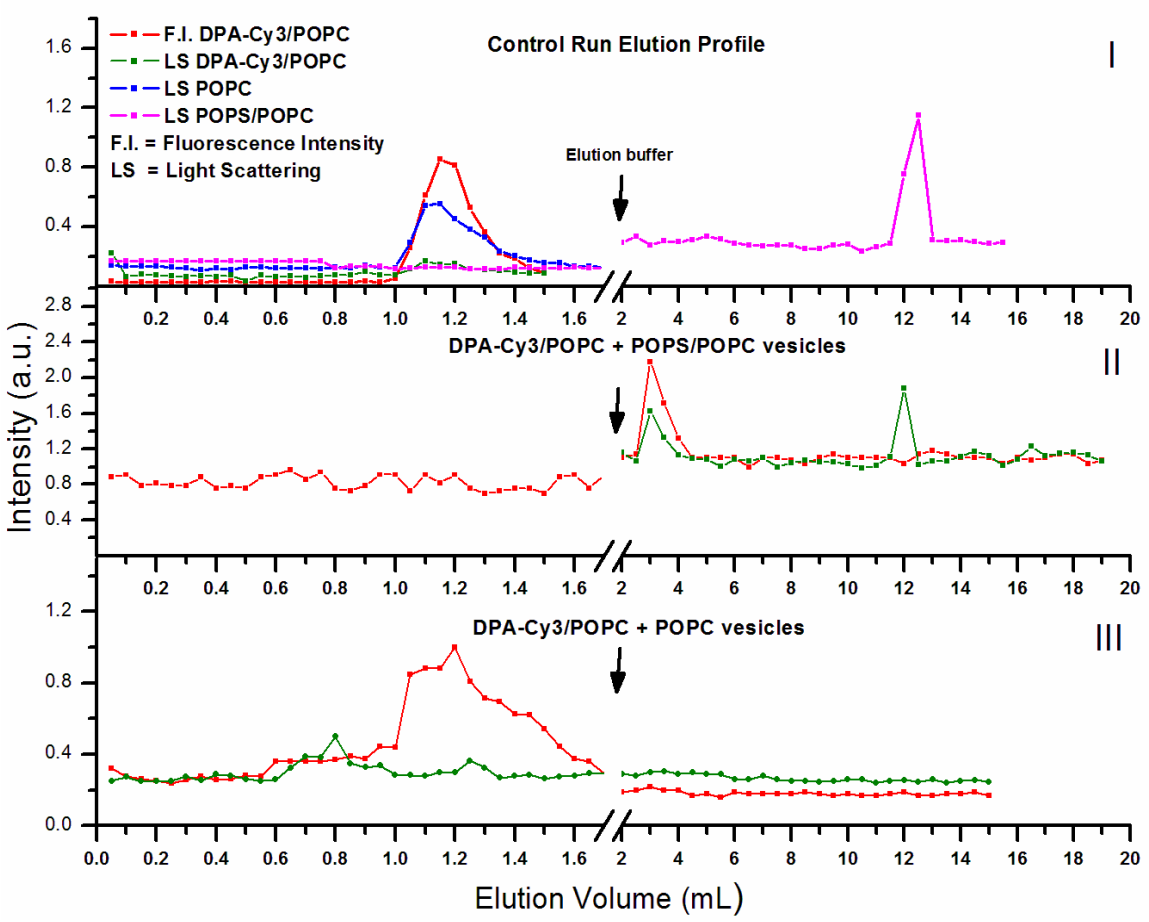

Figure 9: Anion exchange chromatography showing affinity of DPA-Cy3[22,22]/POPC liposomes to PS containing liposomes

DPA-Cy3/POPC liposomes incubated with POPS/POPC liposomes and POPC liposomes for 3 hours at room temperature. (I) DPA-Cy3/POPC, POPC, and POPS/POPC liposomes eluted separately. (II) Mixture of DPA-Cy3/POPC liposomes and POPS/POPC liposomes after incubation (3h). (III) Mixture of DPA-Cy3/POPC and POPC liposomes after incubation (3h). Sample was collected using the "equilibrating buffer" up to 2mL. Arrow indicates the time when the "elution buffer" was used (see Materials and Methods for details).

1.3 Binding of DPA-Cy3[22,22]/POPC Liposome to MCF-7 Cells

1.3.1Quantifying PS on the membrane surface of MCF-7 and MCF-12A cells

Tumor cells and blood vessels bear different levels of PS and other anionic phospholipids exposed on the cell membrane bilayer (Lima, Chammas, Monteiro, Moreira, & Barcinski, 2009; Segawa, et al., 2011; Stafford & Thorpe, 2011). Previous studies demonstrate that the outer membrane of MCF-7, human derived breast cancer cells, have higher percentage of PS content than healthy or non-cancerous cells, and that MCF-7 anti-cancer drug resistant cells have an even higher level of PS exposure (Todor, Lukyanova, & Chekhun, 2012; Woehlecke et al., 2003). Before testing DPA-Cy3[22,22]/POPC liposome biding to cells, I examined the level of PS content outside of MCF-7 cancer cells and compared it to non-cancer breast cells MCF-12A using cell live/dead staining and flow cytometry. MCF-7 and MCF-12A were analyzed by staining with annexin V-FITC and 7AAD to observe PS exposure and cell death, respectively (Figure 10). In physiological conditions, annexin V-FITC binds to PS with high affinity in a calcium-dependent manner (Riedl et al., 2011). 7AAD, a fluorescent dye, was used to stain apoptotic and necrotic cells. Intracellular 7AAD signal was detected after 7AAD entered cells as a result of loss of plasma membrane integrity during cell death.

The plots in Figure 10 A&B show annexin V-FITC positive (+) or PS exposed cells in live and dead cell populations indicated by cells that are either negative or positive for 7AAD staining, respectively. The level of PS exposure was quantified using cells expressing positivity for annexin V-FITC (annexin V+). The density plots show MCF-7 cells have a higher percent (8.75) of annexin V+ 7AAD- cells (Figure 10B Q1),

live cells with PS exposure, than that of non-cancer (1.75) cells MCF-12A (Figure 10A, Q1). Overall, MCF-7 cancer cells bear 3-5 times higher PS than non-cancerous cell line MCF-12A (Figure 10C). Also, similar to our experimental findings, PS content in MCF-7 has been previously determined to be 6-10% in the literature (Todor et al., 2012). The difference in PS exposure between cancer and non-cancer cells is potentially a way to target PS on cancer cells for drug delivery. DPA containing liposomes, (DPA-Cy3[22,22]/POPC liposomes) may have the ability to bind PS and enter highly PS exposed cancer cells allowing drugs to be selectively targeted to diseased tissues.

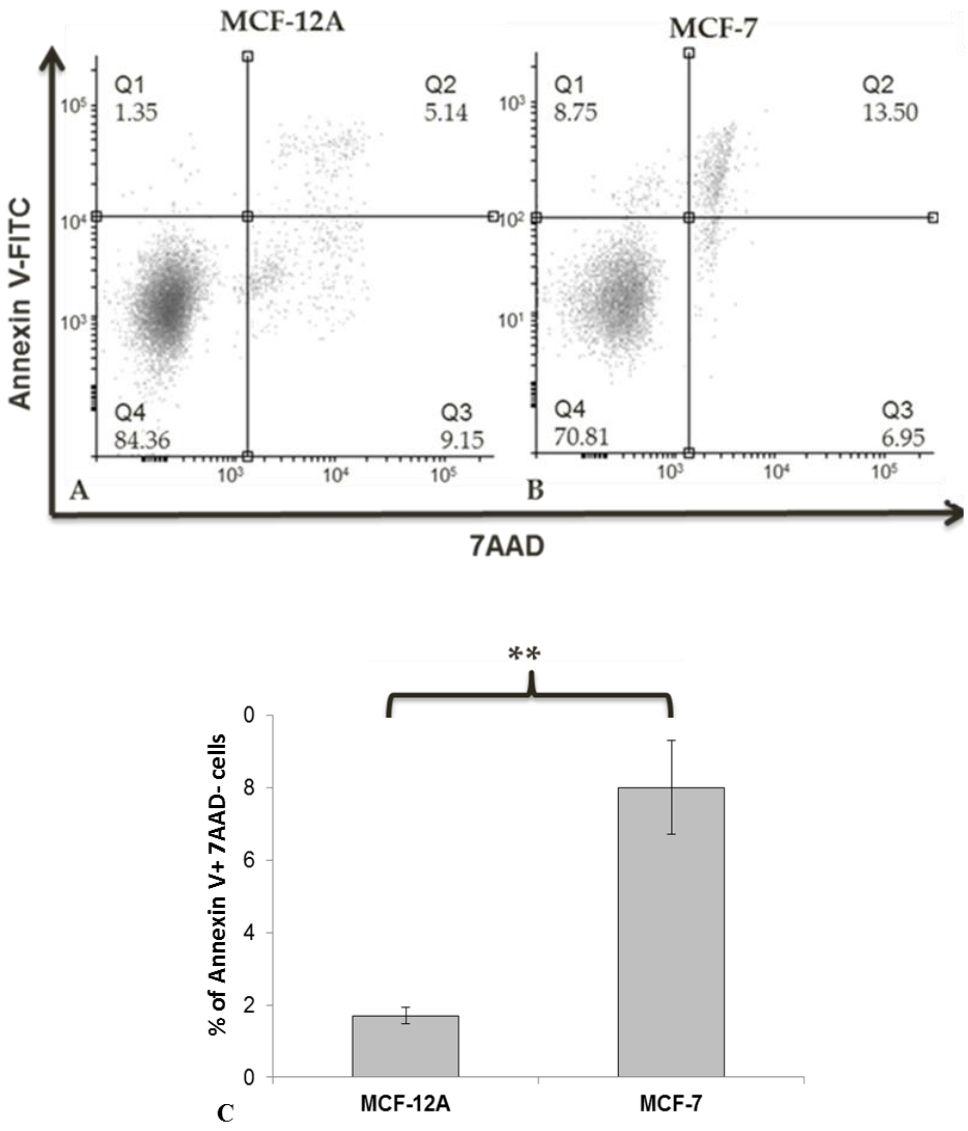

Figure 10: Flow cytometry analysis of MCF-7 and MCF12A cells stained with annexin V-FITC and 7AAD. **p<0.05

A & B are density dot plots of fluorescence intensities of cells stained with annexin V–FITC (y-axis) and 7AAD (x-axis). Annexin V-FITC binds pre-apoptotic and late apoptotic cells with PS exposure, and 7AAD stains necrotic and dead cells. The Number in each quadrant indicates the percentage of cells in that quadrant: Q1: annexin V + 7AAD – (pre-apoptotic); Q2: annexin V + 7AAD+ (dead); Q3: annexin V- 7AAD+ (necrotic); and Q4: annexin V- 7AAD- (alive). PS exposed live cells are located in Q1. (C) Percent of total annexin V + live cells (or PS exposed live cells) in MCF-12 and MCF-7 cell lines. Standard deviations are from 4 independent measurements and the data has a **p value of < 0.05.

1.3.2 Quantifying binding of DPA-Cy3[22,22]/POPC liposomes to MCF-7 cells using flow cytometry

To determine binding of DPA-Cy3[22,22]/POPC liposome to the cell surface, MCF-7 cells were treated with DPA-Cy3[22,22]/POPC liposomes of varying molar content of DPA-Cy3[22,22] (4.8, 2, or 1 mol%) in POPC liposomes. Subsequently, cells were stained with annexin V-FITC and 7AAD to differentiate between live and dead cells. The presence of DPA-Cy3[22,22]/POPC liposomes on the cell surface was detected using flow cytometry by measuring the Cy3 fluorescence from the treated cells. Fluorescence intensities of annexin V-FITC and 7AAD were also recorded. Cy3 fluorescence given by 7AAD negative cell population was analyzed to determine binding or uptake of DPA-Cy3[22,22]/POPC liposomes by live cells.

Figure 11A presents histograms of relative number of cells (cell count) with Cy3 fluorescence (x-axis) after treatment with 20 μM of 4.8 or 2 mol% DPA-Cy3[22,22]/POPC and 4.8 mol% Comp1/POPC liposomes. In Figure 11A, the Cy3+ gate (blue) was defined as the area containing number of cells with Cy3 fluorescence (red part of the peak). The untreated or unstained cells show auto-fluorescence (peak closer to 0) and are Cy3 negative. MCF-7 cells treated with DPA-Cy3[22,22]/POPC liposome display higher Cy3 fluorescence indicated by the peak shifting to the right, into the gate marked Cy3+. The peak shift occurs as a result of liposome binding to cells. Cells treated with a higher mole% DPA-Cy3[22,22]/POPC (4.8 mol%) liposomes experience a greater peak shift or Cy3 positivity (red) because increasing DPA-Cy3[22,22] content in liposomes increases liposome binding to cells. Cells treated with Compound 1 in POPC liposomes (Comp1/POPC) exhibit less significant shift in the peak, or display fewer Cy3+ cell, due

to the lack of the DPA moiety. The percentage of Cy3+ cells was determined using the number of cells in the Cy3+ gate, and it is expressed quantitatively in Figure 11B.

Figure 11B shows the percentage of Cy3+ MCF-7 cells after treatment with 0-20 μM of 4.8, 2, or 1 mol% DPA-Cy3[22,22]/POPC liposomes. Generally, cells treated with DPA-Cy3[22,22]/POPC liposomes have a higher % of Cy3+ cells compared to untreated and 4.8 mol% Comp1/POPC treated cells. In Figure 11A, the first thing to note is that without the DPA moiety in liposomes (Comp1/POPC), Cy3 fluorescence is significantly low. Also, treatment with 20μM of 1 mol% DPA-Cy3[22,22]/POPC liposomes results in very little Cy3+ (~10%) cells. When MCF-7 cells were treated with 20μM of 4.8 mol% and 2 mol% DPA-Cy3[22,22]/POPC liposomes, the percentage Cy3+ cells increase 10 fold (Figure 11B). This set of data illustrates that DPA is essential for liposome binding to cells, and 1 mol%DPA-Cy3[22,22]/POPC liposome formulation will not be an effective for targeted delivery since it resulted in very little binding even at higher concentrations due to low DPA-Cy3[22,22] content in liposomes. Higher DPA-Cy3[22,22] mol% (2 mol% and 4.8 mol%) yield more DPA-Cy3[22,22]/POPC fluorescence on the cell surface as a result of higher affinity to PS. To verify this finding, next, cell binding was observed using a confocal microscope.

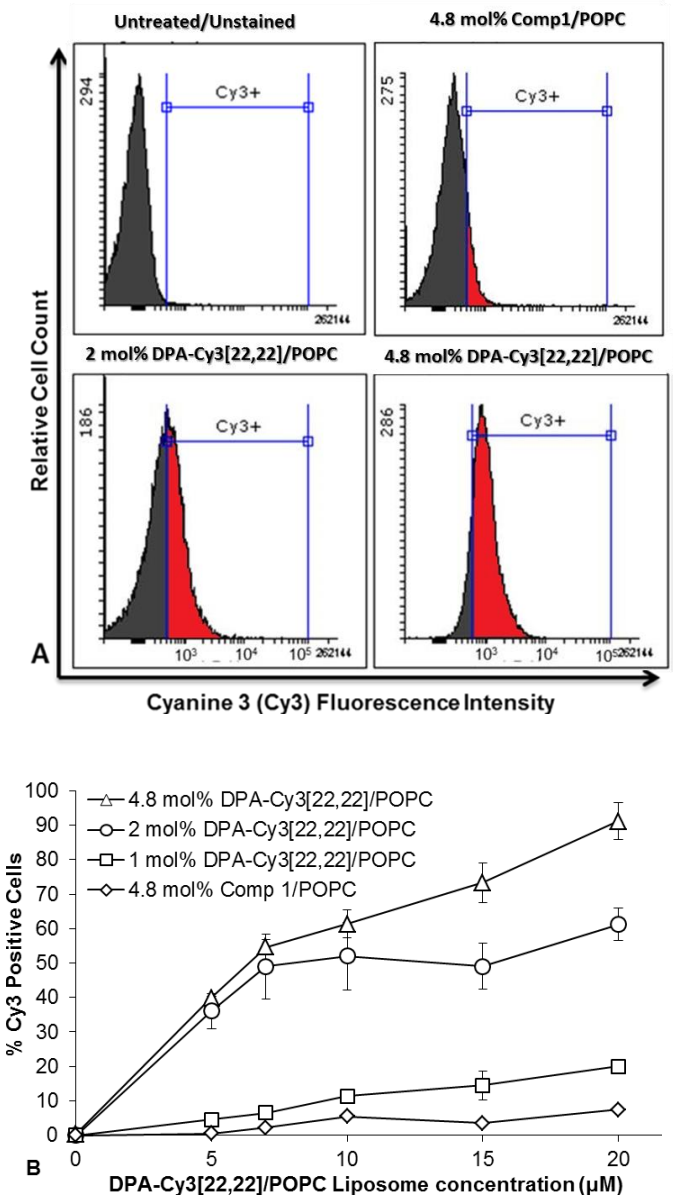

Figure 11: MCF-7 and MCF-12A cells with cyanine 3 fluorescence enhancement on surface of cells.

(A) Histogram of cells treated with Comp 1/POPC and DPA-Cy3[22,22]/POPC liposomes with 4.8 mol% and 2 mol% DPA-Cy3[22,22]. [POPC] = 20 μM. Y-axis shows relative cell counts and the x-axis is Cy3 fluorescence. Untreated cells with auto-fluorescence were used as a control to set Cy3+ gates (blue). More Cy3 positive cells (red, in Cy3+ gate) cells were detected when treated with DPA-Cy3[22,22]/POPC liposomes. (B) Percentage of total live cells that are Cy3 positive (determined from number of cells in the Cy3+ gate) after cells were treated with 0-20 μM DPA-Cy3[22,22]/POPC liposomes (1, 2, and 4.8 mol%) and Comp 1/POPC (4.8 mol%).

1.3.3 Visualizing binding and uptake of DPA-Cy3[22,22]/POPC liposome by MCF-7 cells

MCF-7 cells were treated with DPA-Cy3[22,22]/POPC liposomes and observed using a confocal microscope to assess the effect of DPA-Cy3[22,22] on liposome binding and uptake by cells. As a control, cells were also treated with liposomes containing Compound 1 (Comp 1), Compound 2 (Comp 2) or Compound 3 (Comp 3). These compounds lack the DPA moiety, but they retain Cy3 and the $C_{22}H_{45}$ hydrocarbon chains. Their structural differences are shown in Figure 12B. Cells were also stained with nuclear and cytosolic dyes. In Figure 12, the first column (channel 1) shows the cell nucleus labeled with the blue nuclear dye Hoechet 33342. The second panel (channel 2) shows the cell body with green fluorescence from calcein. The third panel (channel 3), shows fluorescence intensity from cyanine 3 present in Comp 1, 2, 3, and DPA-Cy3[22,22] in POPC liposomes. And, the last column is the merged images of all channels. "Untreated cells" were not treated with liposomes and therefore Cy3 fluorescence was not detected from these cells. As seen in Figure 12, cells treated with DPA containing liposome DPA-Cy3[22,22]/POPC show higher Cy3 fluorescence intensity accumulated inside cells compared to DPA lacking liposomes such as Comp 1/POPC, 2/POPC, and 3/POPC. Cells treated with DPA-Cy3[22,22]/POPC and Comp3/POPC liposomes display more liposomes inside cells compared to cells that are treated with liposomes containing Comp 1 and 2. Typically, liposomes without target molecules can be internalized by cells, but, presence of target molecule in liposomes can greatly enhance cellular uptake (Mossalam, Dixon, & Lim, 2010). There are more liposomes present inside the cells when liposomes comprise of the DPA moiety, and

therefore confirm the findings of flow cytometry data that DPA has affinity for PS and is required for cell binding. Furthermore, the images illustrate that the presence of DPA plays a role in the internalization of liposomes by MCF-7 cells.

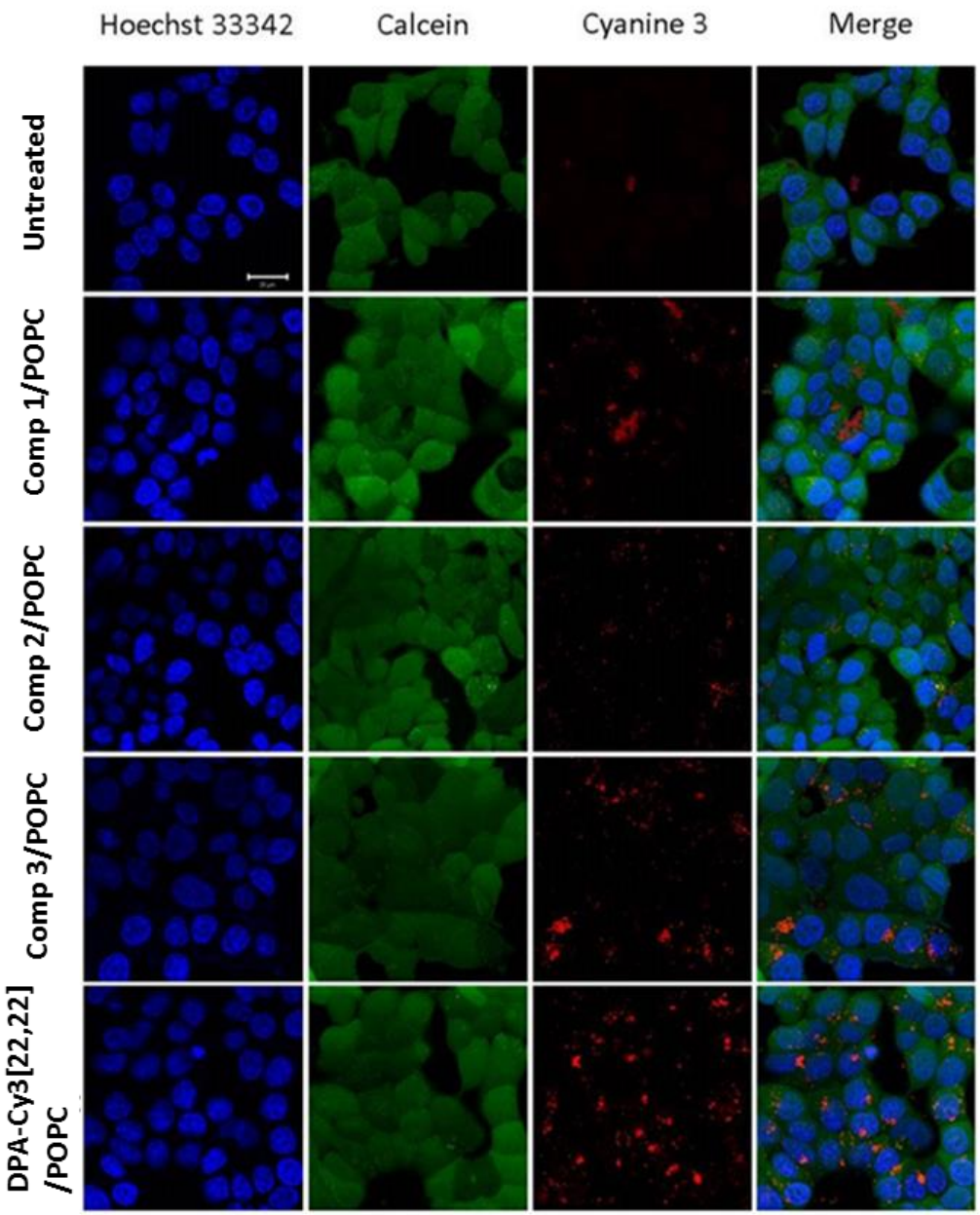

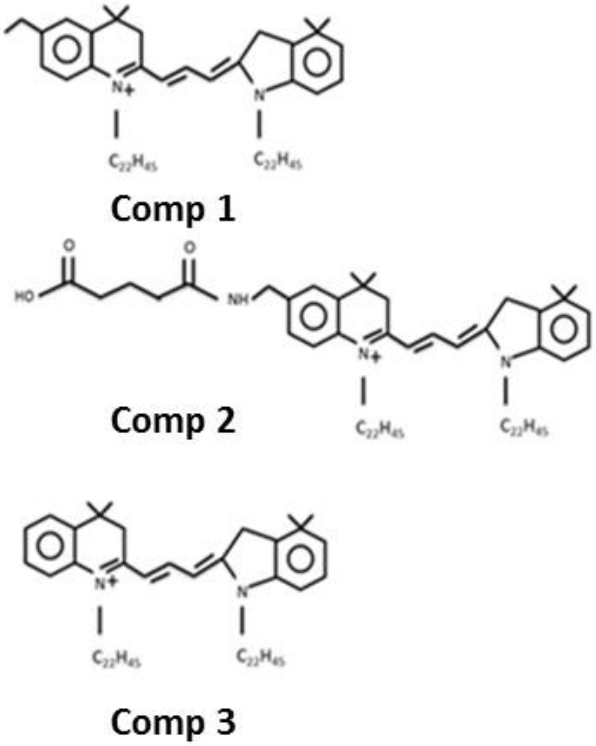

Figure 12: (A) Confocal microscopy images of MCF-7 cells treated with liposomes composed of DPA-Cy3[22,22], Comp 1, Comp 2 or Comp 3 and POPC for 4 hours. Cells were stained with calcein (cytoplasm), Hoechst 33342 (nucleus) and their fluorescence was observed along with Cy3. (B) Structure of Comp 1, Comp 2, and Comp 3.

Cells treated with liposomes have different levels of Cy3 fluorescence observed inside the cells. Cells treated with Comp 1/POPC, Comp 2/POPC, and Comp 3/POPC have the least Cy3 fluorescence present inside the cells. Cells treated with DPA-Cy3[22,22]/POPC displays the most Cy3 fluorescence inside cells.

1.4 Binding of DPA-Cy3[22,22]/POPC Liposomes to Cancer Versus Non-Cancer Cells

Using a flow cytometer, the Cy3 fluorescence on the cell surface of MCF-7 cancer cells and MCF-12A non-cancer cells was measured after treatment with 2 mol% or 4.8 mol% DPA-Cy3[22,22]/POPC liposomes. In Figure 13, DPA-Cy3[22,22]/POPC liposome binding to cells is presented in a histogram (A-D) and a binding curve . Figure 13 A-D histogram shows red peaks representing MCF-7 (Figure 13 A&C) and MCF-12A cells (Figure 13 B&D) treated with 20μM of 2 mol% or 4.8 mol% DPA-Cy3[22,22]/POPC liposomes. Each histogram also shows black peaks, representing untreated cells. As a result of liposome binding on the cell surface, red peaks (treated cells) shift to the right of black peaks (untreated cells) which suggests that Cy3 fluorescence is present in the treated cell population. Using this data, the percentage of Cy3+ cell is determined.

Liposome binding to cell is also described in Figure 13E-F in which the percentage of Cy3+ cells is quantitatively presented and compared between MCF-7 and MCF-12A treated with 0-20 μM 4.8 mol% or 2 mol% DPA-Cy3[22,22]/POPC liposomes. Figure 13E-F shows that when the MCF-7 and MCF-12A cells were treated with 0-20 μM of DPA-Cy3[22,22]/POPC liposomes (4.8 mol% and 2 mol%), a dose dependent increase in Cy3 fluorescence (% Cy3+, y axis) occurs. However, there is a difference in the percentage of Cy3+ cells between MCF-7 and MCF-12A cells after treatment with DPA-Cy3[22,22]/POPC liposomes. At each DPA-Cy3[22,22]/POPC liposome (4.8 mol% and 2 mol%) concentration, the percentage of Cy3+ cell is higher in

MCF-7 than in MCF-12A cells. This difference could be due to the MCF-7 cells bearing more PS than the MCF-12A cells.

Additionally, after treatment with 2 mol% DPA-Cy3[22,22]/POPC liposomes, the percentage of Cy3+ cells is higher in the MCF-7 cell population than the MCF-12A cell population at all liposome concentrations. However, when cells were treated with 4.8 mol% DPA-Cy3[22,22]/POPC, the difference in the percentage of Cy3+ cells is more apparent only at lower concentrations (5-10 μM) (Figure 13F). Surprisingly, when cells were treated with 15-20 μM of 4.8 mol% DPA-Cy3[22,22]/POPC liposomes, both MCF-7 and MCF-12A cells display high percentage of Cy3+ cells. Unexpectedly, non-cancer cells MCF-12A treated with 15-20 μM of 4.8 mol% DPA-Cy3[22,22]/POPC liposomes displayed 60-70 % Cy3+ cells. Since there is an evidence that MCF-12A cells have very low PS exposure, at higher concnetrations of 4.8 mol% DPA-Cy3[22,22]/POPC (15-20 μM), liposomes bind to MCF-12A cells, non-specifically. Another possibility is that higher concenetration of 4.8 mol% DPA-Cy3[22,22]/POPC could be inducing either membrane preturbation or endocytosis. Threfore, 0-20 μM of 2 mol% DPA-Cy3/POPC liposomes or 0-10 μM of 4.8 mol% DPA-Cy3/POPC liposomes may be better for targeting cancer cells over non-cancer cells.

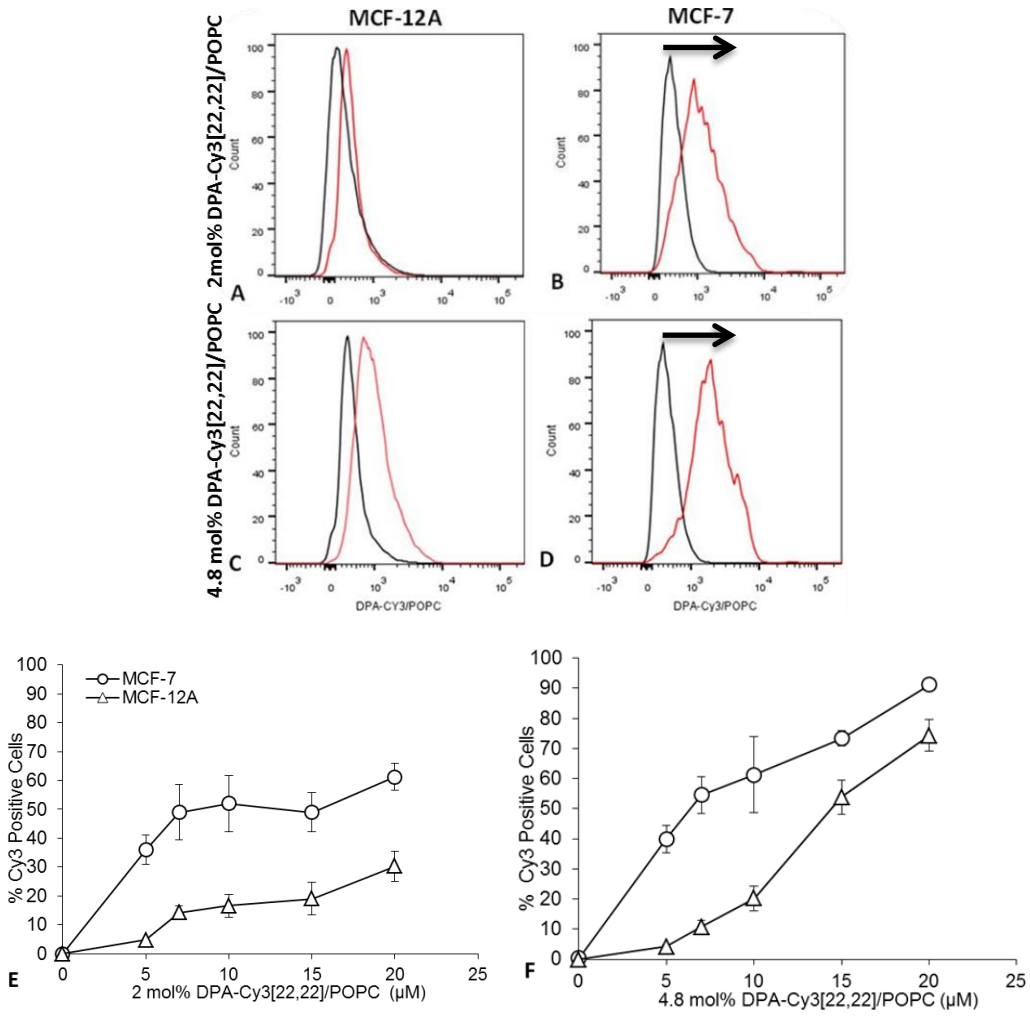

Figure 13: (A-D) histogram of cyanine 3 fluorescence intensity on surface of MCF-7 and MCF-12A cells treated with 4.8 mol% and 2 mol% DPA-Cy3[22,22]/POPC at [POPC] = 20 μM. (E-F) The percentage Cy3+ cells after treatment with 2 mol% and 4.8 mol% DPA-Cy3[22,22]/POPC at [POPC] = 0-20μM

Cells treated with DPA-Cy3[22,22]/POPC liposomes (2 and 4.8 mol% DPA-Cy3[22,22]) for 15 min then stained with annexin V–FITC and 7AAD. The y-axis shows the cell count and the x-axis is the Cy3 fluorescence intensity. Untreated cells (black peaks) has auto fluorescence, and treated cells display Cy3 fluorescence (red peaks). Untreated cells are used to set the thresh-hold above the auto fluorescent peak (above 10^3) to quantify the percentage of Cy3+ cells in treated sample. (A) MCF-12A cells treated with 2 mol% DPA-Cy3[22,22]/POPC. (B) MCF-7 cell treated with 2 mol% DPA-Cy3[22,22]/POPC liposomes. (C) MCF-12A cells treated with 4.8 mol% DPA-Cy3[22,22]/POPC (D) MCF-7 cells treated with 4.8 mol% DPA-Cy3[22,22]/POPC. (E-F) The percentage of Cy3+

cells (from total live cells) after MCF-12A and MCF-7 cells were treated with 0-20 μM concentration of 2 mol% (E) and 4.8 mol% (F) DPA-Cy3[22,22]/POPC liposomes.

1.5 Studies Using PS Inducer Camptothecin to Increase PS Exposure in MCF-7 Cells

1.5.1 PS exposure on MCF-7 cells after treatment with camptothecin determined using flow cytometry

In order to further determine whether the binding of DPA-Cy3[22,22]/POPC liposome to cells is PS dependent, I used camptothecin to induce pre-apoptotic PS exposure in MCF-7 cells. Camptothecin is a drug that can bind DNA and inhibit the enzyme topoisomerase resulting in DNA damage and apoptosis (Liu et al., 2000). Treatment with camptothecin shows higher PS exposure and more cell death (Figure 14-1). The density plot in Figure 14-1 shows that MCF-7 cells treated with 10 μM camptothecin for 2 hours (Figure 14-1B) have much higher percentage of pre-apoptotic cells (annexin V + 7AAD- : Q1) in comparison to untreated cells in Figure 14-1A. Cells treated with camptothecin experience more PS externalization, thus, camptothecin-treated cells bind more annexin V-FITC and have higher FITC fluorescence with longer treatment. Untreated MCF-7 cells have approximately ~7% of PS exposed cells (annexin V+ 7AAD-) as expected from our previous experiment (Figure 10B), while camptothecin treated cells have more than 2 times higher PS exposure (Figure 14-1).

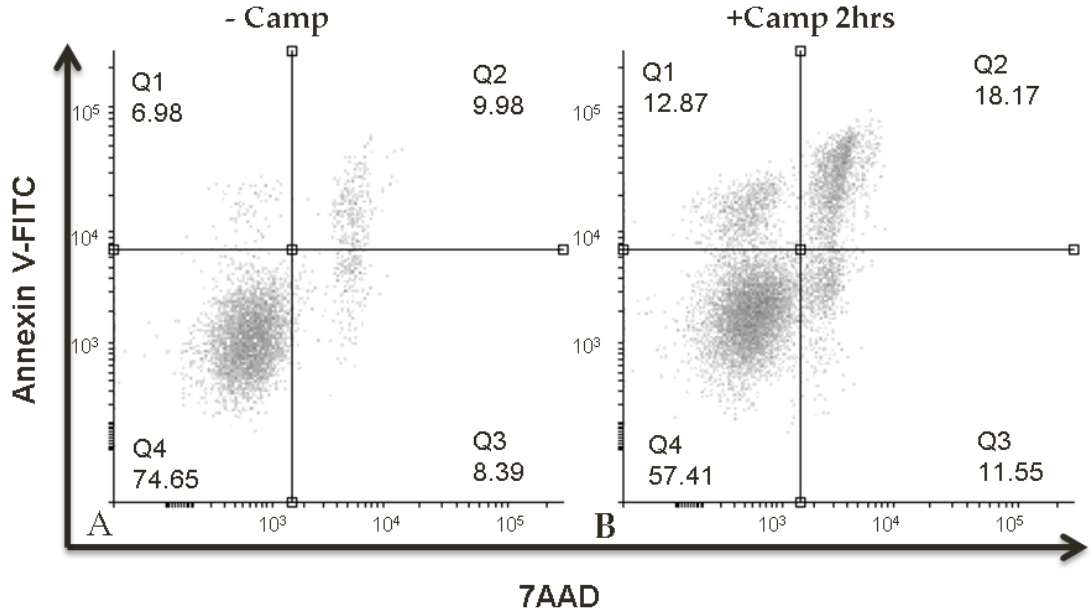

Figure 14-1: Density plots of MCF-7 cells treated with apoptotic inducer camptothecin and stained with annexin V and 7AAD

Annexin V-FITC and 7AAD stained MCF-7 cells (A) untreated and (B) treated with 10μM camptothecin for 2 hrs. A & B show a dot plots of fluorescent intensity of cells stained with annexin V–FITC (y-axis) and 7AAD (x-axis). Annexin V binds pre-apoptotic and late apoptotic cells with PS exposure and 7AAD stains necrotic and dead cells. Numbers in each quadrant indicates % of cells in that quadrant: Q1: annexin V+ 7AAD– (pre-apoptotic), Q2: annexin V+ 7AAD+ (dead), Q3: annexin V- 7AAD+ (necrotic), Q4: annexin V- 7AAD- (alive)

1.5.2 DPA-Cy3[22,22]/POPC liposome binding to camptothecin treated cells observed using confocal microscope

To investigate the effects of increasing PS exposure on DPA-Cy3[22,22]/POPC liposome binding to the cell membrane, first, higher PS exposure was induced in MCF-7 cells using camptothecin. Then, cells were treated with 10 μM of 4.8 mol% DPA-Cy3[22,22]/POPC liposomes. As a control, cells were stained with annexin V-FITC, which can also bind PS on the cell surface. With a confocal microscope, MCF-7 cells were detected using Cy3 and FITC fluorescence to analyze DPA-Cy3[22,22]/POPC liposome and annexin V-FITC binding, respectively. Visually, the Cy3 fluorescence is sparsely distributed around the cell membrane of camptothecin (-) cells (Figure 14-2a), but, for camptothecin (+) cells, the Cy3 fluorescence (red) was considerably higher and more evenly distributed all around the cell membrane of most cells (Figure 14-2b-d). Quantitatively, there is a 2 times increase in the Cy3 fluorescence from cells when camptothecin was used for 2-6 hours before treatment with DPA-Cy3[22,22]/POPC liposomes (Figure 14-2b-d), and a small increase in annexin V-FITC fluorescence is also detected on the cell surface. Compared to untreated cells, camptothecin-treated cells have higher annexin V-FITC (green) and 3 times greater Cy3 fluorescence which led me to believe that camptothecin-induced PS exposure resulted in higher annexin V and DPA-Cy3[22,22]/POPC liposome binding on the cell surface.

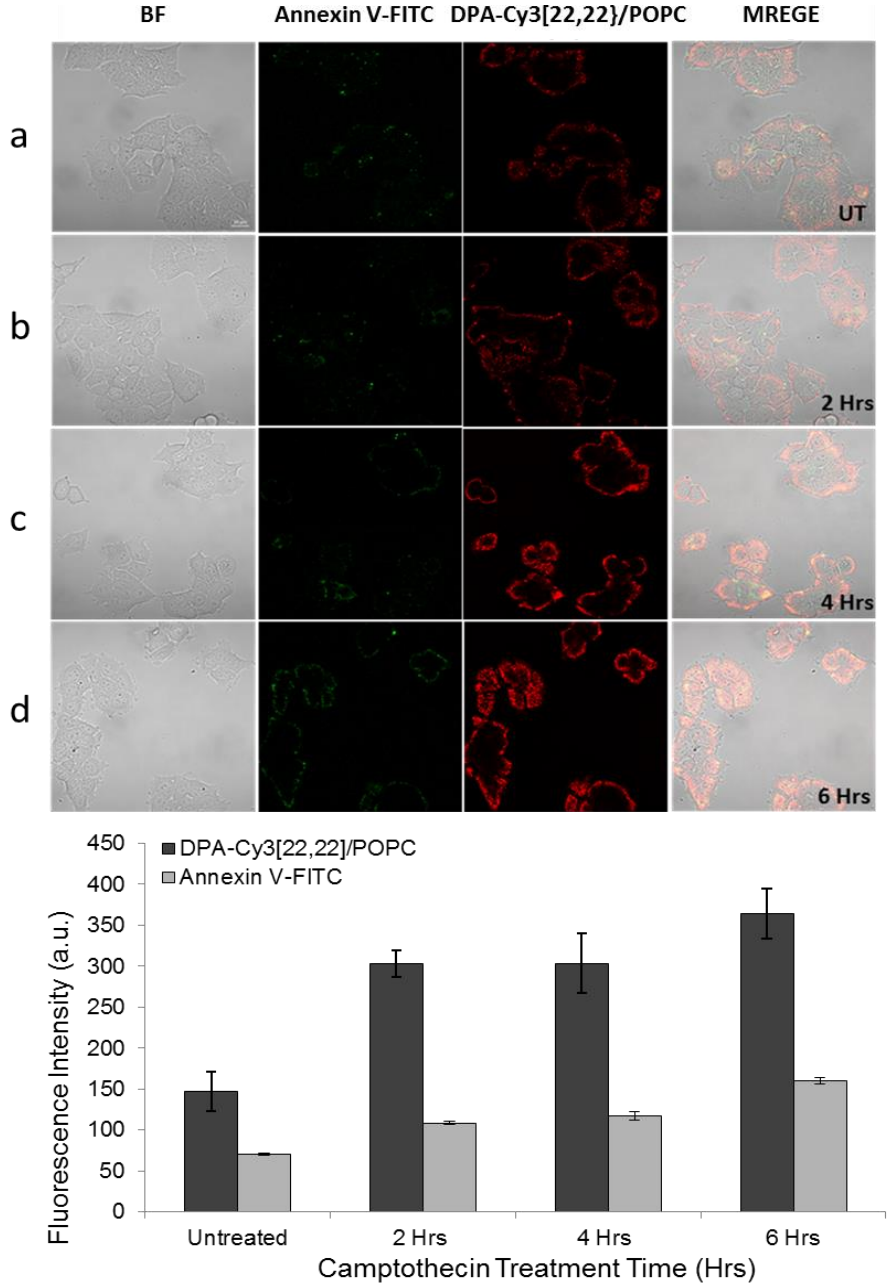

Figure 14-2: Confocal images of MCF-7 cells stained with annexin V-FITC and DPA-Cy3[22,22]/POPC liposomes.

Cells were first treated with 10 µM camptothecin for 0, 2, 4, 6 hrs then treated with 10 µM of 4.8 mol% DPA-Cy3[22,22]/POPC and annexin V for 15 min. (Bottom) Confocal image of MCF-7 cells with annexin V (green) and DPA-Cy3[22,22]/POPC (red). (Top) Quantification of total fluorescence intensity of FITC and Cy3 on MCF-7 cells (~20 cells/image). Standard deviations were determined by quantifying cells from 3 images using Zen software (Zeiss).

1.5.3 Quantifying DPA-Cy3[22,22]/POPC liposome binding to total live MCF-7 cells after treatment with camptothecin

Since DPA-Cy3[22,22] is anticipated to bind cells in a PS dependent manner, next, I test whether camptothecin-induced increase in cells PS exposure can increase DPA-Cy3[22,22]/POPC liposome binding to cells. To verify and quantify DPA-Cy3[22,22]/POPC liposome binding to cells after treatment with camptothecin, I analyzed Cy3 fluorescence on the cell surface using flow cytometry. After camptothecin treated (+) and untreated (-) MCF-7 cells were subsequently treated with DPA-Cy3[22,22]/POPC liposomes, both camptothecin (+) and (-) cells expressed Cy3 fluorescence, but higher Cy3 fluorescence was detected for camptothecin (+) cells. Camptothecin (+) MCF-7 cells treated with both 4.8 mol% and 2 mol% DPA-Cy3[22,22]/POPC liposomes yielded higher Cy3 fluorescence than camptothecin (-) cells that had been treated with the same liposomes (Figure 15A & B). For cells treated with 0-20μM of 2 mol% DPA-Cy3[22,22]/POPC, the percent Cy3 + cells between camptothecin treated and untreated cells is much greater than 4.8 mol% DPA-Cy3[22,22]/POPC treatment (Figure 15C&D). There was a clear difference in the percent Cy3+ cells between camptothecin-treated and camptothecin-untreated cells when cells were treated with 2-10 μM 4.8 mol% DPA-Cy3[22,22]/POPC liposomes. But, when cells were treated with 15-20 μM of 4.8 mol% DPA-Cy3[22,22]/POPC liposome, the difference in percent Cy3+ cells between capmtothecin (+) and (-) cells is reduced (Figure 15D). As predicted, increasing the PS exposure increased DPA-Cy3[22,22]/POPC liposomes binding to cells when 2 mol% DPA-Cy3[22,22]/POPC liposomes are used. However, inducing PS exposure did not significantly affect binding of 4.8 mol% DPA-Cy3[22,22]/POPC

liposomes to cells. This supports our theory that treatment with higher concentration of 4.8 mol% DPA-Cy3[22,22]/POPC may either increase non-specific binding or induce membrane perturbation resulting in higher cell binding at low PS level.

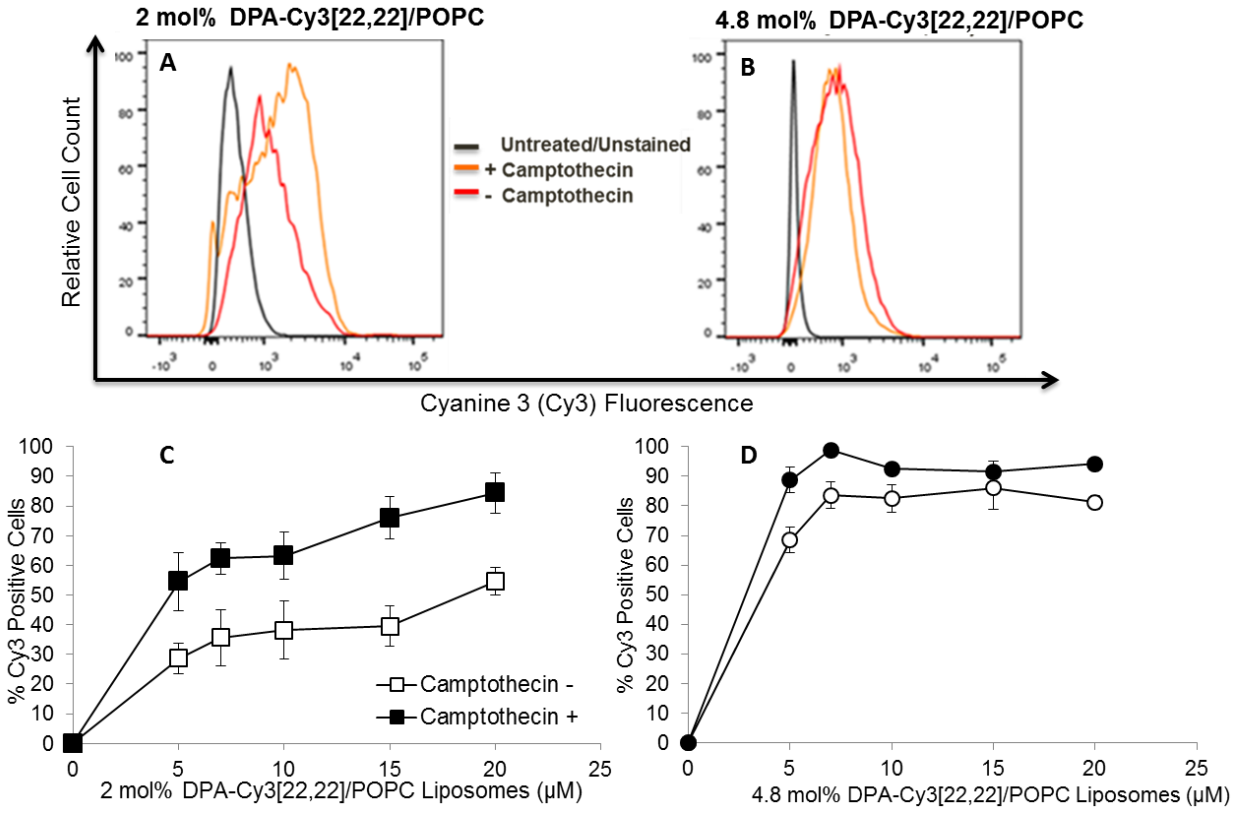

Figure 15: The percentage of MCF-7 cells with Cy3 fluorescence after being treated with camptothecin for 2 hrs followed by treatment with DPA-Cy3[22,22]/POPC liposomes.

A and B show histograms with the number of total live MCF-7 cells (cell count on y-axis) and cells' Cy3 fluorescence intensity (x-axis) after cells were either untreated (red) or with treated with camptothecin (orange) for 2 hours, subsequently, treated with the DPA-Cy3[22,22]/POPC liposomes (either 2 mol% (A) or 4.8 mol% (B)).Black peak shows cells without camptothecin and DPA-Cy3[22,22]/POPC liposomes treatment. C and D show the percentage of Cy3+MCF-7 cells after treatment with 2 mol% (C) and 4.8 mol% (D) DPA-Cy3[22,22]/POPC liposomes.

1.5.4 Treatment with camptothecin increase DPA-Cy3[22,22]/POPC liposome binding to annexin V+ (PS exposed) cells

Thus far, DPA-Cy3[22,22]/POPC liposome binding to cell was quantified using flow cytometry data from total live cells. In this section, DPA-Cy3[22,22]/POPC liposome binding to MCF-7 cells was analyzed in annexin V+ and annexin V– cell populations to determine whether DPA-Cy3[22,22]/POPC liposomes favorably bind to PS expressed live cells over non-PS expressed cells when PS expression is enhanced with camptothecin. Cells treated with 2-20 μM of 2 mol% and 4.8 mol% DPA-Cy3[22,22]/POPC liposomes generally show higher Cy3 positivity on the cell surface in annexin V+ cell population (Figure 16 A-D). When cells were treated with 2 mol% DPA-Cy3[22,22]/POPC liposomes at lipid concentration of 2-20 μM, more liposomes bind annexin V+ cells opposed to annexin V- cells (Figure 16B). Additionally, camptothecin (+) cells treated with 2 mol% DPA-Cy3[22,22]/POPC liposomes show significantly higher liposome binding to annexin V+ cells (Figure 16 A & B). Since camptothecin treatment increases annexin V+ or PS exposed cells, DPA-Cy3[22,22]/POPC liposomes preferably bind to cells with more PS exposure. However, cells treated with 4.8 mol% DPA-Cy3[22,22]/POPC liposomes show little difference in % Cy3+ cells between the annexin V+ and annexin V- cell populations even after treatment with camptothecin.

The most interesting finding is that camptothecin (+) cells treated with 2 mol% DPA-Cy3[22,22]/POPC liposomes display an increase in binding to annexin V+ cells and a decrease in binding to annexin V- cells (Figure 16 A&B) which can be interpreted in either one of two ways. First, it can be assumed that DPA-Cy3[22,22]/POPC liposomes bind strongly to PS exposed cells and weakly to non-PS exposed cells. When

camptothecin induce more PS exposure, 2 mol% DPA-Cy3[22,22]/POPC liposomes bind more PS exposed cells over non-PS exposed cells as a result of strong affinity to PS. Second, the interaction of DPA-Cy3[22,22]/POPC liposomes with non-PS expressing cells induce PS exposure which is the reason for DPA-Cy3[22,22]/POPC liposome binding to non-PS exposed cell population. Upon availability of more PS expressing cells (camptothecin +), 2 mol% DPA-Cy3[22,22]/POPC liposomes are drawn away from non-PS expressing cells. Once again, 4.8 mol% DPA-Cy3[22,22]/POPC liposomes does not show the same outcome as 2 mol% DPA-Cy3[22,22]/POPC liposomes. The DPA-Cy3[22,22] content is higher in 4.8 mol% liposomes which could result in stronger interaction with non-PS exposed cells with or without camptothecin. Therefore, 2 mol% DPA-Cy3[22,22]/POPC liposomes have better specificity to PS than 4.8 mol% DPA-Cy3[22,22]/POPC liposomes especially when there are more PS- exposed cells available.

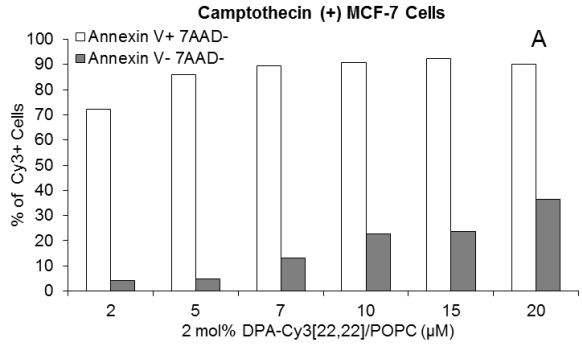
Camptothecin (+) MCF-7 Cells
A
Annexin V+ 7AAD-
Annexin V- 7AAD-
% of Cy3+ Cells
100
90
80
70
60
50
40
30
20
10
0
2
5
7
10
15
20
2 mol% DPA-Cy3[22,22]/POPC (μM)

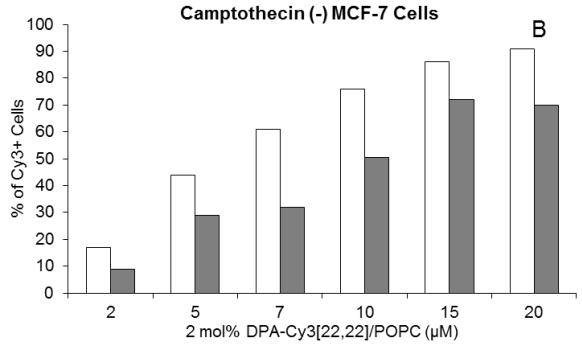
Camptothecin (-) MCF-7 Cells
B
% of Cy3+ Cells
100
90
80
70
60
50
40
30
20
10
0
2
5
7
10
15
20
2 mol% DPA-Cy3[22,22]/POPC (μM)

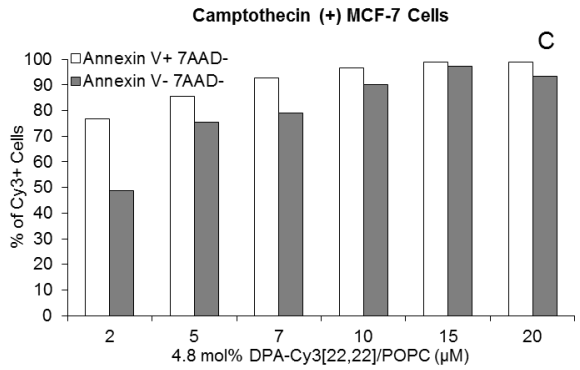
Camptothecin (+) MCF-7 Cells
C
Annexin V+ 7AAD-
Annexin V- 7AAD-
% of Cy3+ Cells
100
90
80
70
60
50
40
30
20
10
0
2
5
7
10
15
20
4.8 mol% DPA-Cy3[22,22]/POPC (μM)

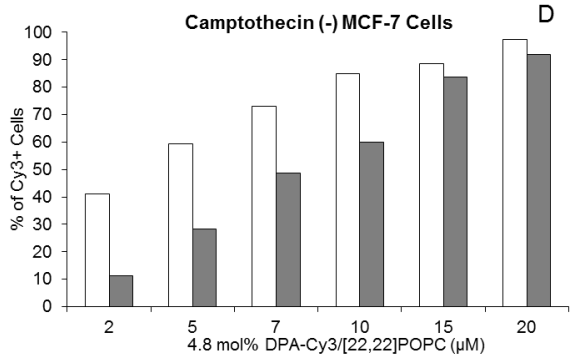
Camptothecin (-) MCF-7 Cells
D
% of Cy3+ Cells
100
90
80
70
60
50
40
30
20
10
0
2
5
7
10
15
20
4.8 mol% DPA-Cy3/[22,22]POPC (μM)

Figure 16: Annexin V+ (PS exposed) and Annexin V- cells expressing Cy3 fluorescence (% cells Cy3+) after treatment with camptothecin and treated with DPA-Cy3[22,22]/POPC liposomes (2 mol% and 4.8 mol% DPA-Cy3[22,22]).

(A) Camptothecin treated (+) and (B) untreated (-)MCF-7 cells incubated with 2 mol% DPA-Cy3 [22, 22]/POPC liposomes shows significant differences in the percentage of cells with Cy3 fluorescence between annexin V + (or PS exposed cells) and annexin V- (or non-PS exposed) cell populations. (C) Camptothecin (+) and (D) (-) MCF-7 cells were incubated with 4.8 mol% DPA-Cy3[22, 22] in POPC liposomes. The data were analyzed with same parameters for all samples. All cells analyzed were from one data set selectively 7AAD- or live cells.

1.6 Cellular Uptake and Intracellular Localization of DPA-Cy3[22,22]/POPC Liposomes

For a mechanistic understanding of DPA-Cy3[22,22]/POPC liposome- cell binding and uptake, cells were observed under a confocal microscope to monitor internalization and localization of DPA-Cy3[22,22]/POPC liposomes inside cells after treatment with DPA-Cy3[22,22]/POPC liposomes for 0-8 hours. To visualize cellular compartments, the nuclear and the cytosolic dye Hoechst 3334 and calcein were used respectively. Images were acquired every 30-60 minutes to detect the liposome fate inside the cells. In Figure 17, after treatment with DPA-Cy3[22,22]/POPC liposomes for 30 minutes, cells display Cy3 fluorescence on the membrane as a result of DPA-Cy3[22,22]/POPC liposomes binding to cell surface. After 90 min of incubation, DPA-Cy3[22,22]/POPC liposomes are detected inside the cells, specifically, in the cytoplasm. Since liposomes enter and accumulate in the cytosol rather than being dispersed on the cell membrane, it could be assumed that liposomes are internalized via endocytosis which

occurs as a result of electrostatic interaction between liposome and the cell membrane (Mossalam et al., 2010).

Between 4-6 hours of incubation of cells with liposomes resulted in nuclear localization of DPA-Cy3[22,22]/POPC liposomes indicated by co-localization of Cy3 fluorescence (red) and nuclear dye (blue) (Figure 17). Usually, After internalization by cells, liposomes are found in the endosomes unless they are targeted to different cellular compartments such as the endoplasmic reticulum (ER) and nucleus (Mossalam et al., 2010). Otherwise, liposomes are kept within endosome which becomes endo-lysosomes after fusion with lysosomes and results in degradation of the liposomes (Iwamoto, 2013). Since ER membrane comprise of negatively charged lipids (Mossalam et al., 2010), DPA-Cy3[22,22]/POPC liposomes can potentially bind to the ER. In Figure 17, we found evidence of liposomes inside the nucleus which indicates that DPA-Cy3[22,22]/POPC liposomes were able to escape lysosomal degradation and enter the nucleus.

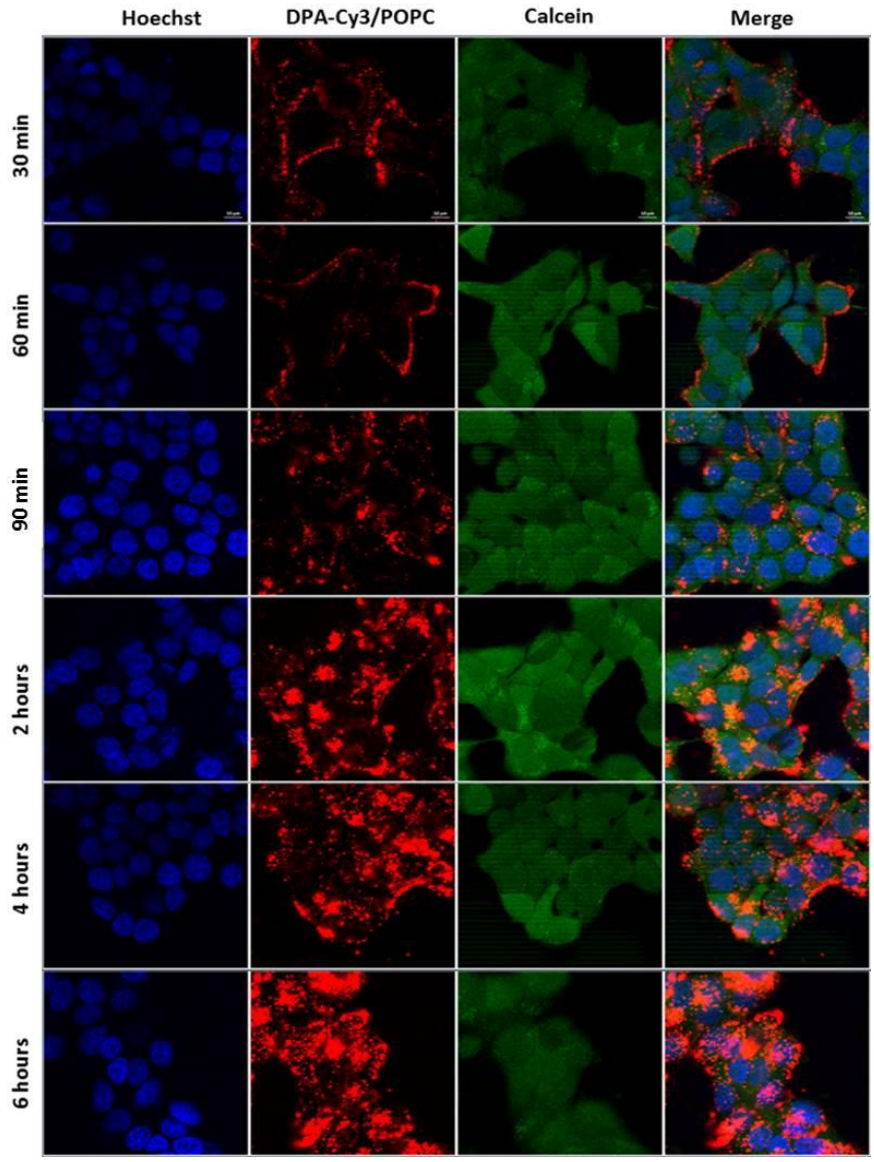

Figure 17: Confocal microscope (Zeiss LSM 510) image of MCF-7 cells treated with DPA-Cy3[22,22]/POPC liposome for 0-6 hours. DPA-Cy3[22,22]/POPC liposomes in the nucleus and cytosol were observed using Cy3 (red), Hoechst (blue), and calcein (green) fluorescence, respectively.

1.7 The Cytotoxic Effect of DPA-Cy3[22,22]/POPC Liposome on Cells

1.7.1 The effect of various DPA-Cy3[22,22] and POPC molar ratio and DPA-Cy3[22,22]/POPC liposome concentration on MCF-7 cell viability

To test the effects of DPA-Cy3[22,22]/POPC liposomes on cell survival, cells were treated for 0-48 hours with various liposome concentrations and with different mol% of DPA-Cy3[22,22] in POPC liposomes. The results are shown in Figure 18-1. Liposome concentration is expressed in terms of the concentration of total lipids in the sample. MCF-7 cells treated with 10-40μM 4.8 mol% DPA-Cy3[22,22]/POPC liposomes show the least cell death (<10%) after treatment with the lowest concentration (10μM) of 4.8 mol% DPA-Cy3[22,22]/POPC and POPC liposomes. The highest cell toxicity is observed at the longest treatment time (48 hours) with 20μM of 4.8 mol% DPA-Cy3[22,22]/POPC liposomes. (Figure 18-1A). The percentage viability between 20μM and 40μM 4.8 mol% DPA-Cy3[22,22]/POPC liposome treatment is similar at most time point, therefore, it can be assumed that the killing effect is similar at higher concentrations (20-40μM) of 4.8 mol% DPA-Cy3[22,22]/POPC.

In addition to testing dose-dependent toxicity, different mol% of DPA-Cy3[22,22] in POPC liposomes were also tested on cells, which show similar findings (Figure 18-1B). The lower mol% (2 mol%) had the lowest effect on cell viability. A more pronounced effect was seen after 48 hours of treatment with 10 μM of 17 mol% and 9.1 mol% DPA-Cy3[22,22]/POPC liposomes, which resulted in ~50% cell death (Figure 18-1B). There is a possibility that higher amount of DPA-Cy3[22,22] in POPC liposomes display a more effective killing effect either by perturbing the cell membrane upon

binding and/or by internalizing liposomes which results in nuclear localization and toxicity.

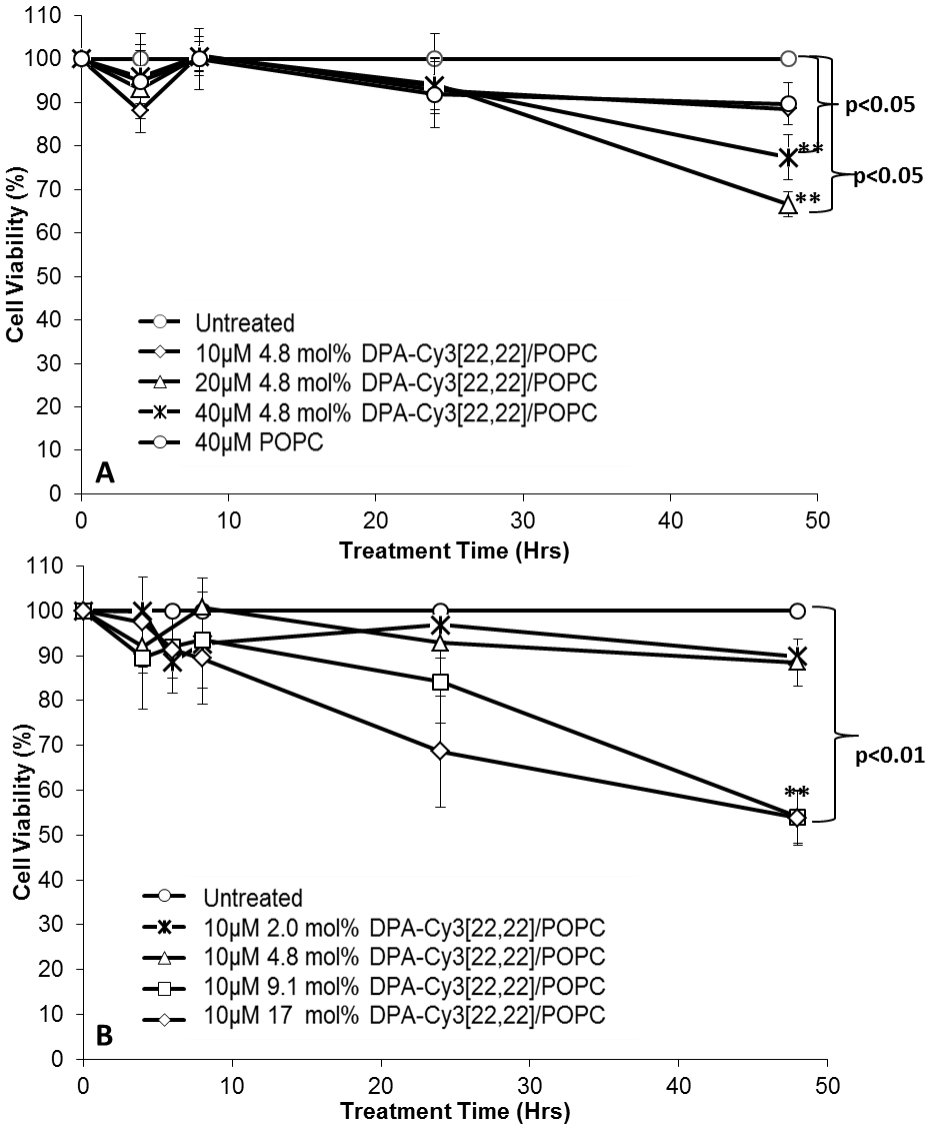

Figure 18-1: Effects of liposome concentration and mol% of DPA-Cy3[22,22] in POPC liposomes on MCF-7 cell viability.

(A) 1000 MCF-7 cells plated in a 96 well plate were treated with 10, 20, and 40 μM of DPA-Cy3[22,22]/POPC liposomes (4.8 mol%) for 0- 48 hours at 37°C. (B) 1000 MCF-7 cells treated with 10 μM at different mol% of DPA-Cy3[22,22] in POPC liposomes (17, 9.1, 4.8, and 2 mole %) for 0-48 hours at 37°C.

1.7.2 The cytotoxic effect of DPA-Cy3[22,22]/POPC liposome on MCF-7 cancer cells versus MCF-12A non-cancer cells

The cytotoxic effects of DPA-Cy3[22,22]/POPC liposomes on non-cancer MCF-12A cells were also investigated. MCF-12A cells were treated with 10 μM of various mol% DPA-Cy3[22,22]/POPC liposomes for 0-48 hours after which the number of cells remaining alive was determined using Invitrogen Cyquant assay. In Figure 18-2, the percent of cells remaining alive is plotted for MCF-7 (data from Figure 18-1B) and MCF-12A cell lines after treatment with (10 μM) DPA-Cy3[22,22]/POPC liposomes at different mol% DPA-Cy3[22,22]/POPC (9.1, 4.8 mol% and 2 mol%). Figure 18-2 shows that DPA-Cy3[22,22]/POPC liposomes exhibit less cytotoxicity to MCF-12A even when using a high mol% of DPA-Cy3[22,22]/POPC liposomes.(Figure 18-2B). MCF-7 cells experience 20-50% cell death after treatment with DPA-Cy3[22,22]/POPC liposomes for 48 hours (Figure 18-2B), whereas MCF-12A cells show only up to 20% cell death using the same liposome concentrations and mole % of DPA-Cy3[22,22] in POPC liposomes. Longer incubation with DPA-Cy3[22,22]/POPC liposomes does not exacerbate the cytotoxic effect on MCF-12A cells more than that on MCF-7 cells. This supports our theory that higher PS content on the cancer cell surface can cause higher DPA[22,22]-Cy3/POPC liposome binding (Figure 15), resulting in more liposome uptake and cell toxicity, whereas non-cancer cells do not exhibit the same level of binding and toxicity.

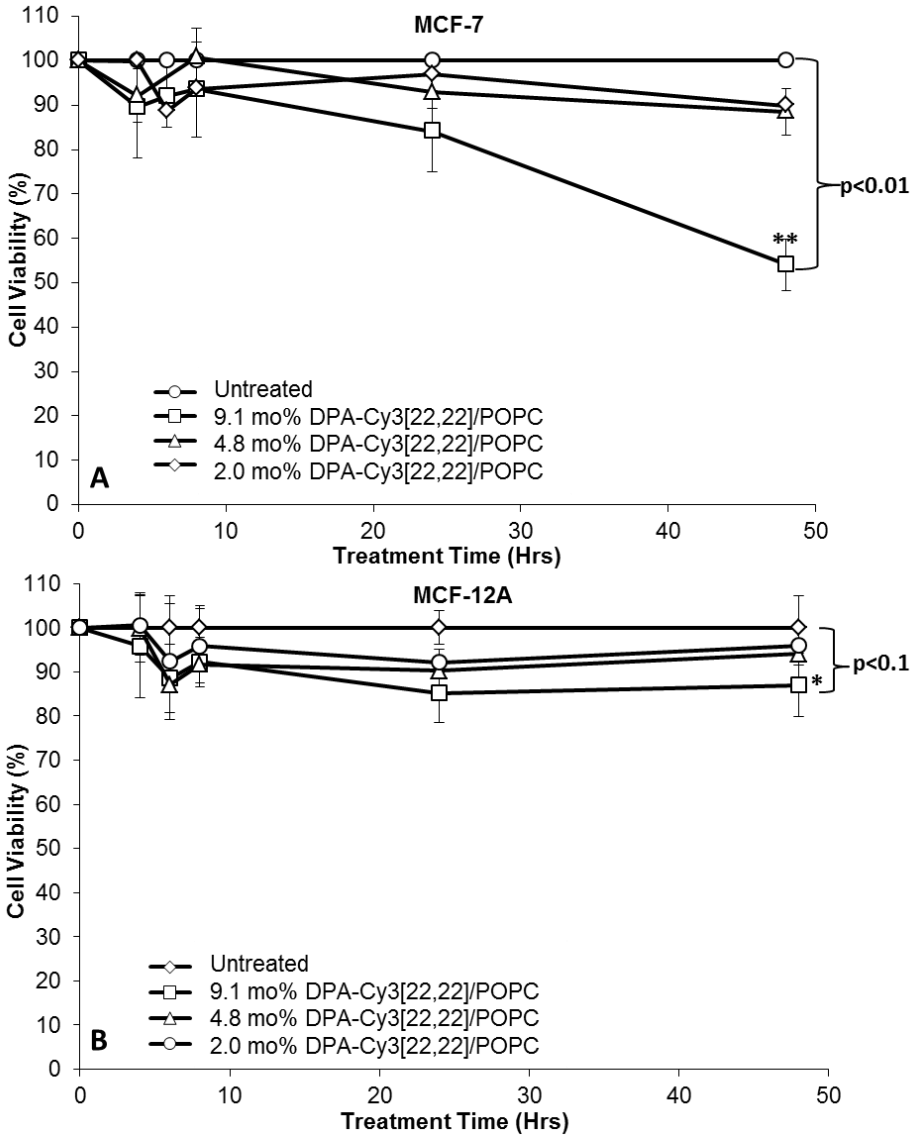

Figure 18-2: Cytotoxicity assay of MCF-7 and MCF-12A cells treated with DPA-Cy3[22,22]/POPC liposome for 0-48 hrs

10 μM of 9.1, 4.8, and 2 mol% DPA-Cy3[22,22] in POPC liposomes were used to treat MCF-7(A) and MCF-12A (B) cells for 0-48 hours.

Part II: DPPC/PLFE Diester/Tetraether Hybrid Thermosensitive Liposomes

2.1 Stability of DPPC/PLFE Liposomes

First, hybrid liposomes were prepared with DPPC (a diester lipid) and PLFE (tetraether lipids) at various molar ratios in either 50 mM Tris or 50mM TES buffer with 10 mM EDTA and 0.02% NaN_3 at pH 7.2. The hybrid liposomes were prepared as extruded unilamellar vesicles (LUVs). The stability of DPPC/PLFE LUVs was tested based on size, polydispersity (PDI) and zeta potential measurements. Table 2 shows the size, PDI, and zeta potential of DPPC/PLFE LUVs with varying PLFE mole percent. Size and PDI data indicated that all liposomes examined here are approximately 140-160 nm in size and are monodispersed (Table 2). However, the addition of PLFE affects the zeta potential of liposomes by making ZP more negative until 60 mol% PLFE. Thereafter, zeta potential becomes less negative. This biphasic behavior at 60 mol% PLFE was observed in both Tris and TES buffer (Figure 19-1).

It is generally accepted that when the zeta potential values are more negative than -30 mV or more positive than 30 mV, the particles are considered stable against coalescence. (Hunter, Midmore, & Zhang, 2001; Laouini et al., 2012). Therefore, data in Figure 19-1 can be taken to indicate that DPPC/PLFE LUVs are stable in Tris buffer at 15-100 mol% PLFE and stable in TES buffer at 30-60 mol% PLFE. The structure of PLFE (Figure 7) contains a negatively charged phosphate on the inositol end of the polar head region which attributes to the low ZP values of PLFE liposomes. Adsorption of charged species in the buffer can affect liposome zeta potential values (Hunter et al., 2001; Laouini et al., 2012). At pH 7.2, the amine group of Tris structure (pKa= 8.3) bear

a positive charge. In TES, at pH 7.2, the negative charge on the sulfate group (pKa= 7.5) coexists with neutral charged species (Figure 19-1). This may explain the difference in zeta potential values in different buffer systems (Figure 19-1).

Table 2: Effect of DPPC/PLFE composition on the size, PDI, and zeta potential

Liposome Composition (mol%)	Size (nm)	PDI	Zeta Potential (mV)
100 % DPPC	162.6 ± 1.9	.198 ± .040	- 4.6 ± 0.5
85% DPPC 15% PLFE	146.6 ± 1.7	.165 ± .021	- 29.6 ± 0.8
80% DPPC 20% PLFE	157.3 ± 1.8	.265 ± .026	- 33.3 ± 0.6
75% DPPC 25% PLFE	151.7 ± 1.2	.265 ± .027	- 42.5 ± 0.9
70% DPPC 30% PLFE	154.7 ± 1.9	.275 ± .022	- 40.6 ± 0.9
65% DPPC 35% PLFE	147.1 ± 1.7	.265 ± .025	- 42.6 ± 1.2
60% DPPC 40% PLFE	144.1 ± 0.8	.257 ± .010	- 47.6 ± 0.2
50% DPPC 50% PLFE	144.9 ± 1.9	.113 ± .010	- 54.5 ± 1.6
40% DPPC 60% PLFE	146.6 ± 1.7	.127 ± .020	- 69.8 ± 1.8
20% DPPC 80% PLFE	146.3 ± 1.5	.125 ± .012	- 58.4 ± 0.6
100% PLFE	159.3 ± 0.9	.232 ± .021	- 43.6 ± 1.6

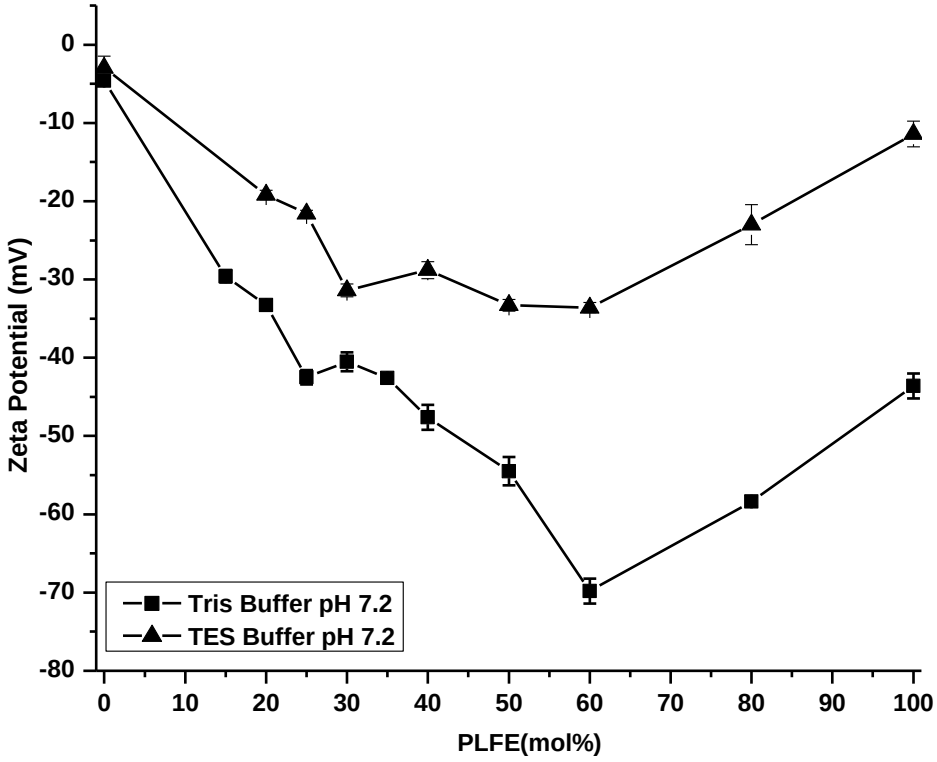

Figure 19-1: Effect of PLFE mole percent on the zeta potential of DPPC/PLFE liposomes suspended in Tris buffer and TES buffer at room temperature.

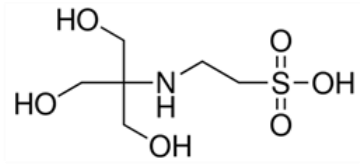

N-[Tris(hydroxymethyl)methyl]-2-aminoethanesulfonic acid (TES)

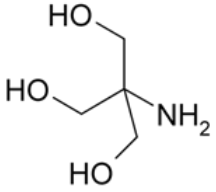

Tris(hydroxymethyl)aminomethane

Figure 19-2: Chemical Structure of Tris and TES

2.2 Membrane Packing of DPPC/PLFE Hybrid Liposomes

To further investigate membrane properties of DPPC/PLFE liposomes, I utilized fluorescent membrane probes to study membrane packing of DPPC/PLFE liposomes. The membrane probe, 6-lauroyl-2-dimethylamino naphthalene, Laurdan (Figure 20) was first designed and synthesized by Gregorio Weber to study dipolar relaxation (T. G. Parasassi, Krasnowska, & Bagatolli, 1998). The sensitivity of Laurdan to the environment polarity can be used to study the polarity in bilayers, micelles, giant unilamellar vesicles (GUVs) and natural membranes (Bagatolli et al., 2000; Harris, Best, & Bell, 2002). Laurdan could experience an emission spectral shift from 450 nm to 500 nm when the probe in the membrane is in a more hydrated environment. A spectral parameter called generalized polarization (GP) was created to quantitatively assess membrane packing using the probe Laurdan. GP_{ex} is defined as shift in the emission maximum of Laurdan quantified by generalized polarization function (see material and methods). In general, GP_{ex} decreases as membrane packing becomes loose (Picardi, Cruz, Orellana, & Perez-Gil, 2011; Sanchez, Tricerri, & Gratton, 2012).

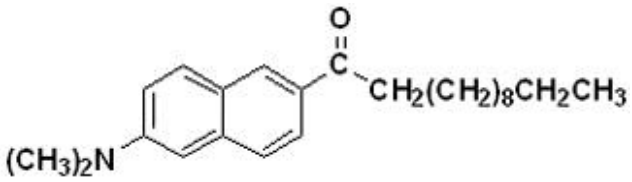

Figure 20: Structure of 6-dodecanoyl-2-dimethylaminonaphthalene (Laurdan)

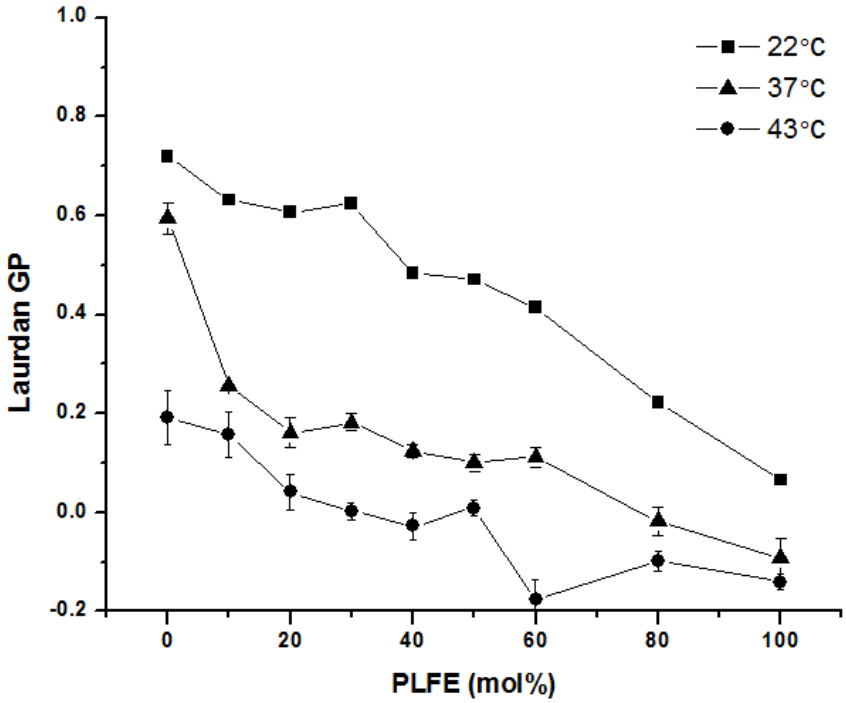

Figure 21: Laurdan GP_{ex} in DPPC/PLFE Liposomes containing 0-100 mol% PLFE. λ_{ex} = 380 nm

In this study, Laurdan fluorescence in DPPC/PLFE was measured to see the effect of PLFE content and temperature on GP_{ex} or membrane packing. GP_{ex} decreased with increasing mol% PLFE (Figure 21). This trend seems counter-intuitive because PLFE is thought to increase membrane packing tightness. This phenomenon has been reported before and could be explained in terms of probe relocation. A previous study using PLFE GUVs showed low Laurdan GP in PLFE liposomes occurs due to rigid packing of the liposome membrane which affect the probe's position and orientation (Bagatolli et al., 2000). In PLFE membranes, Laurdan is believed to be in a L-shaped configuration with the naphthalene ring parallel to the membrane, leading to lower GP (Bagatolli et al., 2000).

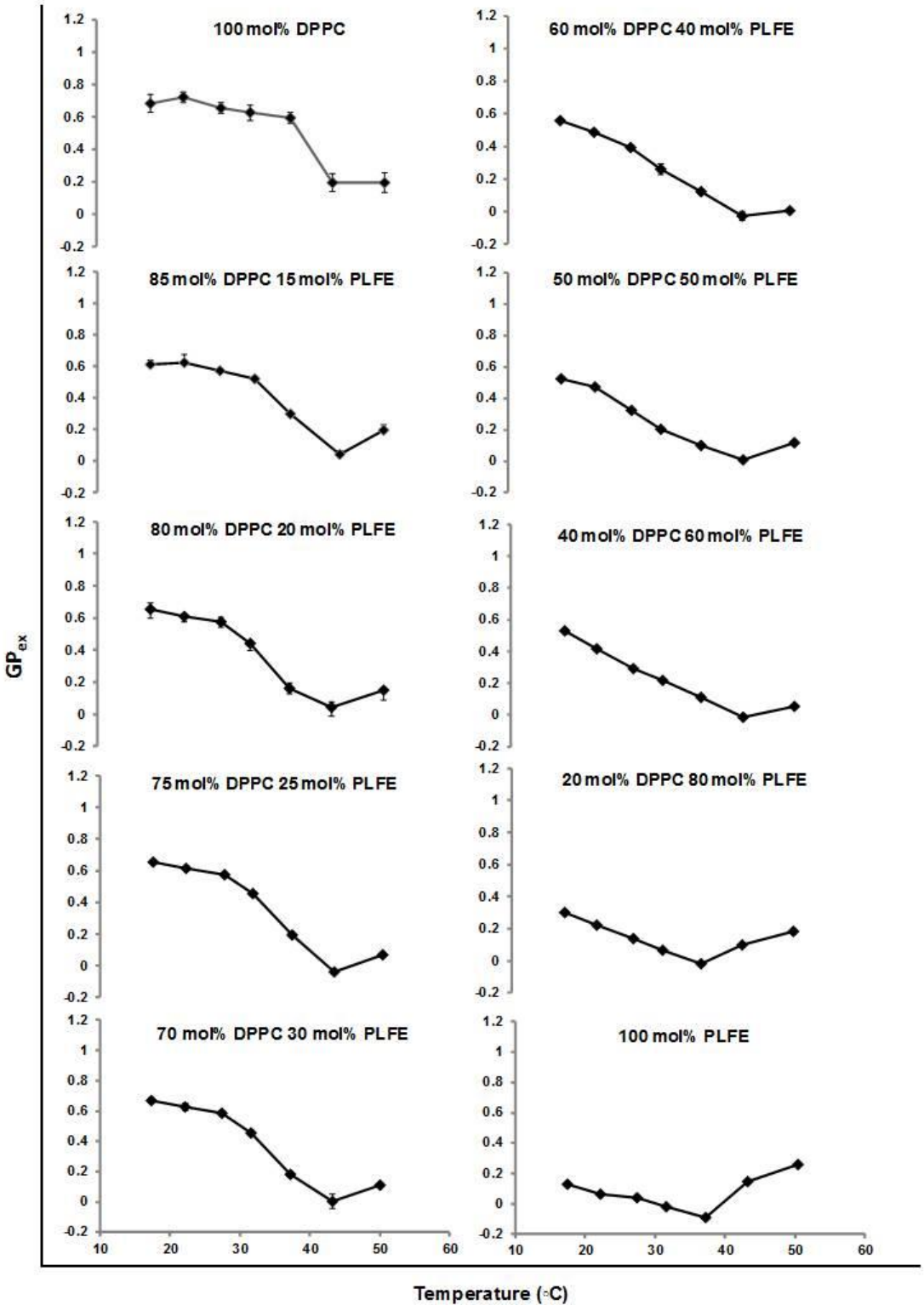
100 mol% DPPC
60 mol% DPPC 40 mol% PLFE
85 mol% DPPC 15 mol% PLFE
50 mol% DPPC 50 mol% PLFE
80 mol% DPPC 20 mol% PLFE
40 mol% DPPC 60 mol% PLFE
75 mol% DPPC 25 mol% PLFE
20 mol% DPPC 80 mol% PLFE
70 mol% DPPC 30 mol% PLFE
100 mol% PLFE
GP_ex
Temperature (°C)

Figure 22: Effect of temperature on Laurdan GP_{ex} in DPPC/PLFE liposomes at various PLFE mole percent.

GP_{ex} was determined using I_{450} and I_{500} when sample was excited at 340 nm. Measurements were repeated in triplicates. Probe-to lipid ratio = 1/400. The measurement was done in heating mode.

Figure 22 shows the effect of temperature on Laurdan GP_{ex} in DPPC/PLFE liposomes at different PLFE mole fractions. The GP_{ex} of DPPC exhibits a sharp decrease between 41°C-42°C, which is near the main transition temperature of DPPC (T_m= ~41.6°C). GP_{ex} decrease near the T_m is in good agreement with previously published data (T. Parasassi et al., 1990). Addition of PLFE in DPPC/PLFE liposomes broadens the transition, and by increasing the amount of PLFE, the broadening of the transition becomes even more noticeable (Figure 22). After addition of 40 mol% PLFE, there is no sharp change in GP_{ex}, instead, GP_{ex} gradually decreases when the temperature is increased. In the range of 10-30mol% PLFE, the DPPC phase transition is retained but the phase transition is broadened possibly due to the co-existence of DPPC and PLFE domains(T. Parasassi, Di Stefano, Loiero, Ravagnan, & Gratton, 1994). The existence of DPPC-rich and DPPC-poor domains implies the existence of interfacial regions between domains. In the interfacial regions the packing is defective which enables the entrapped drug molecules to leak out. Thus, domain formation at certain PLFE mole fractions in PLFE/DPPC mixtures could be developed into a mechanism for drug release.

.

2.3 Surface Properties of DPPC/PLFE Hybrid Liposomes

The effect of temperature on zeta potential (ZP) of DPPC/PLFE liposome was also studied. ZP measurements reveal surface characteristics of DPPC/PLFE liposomes. We have studied the effect of temperature (25-60 °C) on the zeta potential (ZP) of DPPC/PLFE hybrid liposomes in Tris buffer at various DPPC/PLFE mixing ratios (Figure 23-1). The most striking result was obtained from 20-30 mol% PLFE in DPPC. At these mole fractions, there is an abrupt change of ZP with temperature. The 30 mol% PLFE/DPPC hybrid liposomes exhibit a ZP value of ~-45mV below 40°C and undergo a sharp increase to ~-5mV at 50°C, with the most dramatic ZP change occurring at 42°C. For 25 and 27 mol% PLFE, the hybrid liposomes display a similar but less steep increase in ZP with increasing temperature, showing the 50% change occurring at ~47°C and 45°C, respectively. For 20 mol% PLFE, the ZP transition is much broader, and only a half transition is revealed in the temperature range examined (Figure 23-1). For 40 mol% PLFE, no abrupt ZP transition was detected (not shown). To the best of our knowledge, the large and abrupt ZP change with temperature detected in 20-30 mol% PLFE/DPPC liposomes is a novel finding. This phenomenon has not been reported in any other liposomal systems.

Such dramatic change in ZP with temperature observed in 25-30 mol% PLFE in DPPC cannot be attributed simply due to the phase transition of DPPC domains. In DPPC/PLFE hybrid liposomes, DPPC may form its own domain segregated from PLFE domains. It is well know that DPPC has a main gel-to-liquid crystalline phase transition at ~41°C. However, as shown in the top panel of Figure 23-1, the ZP value of 100 mol% DPPC in Tris buffer (pH 7.2) becomes just slightly more negative as the temperature

increases from 25°C (~-5mV) to 60°C (~-11mV) (top panel, Figure 23). The lack of a large and abrupt change in ZP in 100 mol% DPPC suggests that the dramatic change in ZP observed in 20-30 mol% PLFE (Figure 23-1) is not simply due to the melting of the gel phase of DPPC domains in DPPC/PLFE hybrid liposomes.

For 100 mol% PLFE liposomes dispersed in Tris buffer (pH 7.2), ZP undergoes a monotonic change with increasing temperature, becoming more negative with increasing temperature (bottom, Figure 23-1). At a given temperature examined, the ZP value of 100 mol% PLFE is much more negative than that of 100 mol% DPPC (bottom, Figure 23-1).This difference is reasonable because PLFE is negatively charged at neutral pH due to the presence of a phosphate moiety and because the phosphate moiety may reside on the outer surface of the liposomes. In contrast, DPPC, which contains a phosphate and a choline amine, has a net charge near zero at neutral pH. Zeta potential is not the same as membrane surface potential; however, the ZP value is strongly dependent upon membrane surface charge.

Figure 23-2A shows that the large and dramatic increase in ZP from 40°C obtained from 30 mol% PLFE in DPPC dispersed in Tris buffer (pH 7.2) can be reversed by cooling the liposomes. In addition, a similar dramatic change in ZP was observed in 30 mol% PLFE in DPPC liposomes dispersed in TES buffer (Figure 23-2B). In this case, the 50 % change in ZP occurs at a lower temperature (~37°C) while maintaining a good temperature reversibility of ZP change (Figure 23-2B).

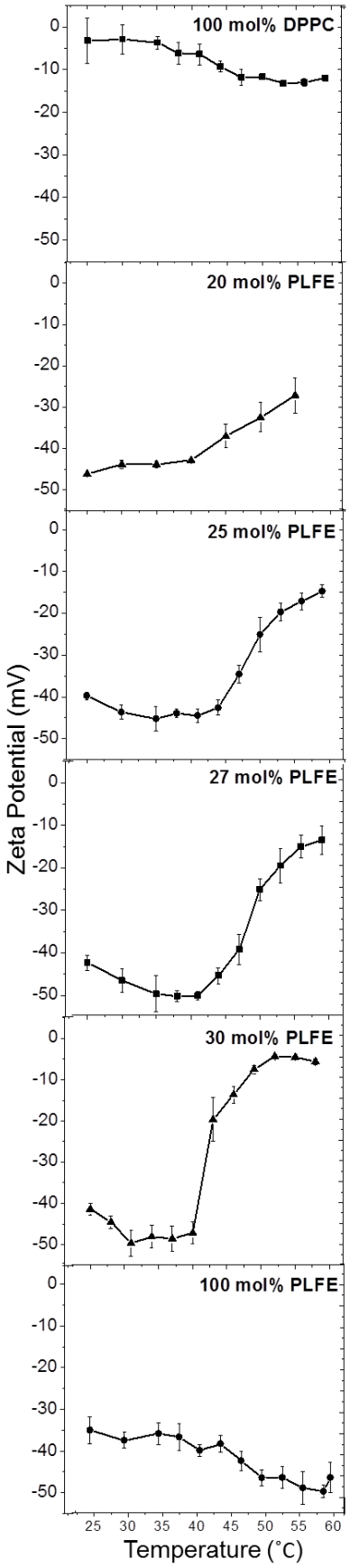
100 mol% DPPC
20 mol% PLFE
25 mol% PLFE
27 mol% PLFE
30 mol% PLFE
100 mol% PLFE
Zeta Potential (mV)
Temperature (˚C)
0
-10
-20
-30
-40
-50
25
30
35
40
45
50
55
60

Figure 23-1: Effect of temperature on zeta potential (ZP) of DPPC/PLFE liposomes at different PLFE mole fraction.

Liposomes (~146± 2.5 nm) in 50 mM Tris buffer with 10 mM EDTA and 0.02% NaN_3 at pH 7.2 were incubated for 10 minutes at each temperature prior to ZP measurement. Liposomes containing 20-30 mol% PLFE show a change in zeta potential with increasing temperature. Above 30 mol% PLFE there is no abrupt change in ZP. Each data point represents the average value from 3 measurements and their standard deviations.

In summary, in 20-30 mol% PLFE in DPPC liposomes, there is a temperature induced dramatic change in zeta potential, which could mean a major change in membrane structure. Initially, the negative ZP of 70 mol% DPPC/30 mol% PLFE liposomes can be attributed to the negative charge on the phosphate of one polar end of PLFE lipids (Figure 7) facing outside the membrane. When the temperature is increased to above 40°C, the negative polar end of PLFE lipid re-orients through flip-flop motion resulting in the negative phosphate head-group to face inside the liposome membrane and increasing the ZP value. This occurrence is only observed when 70-80 mol % DPPC (20-30 mol% PLFE) is present and does not occur in the absence of DPPC. Therefore, the interfacial regions between DPPC and PLFE lipid domain may contribute to the flip-flop phenomenon. This is further investigated using membrane probes.

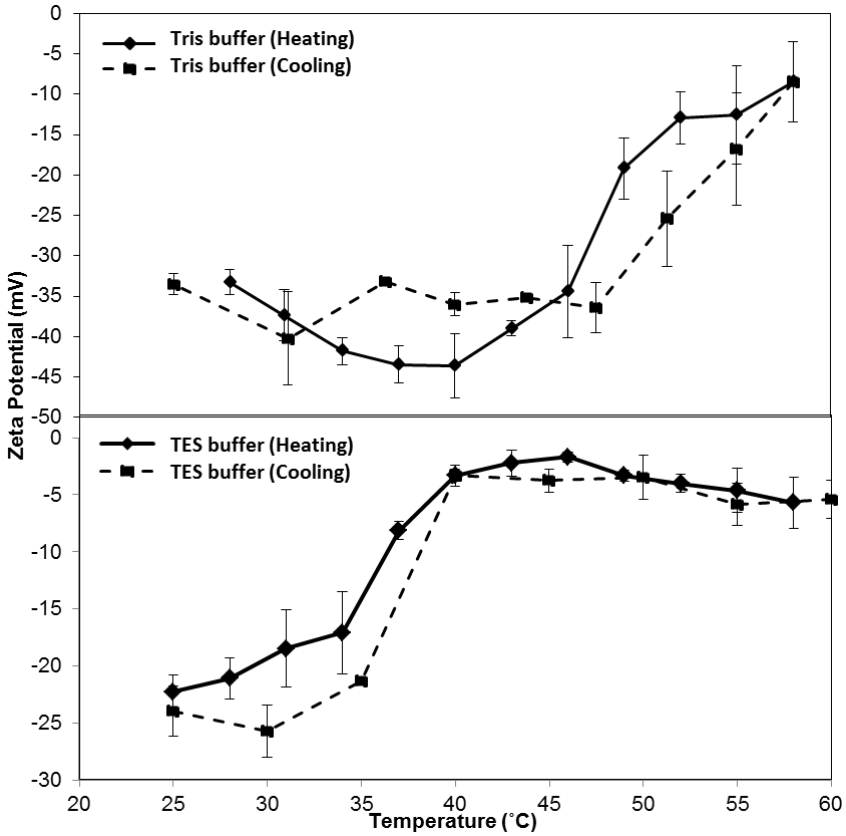

Figure 23-2: Heating and cooling scans measuring ZP of DPPC/PLFE hybrid (30 mol% PLFE) liposomes in 50 mM Tris (A) and 50 mM TES (B) buffers at pH 7.2. Measurements were taken in triplicates to determine the standard deviations.

2.4 DPPC/PLFE Liposome Membrane Packing Studied Using Laurdan and DPH Probes

2.4.1 DPH steady state polarization and laurdan generalized polarization

The hybrid PLFE/DPPC liposomes containing 30 mol% PLFE appear to be most interesting because they exhibit a dramatic change in ZP at ~42°C, which is suitable for use as thermos-sensitive liposomes in hyperthermic treatment of diseased tissue (Anyarambhatla & Needham, 1999; Kong et al., 2001; Manzoor et al., 2012). Therefore, we have used DPH and Laurdan to conduct a more detailed study of membrane packing in liposomes of this particular formulation. In Figure 24, the excitation generalized polarization (GP_{ex}) of fluorescent probe Laurdan and the steady state fluorescence polarization of DPH was measured at 18°C-55°C in 0, 30, and 100 mol % PLFE liposomes.

In figure 24A, Laurdan GP_{ex} in 0, 30, and 100 mol% PLFE is represented. As expected, 100 mol% DPPC (0 mol% PLFE) liposomes experiences a sharp decrease in Laurdan GP_{ex} between 40-43°C due to DPPC phase transition (Repakova et al., 2005; Sanchez et al., 2012) (Figure 24A). The GP_{ex} data of 100 mol% PLFE liposomes show that initially, at room temperature, Laudan GP_{ex} is low (~0.1), then, when the temperature was increased, GP_{ex} begin decreasing until 38°C. This is consistent with the previous finding by Begatolli et. al. 30 mol% PLFE in DPPC behaves somewhat differently than either 0 or 100 mol% PLFE. Laurdan GP_{ex} in 30 mol% PLFE/DPPC liposomes begins decreasing at ~30°C to ~45°C, much broader than the GP_{ex} profile in 100 mol% DPPC liposomes (Figure 24A).

Figure 24B shows that in 100 mol % DPPC (0 mol% PLFE) liposomes, DPH steady state polarization undergoes a sharp decrease between 40-42°C. In 30 mol% PLFE/DPPC liposomes, DPH polarization, similar to GP_{ex} trend, decreases with increasing temperature (Figure 24B). DPH polarization in 30 mol% PLFE/DPPC liposomes show broadening of the DPPC phase transition temperature span which changes from 40-42°C (in 100 mol% DPPC) to 38°C to 45°C (in 70 mol% DPPC/30 mol% PLFE) (Figure 24B). Also, at ~55°C, the DPH polarization value of 30 mol% PLFE/DPPC liposomes decreased almost as much as 100 mol% DPPC. However, 100 mol% PLFE liposomes exhibit a small but steady decrease in DPH polarization from ~0.44 at room temperature to ~0.30 at 60°C (Figure 24B) but not as much as either 0 and 30 mol% PLFE containing liposomes.

Overall, at room temperature (~18°C), DPH polarization in all three systems is similar (0.40-0.45) (Figure 24B). GP_{ex} value at room temperature for liposome mixtures containing 0 and 30 mol% PLFE lipids is ~0.65, however, for 100 mol % PLFE liposomes GP_{ex} is significantly lower. The difference in DPH polarization and Laurdan GP_{ex} in 100 % PLFE containing liposomes can be explained by the difference in DPH and Laudan location and orientation in the membrane (Kaiser & London, 1998; T. Parasassi et al., 1990). In addition, for 70 mol% DPPC/30 mol% PLFE liposomes, both Laurdan and DPH showed changes in the membrane fluidity occurring between ~33°C-~45°C. The consistency in the data from laurdan and DPH supports our theory regarding DPPC and PLFE domain formation and existence of weak interfacial regions between the domains where membrane packing might be more loose.

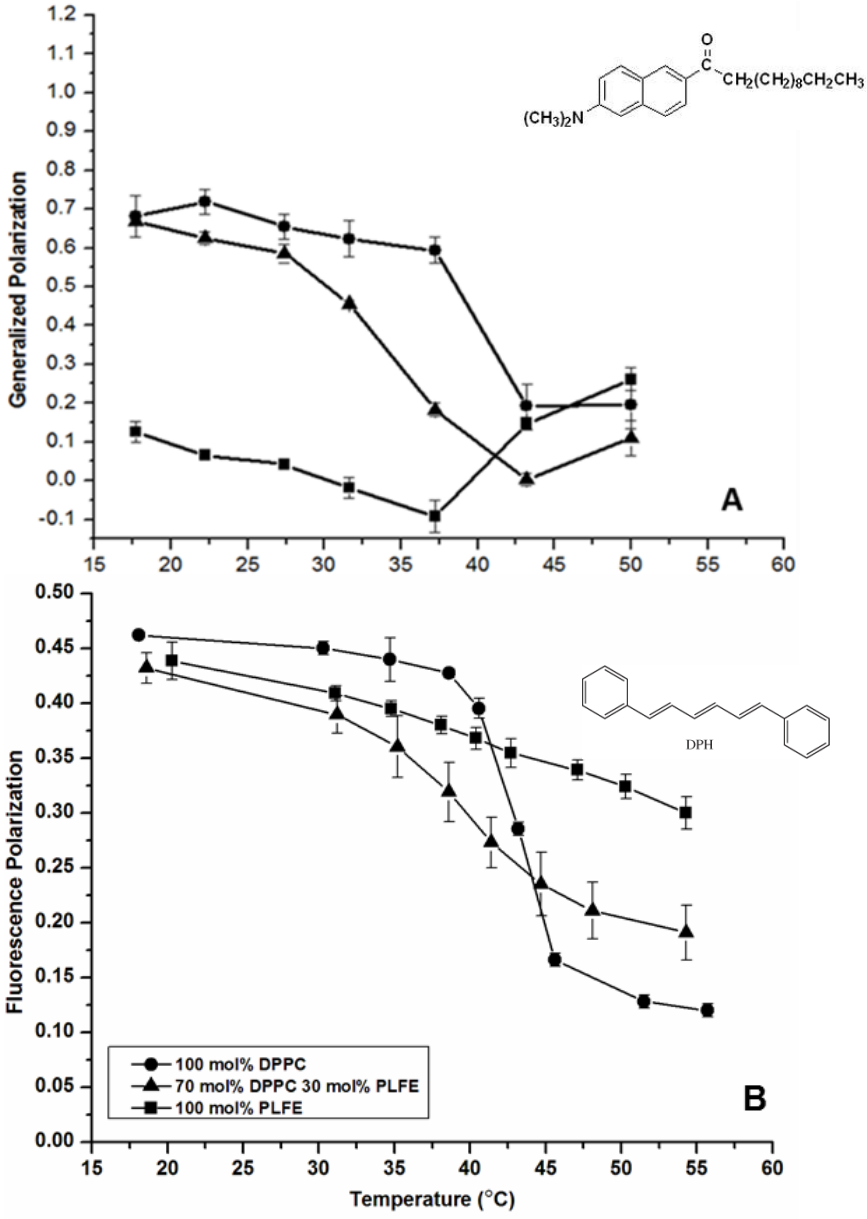

Figure 24: Temperature dependence of generalized polarization of Laurdan (A) and fluorescence steady-state polarization of DPH (B) in 0, 30, 100 mol% PLFE liposomes.

Liposomes (154-160 nm) were labeled with either Laurdan or DPH with a 1:400 probe-to-lipid ratio. Samples were prepared in 50 mM Tris buffer with 10 mM EDTA and 0.02% NaN_3 at pH 7.2.

2.4.2 DPH lifetime measurements in DPPC/PLFE liposome

Liposome membranes display heterogeneity due to differences in composition, physical characteristics, and membrane packing (Chong & Weber, 1983; Fiorini, Valentino, Wang, Glaser, & Gratton, 1987). To further assess the membrane properties of DPPC/PLFE, we investigated the DPH fluorescence lifetime in DPPC/PLFE liposomes. Fluorescence lifetime is a measure of the time a fluorophore spends in the excited state before returning to the ground state, in which it emits photons. (Jameson, 2014). Fluorescence lifetime and differential polarized phase and modulation fluorometry will help evaluate the difference in the membrane heterogeneity of the liposomes containing DPPC and PLFE lipids. The temperature dependence of DPH fluorescence lifetime in PLFE liposomes was determined using frequency domain fluorometry. Lifetime of DPH fluorescence is fit to the exponential decay law:

$$I(t) = \sum \alpha_i \exp(-t/\tau_i)$$

Where *I*(t) is the fluorescence intensity, α_i are pre-exponential factors, τ_i fluorescence lifetime from *i*th component, and t is time in nanoseconds. The data was best fit using two exponential decay equations:

$$F(t) = \alpha_1 e^{\frac{-t}{\tau_1}} + \alpha_2 e^{\frac{-t}{\tau_2}}$$

The goodness of the fit was determined by chi square, χ^2, and the average lifetime is determined by equation:

$$\langle \tau \rangle = (\tau_1) f_1 + (\tau_2) f_2$$

$\langle\tau\rangle$ is average lifetime in nanoseconds, τ_1 and τ_2 are two lifetime components and f_1 and f_2 are their fractional intensities, respectively.

Table 3 lists the average DPH fluorescence lifetime and their fractional components in 100 mol% DPPC, 70 mol% DPPC /30 mol% PLFE, and 100 mol% PLFE liposomes at various temperatures. The result of the fit gave a short lifetime component τ_1 (~1-3 ns) and a long lifetime component τ_2 (8-10 ns) which is the major component for all three systems. For 100 mol% DPPC, both short and long lifetime values decreases at high temperatures (42°C-51°C). When the temperature is increased to ~50 °C, fractional intensity of the shorter lifetime increases from 0.03 to 0.09 and longer lifetime decreases from 0.95 to 0.88. At low temperatures, the longer lifetime remains steady. At ~40°C, near the DPPC T_m, lifetime values begin decreasing. The change in the lifetime and fractional intensities of short and long lifetime components is caused by change in the membrane volume when the temperature is increased to T_m (Fiorini et al., 1987). Similar observation is made in 70 mol% DPPC/30 mol% PLFE liposomes, in which, the fractional intensity of the short lifetime component at room temperature is much higher (.09) than 100 mol% DPPC liposomes, and it increases even more at higher temperatures (Table 3). In 100 mol% PLFE, the fractional intensity of short lifetime component was higher than 0 and 30 mol% PLFE liposomes, and there was very small change in short and long lifetime component with increasing temperature. The significance of this is discussed later.

Table 3: Analysis of DPH Fluorescence Lifetime

100 mol% DPPC Liposomes

Temperature (°C)	τ_1	f_1	τ_2	f_2	$<\tau>$	X^2
25.2	1.93 ± 0.30	0.03 ± 0.01	10.3 ± 0.1	0.95 ± 0.01	9.91 ± 0.02	1.74
27.6	2.19 ± 0.10	0.05 ± 0.01	10.5 ± 0.1	0.93 ± 0.01	9.94 ± 0.02	1.37
32.3	2.74 ± 0.30	0.04 ± 0.01	10.1 ± 0.1	0.94 ± 0.01	10.1 ± 0.03	2.25
35.0	1.51 ± 0.10	0.03 ± 0.01	10.4 ± 0.1	0.95 ± 0.00	9.92 ± 0.01	1.86
37.8	2.36 ± 0.40	0.05 ± 0.01	10.4 ± 0.1	0.93 ± 0.01	9.83 ± 0.03	1.16
40.5	3.00 ± 0.40	0.05 ± 0.01	9.60 ± 0.1	0.92 ± 0.01	9.01 ± 0.05	1.23
42.9	1.15 ± 0.10	0.04 ± 0.00	9.06 ± 0.0	0.93 ± 0.00	8.50 ± 0.00	1.25
46.1	1.47 ± 0.10	0.09 ± 0.00	8.60 ± 0.0	0.87 ± 0.00	8.17 ± 0.01	1.45
49.1	1.80 ± 0.20	0.09 ± 0.01	8.52 ± 0.1	0.88 ± 0.01	7.64 ± 0.04	2.52
51.2	1.01 ± 0.10	0.07 ± 0.01	8.22 ± 0.1	0.91 ± 0.01	7.51 ± 0.03	2.21

70 mol% DPPC / 30 mol% PLFE Liposomes

Temperature (°C)	τ_1	f_1	τ_2	f_2	$<\tau>$	X^2
23.2	2.39 ± 0.20	0.09 ± 0.01	10.3 ± 0.1	0.90 ± 0.01	9.43 ± 0.03	1.69
26.7	3.03 ± 0.20	0.14 ± 0.01	10.7 ± 0.1	0.83 ± 0.01	9.42 ± 0.04	1.93
30.3	3.39 ± 0.20	0.16 ± 0.01	10.8 ± 0.1	0.82 ± 0.01	9.40 ± 0.04	1.72
33.4	3.36 ± 0.20	0.19 ± 0.01	10.8 ± 0.2	0.79 ± 0.01	9.21 ± 0.11	1.40
36.3	3.08 ± 0.20	0.16 ± 0.01	10.5 ± 0.1	0.82 ± 0.01	9.10 ± 0.04	2.27
39.1	2.41 ± 0.10	0.14 ± 0.01	10.1 ± 0.1	0.83 ± 0.01	8.65 ± 0.02	1.09
42.0	2.68 ± 0.10	0.17 ± 0.01	10.2 ± 0.1	0.82 ± 0.01	8.69 ± 0.02	1.82
44.9	2.77 ± 0.10	0.20 ± 0.01	10.4 ± 0.1	0.76 ± 0.01	8.53 ± 0.02	1.39
48.2	2.33 ± 0.10	0.17 ± 0.01	9.88 ± 0.1	0.80 ± 0.01	8.33 ± 0.01	1.78
52.1	2.46 ± 0.10	0.22 ± 0.01	10.3 ± 0.1	0.75 ± 0.01	8.28 ± 0.02	2.61

100 mol% PLFE Liposomes

Temperature (°C)	τ_1	f_1	τ_2	f_2	$<\tau>$	X^2
24.9	2.89 ± 0.10	0.25 ± 0.01	9.59 ± 0.2	0.72 ± 0.01	7.57 ± 0.10	2.52
27.2	2.92 ± 0.10	0.23 ± 0.02	9.53 ± 0.1	0.75 ± 0.01	7.57 ± 0.03	2.71
30.0	2.65 ± 0.10	0.23 ± 0.01	9.56 ± 0.1	0.73 ± 0.01	7.62 ± 0.03	1.67
32.9	2.68 ± 0.10	0.23 ± 0.01	9.59± 0.1	0.73 ± 0.01	7.61 ± 0.03	2.12
35.4	2.89 ± 0.10	0.25 ± 0.02	9.96 ± 0.1	0.70 ± 0.02	7.75 ± 0.04	1.82
37.8	3.36 ± 0.10	0.32 ± 0.01	10.5 ± 0.1	0.64 ± 0.01	7.77 ± 0.03	1.85
41.0	3.23 ± 0.10	0.30 ± 0.01	10.3 ± 0.2	0.66 ± 0.01	7.78 ± 0.09	2.20
43.9	2.34 ± 0.10	0.22 ± 0.01	9.79 ± 0.2	0.73 ± 0.01	7.75 ± 0.10	2.83
47.2	2.70 ± 0.10	0.28 ± 0.01	10.3 ± 0.2	0.67 ± 0.01	7.67 ± 0.09	1.71
50.0	2.36 ± 0.10	0.26 ± 0.01	9.64 ± 0.2	0.69 ± 0.01	7.24 ± 0.10	2.52

**** $<\tau>$, τ_1 and τ_2, lifetime in nanoseconds; *f*1 and *f*2, fractional intensities**

To take a closer look at the differences in DPH fluorescence lifetime in 0, 30, 100 mol% PLFE liposomes, average lifetime is plotted with temperature (Figure 25). In 100 mol% DPPC liposomes, from room temperature (24°C) to 39°C, the DPH fluorescence lifetime (~ 9.9 ns) remains steady (Figure 25A). When the temperature is increased to above 39°C, the DPH fluorescence lifetime begins to decrease (Figure 25A). At lower temperatures, DPPC liposomes remain in gel state. Before the T_m, the onset temperature is defined as the temperature at which membrane begins to exhibit volume fluctuation (Fiorini et al., 1987). Just above the onset temperature, the average lifetime of DPH begins to decrease and continues to decrease beyond the T_m (T_m = ~41.6°C for 100 mol% DPPC). Before the T_m, At the onset temperature, the membrane begins exhibiting more volume fluctuation (Chong et al., 2010; Mabrey & Sturtevant, 1976) which causes more water penetration and consequently a decrease in the DPH lifetime. Then, the highest volume fluctuation occurs at the T_m, which results in even lower DPH lifetime values (Fiorini et al., 1987). For 70 mol% DPPC/30 mol% PLFE liposomes, an abrupt decrease $<\tau>$ is not as obvious as 100 mol% DPPC liposomes instead a gradual decrease in $<\tau>$ is observed (Figure 25B). More interestingly, compared to 100 mol% DPPC, the DPH $<\tau>$ in 70 mol% DPPC/30 mol% PLFE is lower below 40°C and higher above 40°C indicating that presence of PLFE has altered membrane characteristics.

At a given temperature examined, DPH fluorescence lifetime in 100 mol% PLFE liposome is considerably lower (~7.5 ns) than that in 100 mol% DPPC liposomes and in DPPC/PLFE (30 mol%) mixture (Figure 25C). In 100 mol% PLFE, the average lifetime stays steady (7.5-7.6 ns) from 25°C to 47°C. When the temperature is increased above 47°C, there is a small decrease in average DPH lifetime (7.2 ns). Figure 25C also shows

that compared to 100 mol% DPPC and 70 mol% DPPC/ 30mol% PLFE liposomes, 100 mol% PLFE liposomes have no abrupt changes in $<\tau>$ in the temperature range examined. The lower DPH fluorescence lifetime, compared to those in 100 mol% DPPC and 30 mol% PLFE, is surprising because 100 mol% PLFE liposomes have tighter membrane packing, in which case one would expect the DPH fluorescence lifetime to be higher. Lower DPH fluorescence lifetime values in 100 mol% PLFE can be explained by differences in DPH probe location in the membrane of 100 mol% PLFE containing liposomes. Similar to Laurdan, DPH probe might be pushed out closer to liposome membrane surface because of tight membrane packing of PLFE liposomes. This results in DPH existing closer to the surface of the membrane or inner aqueous compartment or parallel to the membrane surface which allows more water molecules to access the probe. Consequently, the DPH probe is in PLFE liposome is in more hydrating environment which results in lower DPH lifetime values. This also explains the reason for higher fractional intensity of short lifetime component in PLFE liposomes.

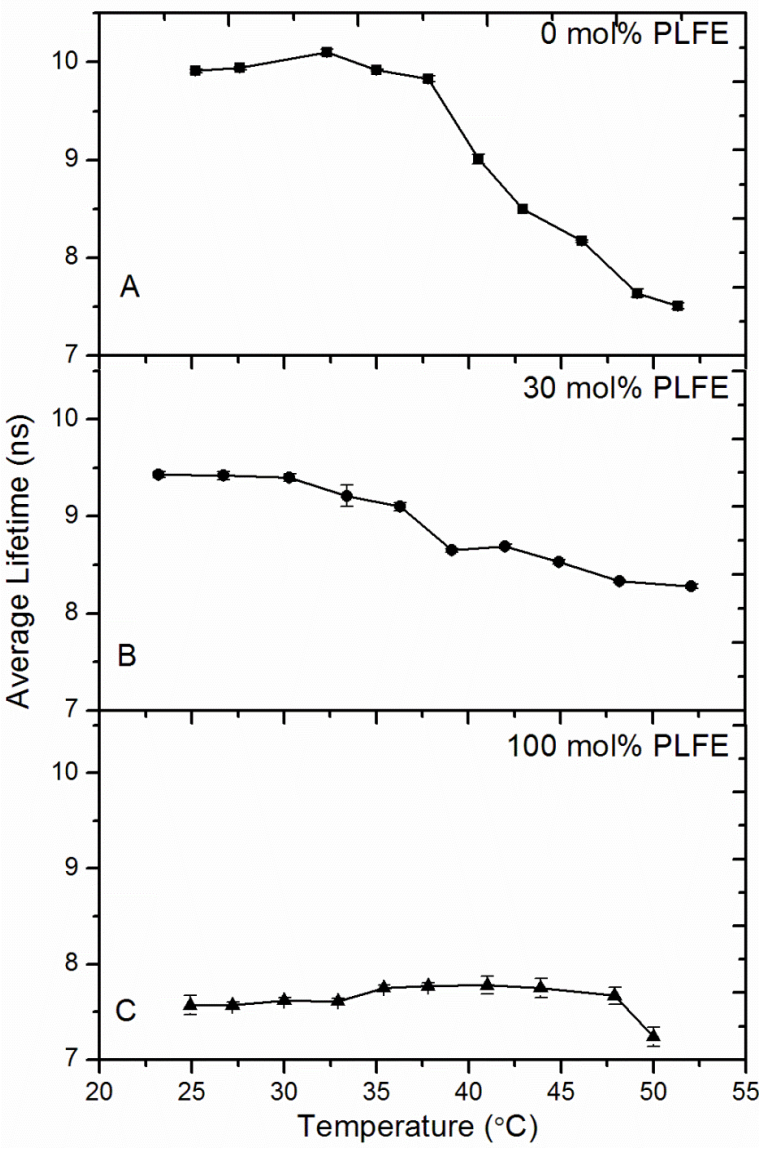

Figure 25: Effect of temperature on DPH average lifetime <τ> measured in 100 mol% DPPC (A), 70 mol% DPPC /30 mol% PLFE (B), and 100 mol% PLFE (C) liposomes.

Liposomes prepared in 50 mM Tris buffer with 10 mM EDTA 0.02% NaN_3 at pH 7.2 was labeled with DPH at a 1:500 probe to lipid ratio. Lifetime was determined using POPOP as a reference. Standard deviation was calculated using the uncertainties of τ and f values obtained experimentally.

2.4.3 Differential polarized phase and modulation study of DPH in DPPC/PLFE liposomes

In addition, the probe dynamics in liposomes was evaluated using differential polarized phase and modulation flourometry (Chong, Cossins, & Weber, 1983; Kao, Chong, Huang, & van der Meer, B. W., 1990). In this study, the sample was illuminated with polarized light (∥ or ⊥) and the phase delay and demodulation ratio (AC) in emission were measured. Measurements were fitted to the equation:

$$r(t) = r_1 e^{\frac{-t}{\theta_1}} + r_2 e^{\frac{-t}{\theta_2}}$$

Where r is the anisotropy, r_1 and r_2 are the anisotropy of component 1 and 2, respectively, θ_1 is the rotational correlation time (in nanoseconds), and t is time. For our studies, θ_2 is fixed to 10,000 ns and therefore, r_2 is limiting anisotropyr_∞. The goodness of the fit was judged based on χ^2. In the data presented, the best fit was achieved when using a two component model. θ_1 and $r_1$as well as r_∞ are used to calculate the rotational rate and molecular order of DPH in liposomes as a function of temperature and PLFE content.

Table 4 lists fitted limiting anisotropy (r_2), and rotational correlation time (θ_1) with respect to temperature at 0, 30, and 100 mol% PLFE. S, the order parameter, is calculated using the equation $r_\infty / r_0 = S^2$ where $r_0 = 0.39$ is anisotropy observed in the absence of rotational motion during the lifetime of the excited state (Kao et al., 1990). The rotational rate, R in ns^{-1}, was calculated using $R = 1/6\ \theta_1$ to describe the probe's rotational movement within the membrane (Repakova et al., 2005). The "wobbling in cone" model have been used previously to describe the motion of DPH in membrane, in which, long axis of DPH probe is believed to be wobbling freely in a cone shaped

space(Kinosita, Ikegami, & Kawato, 1982). DPH rotational motion in membrane is hindered or angular range of rotational motion is limited, in such a case, limiting anisotropy is observed at longer time (10000 ns) (Lakowicz, 1999). Generally, narrow angular range of the probe within the membrane results in higher r_∞ and S values, assuming the system is spherical and DPH is in a cone shaped space (Kinosita et al., 1982).

Table 4: Analysis of DPH Differential Polarized Phase and Modulation Data

100 mol% DPPC Liposomes

Temperature (°C)	θ_1	R	r_1	θ_2	r_2	S	X^2
25.2	2.26 ± 0.10	0.073 ± 0.003	0.067 ± 0.010	10000 FIXED	0.340 ± 0.001	0.93 ± 0.00	2.89
27.6	2.34 ± 0.30	0.071 ± 0.009	0.063 ± 0.002	10000 FIXED	0.365 ± 0.002	0.96 ± 0.00	2.82
32.3	2.79 ± 0.10	0.069 ± 0.003	0.056 ± 0.000	10000 FIXED	0.344 ± 0.002	0.94 ± 0.00	2.68
35.0	2.17 ± 0.07	0.076 ± 0.002	0.096 ± 0.008	10000 FIXED	0.304 ± 0.002	0.88 ± 0.01	2.24
37.8	1.50 ± 0.10	0.111 ± 0.007	0.136 ± 0.004	10000 FIXED	0.290 ± 0.008	0.86 ± 0.02	1.27
40.5	1.34 ± 0.04	0.124 ± 0.003	0.298 ± 0.005	10000 FIXED	0.120 ± 0.005	0.55 ± 0.01	0.66
42.9	1.28 ± 0.01	0.130 ± 0.001	0.333 ± 0.001	10000 FIXED	0.067 ± 0.001	0.41 ± 0.01	1.74
46.1	1.43 ± 0.02	0.126 ± 0.002	0.329 ± 0.001	10000 FIXED	0.072 ± 0.001	0.42 ± 0.00	3.78
49.1	1.37 ± 0.02	0.121 ± 0.001	0.373 ± 0.010	10000 FIXED	0.027 ± 0.001	0.27 ± 0.00	3.42
51.2	1.14 ± 0.04	0.145 ± 0.005	0.400 ± 0.010	10000 FIXED	0.048 ± 0.006	0.32 ± 0.01	2.91

70 mol% DPPC / 30 mol% PLFE Liposomes

Temperature (°C)	θ_1	R	r_1	θ_2	r_2	S	X^2
23.2	4.97 ± 0.40	0.033 ± 0.003	0.090 ± 0.002	10000 FIXED	0.302 ± 0.003	0.88 ± 0.01	2.97
26.7	4.99 ± 0.10	0.033 ± 0.001	0.136 ± 0.001	10000 FIXED	0.240 ± 0.002	0.78 ± 0.00	3.76
30.3	5.05 ± 0.20	0.033 ± 0.001	0.158 ± 0.001	10000 FIXED	0.213 ± 0.003	0.73 ± 0.01	2.38
33.4	4.50 ± 0.10	0.037 ± 0.001	0.197 ± 0.002	10000 FIXED	0.177 ± 0.003	0.67 ± 0.01	2.46
36.3	3.36 ± 0.10	0.050 ± 0.001	0.213 ± 0.001	10000 FIXED	0.169 ± 0.002	0.66 ± 0.00	3.96
39.1	3.65 ± 0.10	0.047 ± 0.001	0.229 ± 0.001	10000 FIXED	0.127 ± 0.002	0.56 ± 0.01	3.76
42.0	3.07 ± 0.09	0.054 ± 0.001	0.247 ± 0.002	10000 FIXED	0.145 ± 0.002	0.61 ± 0.00	2.17
44.9	2.58 ± 0.10	0.064 ± 0.001	0.260 ± 0.003	10000 FIXED	0.130 ± 0.003	0.57 ± 0.01	2.00
48.2	2.15 ± 0.06	0.077 ± 0.001	0.297 ± 0.002	10000 FIXED	0.133 ± 0.002	0.58 ± 0.00	2.41
52.1	2.05 ± 0.09	0.081 ± 0.001	0.312 ± 0.005	10000 FIXED	0.117 ± 0.002	0.55 ± 0.00	1.27

100 mol% PLFE Liposomes

Temperature (°C)	θ_1	R	r_1	θ_2	r_2	S	X^2
24.9	2.73 ± 0.20	0.061 ± 0.002	0.082 ± 0.002	10000FIXED	0.302 ± 0.002	0.88 ± 0.00	2.66
27.2	3.45 ± 0.30	0.048 ± 0.002	0.088 ± 0.002	10000FIXED	0.300 ± 0.002	0.88 ± 0.00	1.00
30.0	2.80 ± 0.20	0.059 ± 0.001	0.099 ± 0.002	10000FIXED	0.290 ± 0.002	0.86 ± 0.00	1.73
32.9	1.92 ± 0.10	0.066 ± 0.001	0.113 ± 0.002	10000FIXED	0.287 ± 0.002	0.85 ± 0.00	1.92
35.4	2.72 ± 0.10	0.061 ± 0.001	0.121 ± 0.003	10000FIXED	0.279 ± 0.002	0.84 ± 0.00	1.68
37.8	3.86 ± 0.30	0.043 ± 0.001	0.125 ± 0.002	10000FIXED	0.262 ± 0.003	0.81 ± 0.01	1.42
41.0	3.11 ± 0.20	0.053 ± 0.002	0.139 ± 0.002	10000FIXED	0.260 ± 0.002	0.82 ± 0.00	1.91
43.9	3.26 ± 0.20	0.051 ± 0.003	0.156 ± 0.002	10000FIXED	0.241 ± 0.002	0.79 ± 0.00	1.80
47.2	2.89 ± 0.20	0.057 ± 0.004	0.177 ± 0.002	10000FIXED	0.229 ± 0.003	0.76 ± 0.01	1.82
50.0	2.80 ± 0.20	0.059 ± 0.004	0.190 ± 0.003	10000FIXED	0.217 ± 0.003	0.75 ± 0.01	3.16

In 100 mol% DPPC liposomes, θ_1, correlation rotational time is steady from 25.2°C - 37.8°C. Between 37.8°C and 40.5°C, there is a significant decrease in rotational correlation time with increasing temperature (Table 4). The rotational rate, R (rad ns^{-1}), is smaller at lower temperatures and increases significantly when the temperature is increased from 35.4°C to 37.8°C, around the DPPC transition onset temperature (Figure 27). The order parameter S also decreases when the temperature is increased from 37.8°C to 40.5°C (Figure 26). This could be explained by proposing that there is an increase in motion and disorder within the restricted cone in the membrane caused by change in temperature. The limiting anisotropy or r_∞ is high at low temperatures because probe rotation is hindered up to a certain angle in the membrane. In 100 mol% DPPC liposomes, when the temperature is increased, especially around T_m, r_∞ decreases dramatically as a result of an increase in the cone angle which allows DPH to move more freely.

The rotational correlation time, θ_1, in 70 mol% DPPC/ 30 mol% PLFE is larger (~ 5ns) than in 100 mol% DPPC (~ 2 ns) at low temperatures suggesting a smaller cone angle is created by PLFE lipids. Both θ_1 and S (Figure 26) in 70 mol% DPPC/ 30 mol% PLFE decreases with increasing temperature especially when the temperature is increased to above 36.3°C. The cone angle increases when temperature is increased due to the DPPC phase transition, as a result, the rotational rate (R) also increases at 36.3°C. At 23-33°C, r_2 values in 70 mol% PLFE/30 mol% DPPC are smaller than in 100 mol% DPPC. This seems counter intuitive because with the addition of PLFE, one would expect higher r_∞ (r_2)value due to smaller cone angle because of less free volume (Chong et al., 2005; Chong et al., 2010). This discrepancy can be explained by the location of DPH probe in

the membrane. The effect of PLFE is more apparent when temperature is increased. With increasing temperature, the decrease in r_2 values and the increase in rotational rates are much less dramatic in 70 mol% DCCP/ 30 mol% PLFE than in 100 mol% DPPC liposomes because PLFE cause restriction of the probe resulting in less motion of the DPH probe in 70 mol% DPPC/ 30 mol% PLFE liposomes.

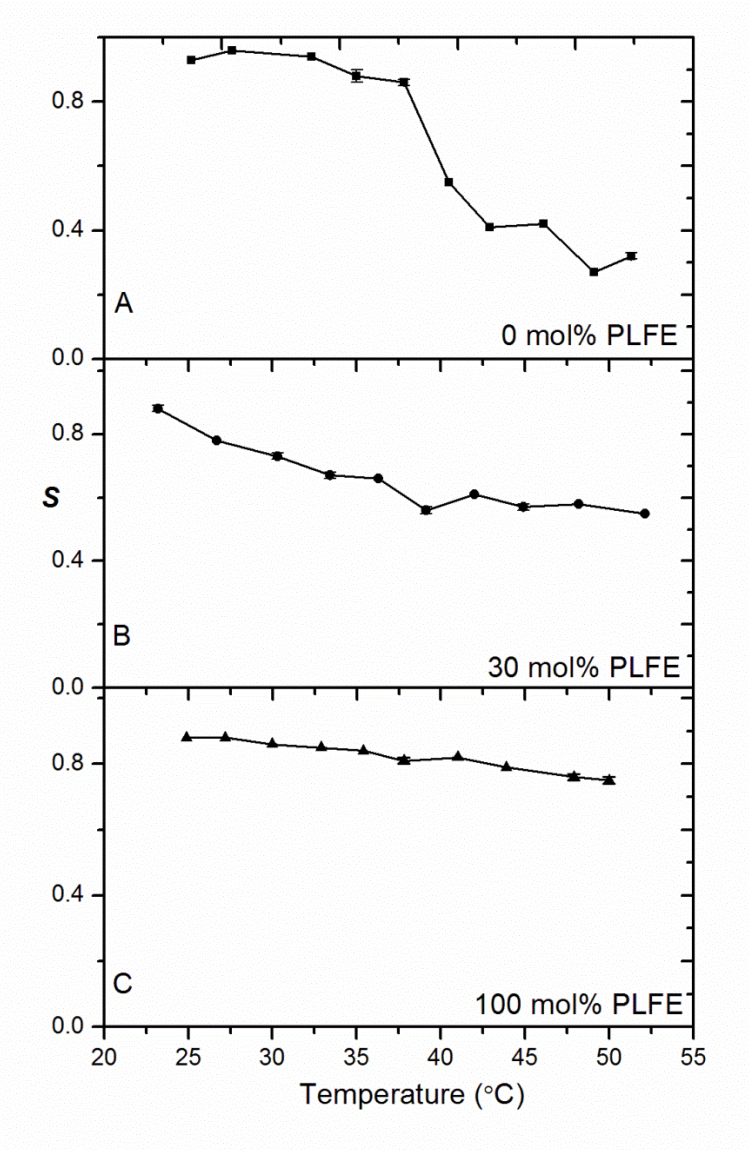

Figure 26: DPH order parameter (S) in 100 mol% DPPC (A), 70 mol% DPPC 30 mol% PLFE (B), and 100 mol% PLFE (C) liposomes. Standard deviations were calculated using propagation of error.

Smaller DPH θ_1 value is found in 100 mol% PLFE liposomes. θ_1 values in 100 mol% PLFE liposomes (~2-3 ns) are similar to 100 mol% DPPC liposomes at low temperatures 24.9℃-35.4 ℃ . But, θ_1 values stay steady and exhibit no significant change when the temperature is increased because there is no DPPC lipid present in the system. The S values do not show any significant decrease either (Figure 26) because 100 mol% PLFE liposomes remain tightly packed. r_2 values in 100 mol% PLFE is similar to 70 mol% DPPC/ 30 mol% PLFE liposomes. Unlike 70 mol% DPPC/ 30 mol% PLFE, r_2 in 100 mol% PLFE liposomes do not show as greater change with increasing temperatures. Due to tight packing of PLFE lipids, when the PLFE content is increased to 100 mol% PLFE, the cone angle decrease results in very little change in DPH motion even at higher temperatures. Previous studies demonstrated that volume fluctuation in DPPC liposome increases around its T_m, but PLFE liposomes have little volume change with increasing temperature. In this study, similar observation is made about DPH in 100 mol% PLFE liposomes. DPH rotational rate, time, and order parameter all show little change with increasing temperature suggesting PLFE liposomal membrane is not affected by temperature.

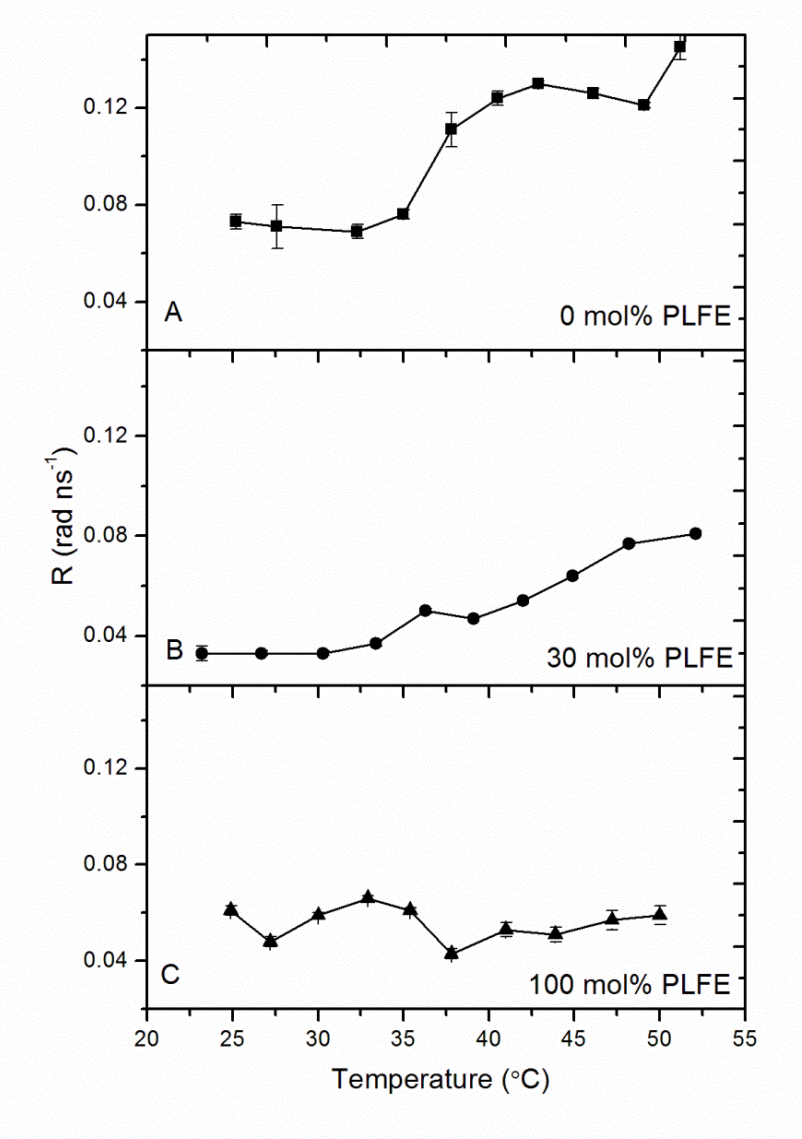

Figure 27: DPH rotational rate (rad ns^{-1}) in 100 mol% DPPC (A), 70 mol% DPPC 30 mol% PLFE (B), and 100 mol% PLFE (C) liposomes. Standard deviation was calculated using propagation of error.

The DPH rotational rate increases in 100 mol% DPPC and 70 mol% DPPC/30 mol% PLFE liposomes when temperature is raised from 37°C to 42°C but not 100 mol% PLFE liposomes. Due to the presence of DPPC lipid in DPPC/PLFE liposomes, increasing the temperature to DPPC T_m increases motion of the fluorescent probe as a result of more fluid environment(Fiorini et al., 1987; Repakova et al., 2005). DPH movement in 100 mol% PLFE shows very little change suggesting membrane remain tightly packed even after increasing temperatures at the presence of 0 and 30 mol% PLFE in DPPC/PLFE liposomes. This finding is in agreement with Laurdan GP_{ex} and DPH polarization data presented earlier (Figure 22 and Figure 24). Unlike DPPC liposome membrane, 100 mol% PLFE liposomes form monolayer because the phytanoyl chains of PLFE are covalently linked from one polar end to the other. Bipolar monolayers do not have the type of gauche-to-trans conformational transition normally seen in bilayers composed of monopolar lipids (Khan & Chong, 2000) which is the reason PLFE membrane is more tightly packed(Komatsu & Chong, 1998), have low volume fluctuations (Chong et al., 2010), and exhibit little DPH movement (Figure 26 & 27).

DPH in PLFE containing liposomes can be described in Diagram 2. Possible location and orientation of DPH in 100 mol% PLFE liposomes can be explained by two possible scenarios (1) DPH is located between the hydrocarbon regions and parallel to the liposome membrane, and (2) DPH is present in two different domains formed by PLFE lipid with either GDNT or GDGT head groups (Diagram 1B: 2). DPH lifetime components determined from the fit has two highly significantly different lifetimes. The longer lifetime component (~10ns) is due to DPH located in the hydrocarbon region of the PLFE lipid membrane and the shorter lifetime component (~2ns) is caused by DPH

near more hydrating environment, parallel to the membrane surface, similar to DPH in DPPC membrane (Fiorini et al., 1987; Repakova et al., 2005), therefore, scenario 1 is more likely. This also explains the reason for higher fractional intensity of the shorter lifetime component in PLFE containing liposomes (Table 3). Increasing the PLFE content prevents DPH from entering deeper hydrophobic core of the membrane (Diagram 1B: 1), as a result, more DPH probe is located parallel to surface of the membrane. Scenario 2 suggests formation of segregated domains by GDGT and GDNT head group lipids results in two different DPH lifetimes. Two photon fluorescence microscopy of PLFE giant unilamellar vesicles show snow flake-like domain formation at low temperatures, which may be caused by separation of GDGT and GDNT containing lipids. However, this occurs at very low temperature (12.8-28.4°C) (Bagatolli et. al., 2000).

Form our results, we can infer that the location of the DPH probe in 70 mol% DPPC /30 mol% PLFE hybrid liposomal membrane differ from 100 mol% DPPC or 100 mol% PLFE. At any given temperature, the DPH rotational rate in 70 mol% DPPC /30 mol% PLFE hybrid liposomes is slower than that in 100 mol% DPPC. Surprisingly, 30 mol% PLFE/DPPC membrane has half the rotation rate as 100 mol% PLFE at 25-35°C. This suggests that the DPH probe in 70 mol% DPPC /30 mol% PLFE is located deeper within the hydrocarbon interior of the membrane, and the slower rotational rate of DPH occurs due to hindrance by cyclopentane rings and branched methyl groups of PLFE lipid. Consequently, at lower temperatures, the rotational correlation time is faster in 70 mol% DPPC /30 mol% PLFE hybrid membrane than 100 mol% PLFE. Also, in 70 mol% DPPC /30 mol% PLFE, DPH rotational rate (R) gradually increases with temperature but not to the extent as 100 mol% DPPC. The DPH probe movement increases with

temperature in the 70 mol% DPPC /30 mol% PLFE perhaps due to DPH locating in the DPPC domains or in the region between DPPC and PLFE segregated domains (Diagram 2C) which are the regions most affected by temperature increase.

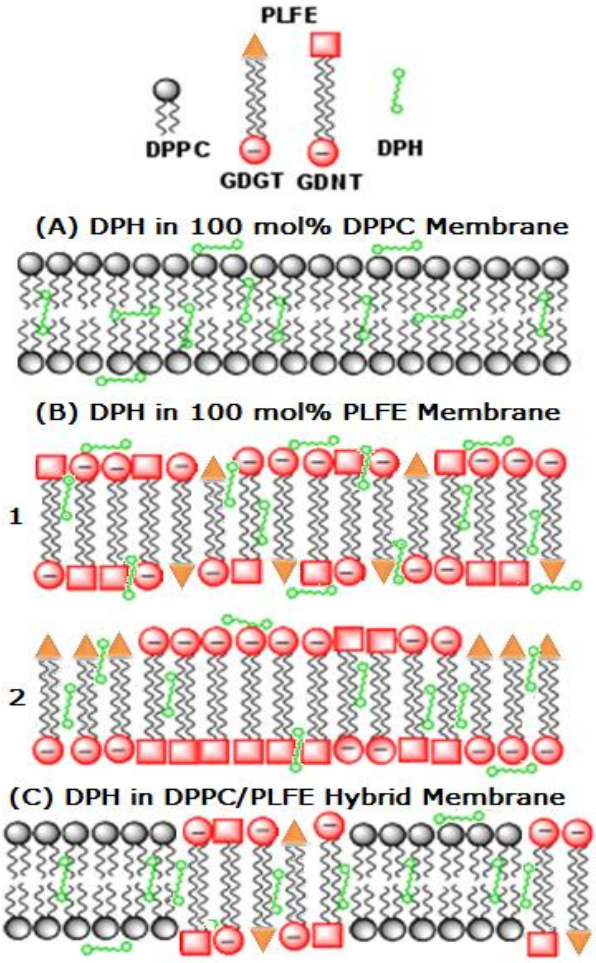

Diagram 4: Location of DPH probe in DPPC and PLFE lipid containing liposomes

The result of the fit gives two DPH lifetime components. (A) DPH in DPPC liposomes is believed to be located either in hydrocarbon core (major component) or parallel to membrane (minor). (B) Location of DPH in PLFE liposomes can be hypothesized to be in 1 of 2 ways. 1) First, DPH may be located in the hydrophobic region of PLFE monolayer and parallel to the membrane 2) Second, PLFE-GDNT and PLFE-GDGT can form segregated domains and DPH in two different domains have different lifetime components.(C) DPH in 70 mol% DPPC /30 mol% PLFE liposome membrane.

2.5 Temperature Dependent Drug Release from DPPC/PLFE Liposomes

2.5.1 Monitoring slow kinetics of DXO release from DPPC and PLFE liposomes using fluorometer

Liposomes with 0, 20, 30 mol % PLFE containing anti-cancer drug doxorubicin (DXO) were utilized to test slow kinetics drug release from liposomes. From the zeta potential measurements, it was determined that DPPC/PLFE liposomes are highly stable in buffer and, particularly, 20-30 mol% PLFE containing liposomes have unique temperature-induced change in membrane surface properties (Figures 19 & 23). Here, we test the effect of temperature on drug release from PLFE containing liposomes. First, after preparing liposomes with DXO entrapped, free drug was separated using size exclusion column. Figure 28A shows the elution profile of sample separated using Sephadex G-50 size-exclusion column. The result also shows that liposomes were able to be separated from free drugs successfully. Liposomes which are larger in size were able to be eluted out of the column (Peak 1) before small-molecule free drugs (Peak 2). Using light scattering, only one peak was detected which overlapped with Peak 1 of fluorescence data, identifying peak 1 to be the liposomes trapped with DXO. Afterwards, slow kinetics of drug release was performed using the liposomal fractions (Figure 28B). The rate constants of DXO were calculated using $F = A + B\,(1 - e^{-kt})$, where k is the rate constant of leakage, t is time, and A and B are constants; $F = F_t/F_{max}$ was used to fit the normalized fluorescence intensity (Komatsu & Chong, 1998). Maximum fluorescence intensity was determined by adding detergent to the liposome dispersant (Figure 28B).

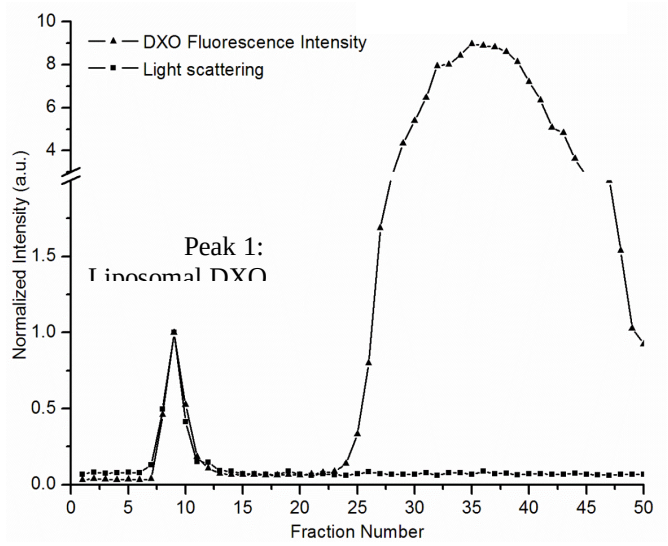

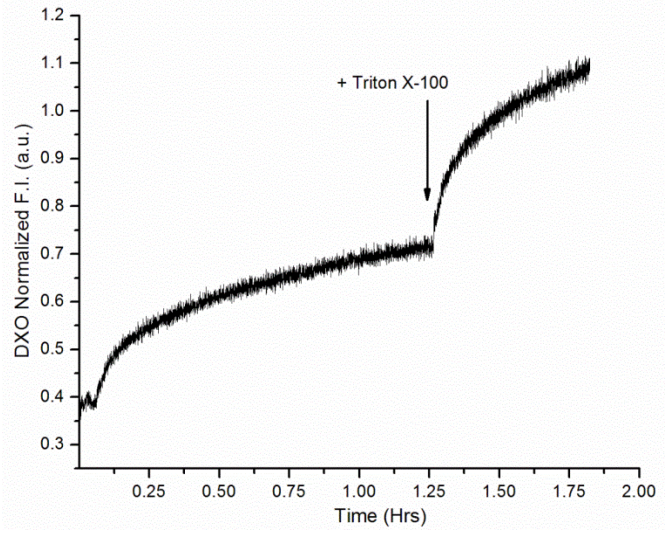

Figure 28: Elution profile of liposomal drug separation from free DXO (A) and (B) DXO release from liposomes in Tris-HCl buffer (50mM Tris, 10mM EDTA, 0.02% NaN_3 at pH 7.2) followed by addition of detergent (0.2% triton x-100) to determine maximum fluorescence.

First, drug release from liposomes with and without PLFE is compared. The rate constants (*k*) of drug release from 100 mol% DPPC, 80 mol% DPPC/20 mol% PLFE, and 70 mol% DPPC/30 mol% PLFE were determined at room temperature, 37 °C, and 41-42°C. 100 mol% DPPC liposomes exhibited a drastic increase in rate constant when temperature was increased from room temperature to 37°C, comparably, PLFE containing liposomes have much smaller release rate constant at 37°C. Liposomes with PLFE show more than 2 fold smaller rate constant than those without PLFE at both room temperature and 37°C (Figure 29). These data agree with the previous finding that PLFE liposomes are stable at 37°C (Figure 23-1) and that PLFE containing membrane is tightly packed (Figure 22) which results in slower drug release. Interestingly, when temperature is increased to above 41°C the rate constant changes dramatically for DPPC/PLFE liposomes (Figure 29) which is also consistent with our previous data which show that increasing the temperature affects the DPPC/PLFE liposomes' membrane and surface properties (Figure 23-1). Particularly, 30 mol% PLFE containing liposomes have higher *k* when temperature is increased to ~42 °C compared to 20 mol% PLFE. Increasing the temperature to 42 °C changes the membrane fluidity (Figure 22), the surface properties (Figure 24), the lipid mobility and order (Figure 25-27) of 70 mol% DPPC/30 mol% PLFE liposomes which results in an increase in drug release.

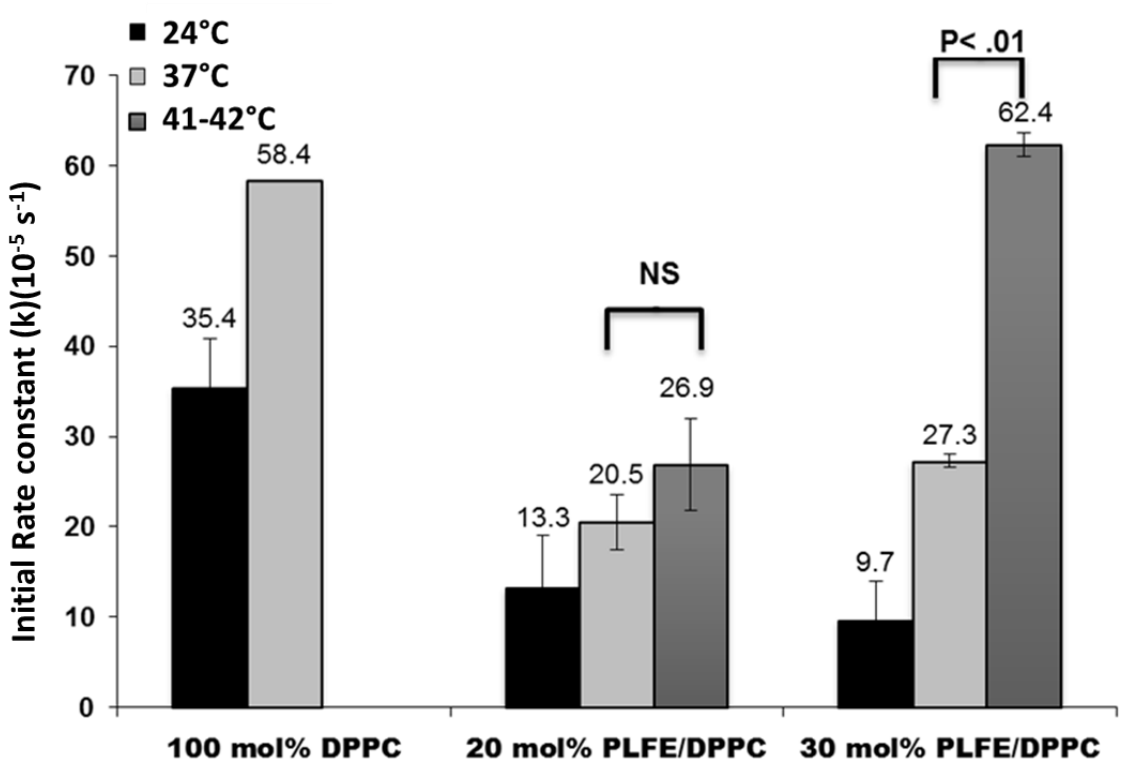

Figure 29: The rate constant (*k*) of DXO release from liposomes with 0, 20, and 30 mol% PLFE (~160-170nm) at 24°C, 37 °C , and 41-42 °C.

Liposomes with ~200 µM doxorubicin entrapped in 100 mol% DPPC, 20 mol% PLFE, 30 mol% PLFE liposomes dispersed in Tris-HCl buffer pH 7.2 (170-200 nm). Liposomal drug was collected after separation from free drug using Sephadex G-50. Liposomes were then analyzed in ISS K-2 fluorometer to observe changes in DXO fluorescence over time. NS = not significant

.

2.5.2 Drug release from 70 mol% DPPC 30 mol% PLFE in buffer and human blood serum

A thorough temperature dependent drug release study was performed using 70 mol% DPPC/30 mol% PLFE liposomal DXO. The temperature range examined was 20-45°C. The rate constants for drug release in both Tris-HCl buffer and in human blood serum were determined at different temperatures (Figure 30). The initial rate constant *k* of DXO release is low in both buffer and serum at temperatures below 37°C (Figure 30). The rate constant increased significantly, in both buffer and serum, when temperature was increased from 37°C to 41°C. Liposomes with passively and actively entrapped DXO in buffer and in serum have the highest *k* near ~41.5 °C, close to ZP transition temperature of 30 mol% PLFE in DPPC (Figure 30). The *k* value decreases a little when temperature was increased from 42°C to 45°C in both buffer and blood serum. At most temperatures, the *k* values observed in serum are smaller. This difference is possibly due to the presence of proteins and small molecules in the blood interacting with liposome surface (Gaber et al., 1995). Also, at all temperature, *k* values are lower for liposomal DXO entrapped using passive loading for the reason being that passive loading method yields lower DXO entrapment efficiency (~40%) than liposomes entrapment using active loading method (~94%).

Overall, in both buffer and serum, *k* is noticeably higher when the temperature is increased from 37°C to ~42°C. It is important to note that, in serum, 70 mol% DPPC/30 mol% PLFE liposomes still exhibits a 2 times increase in *k* when the temperature was increased to ~42°C which demonstrates the potential usefulness of this formulation as a temperature-sensitive drug carrier *in-vivo*.

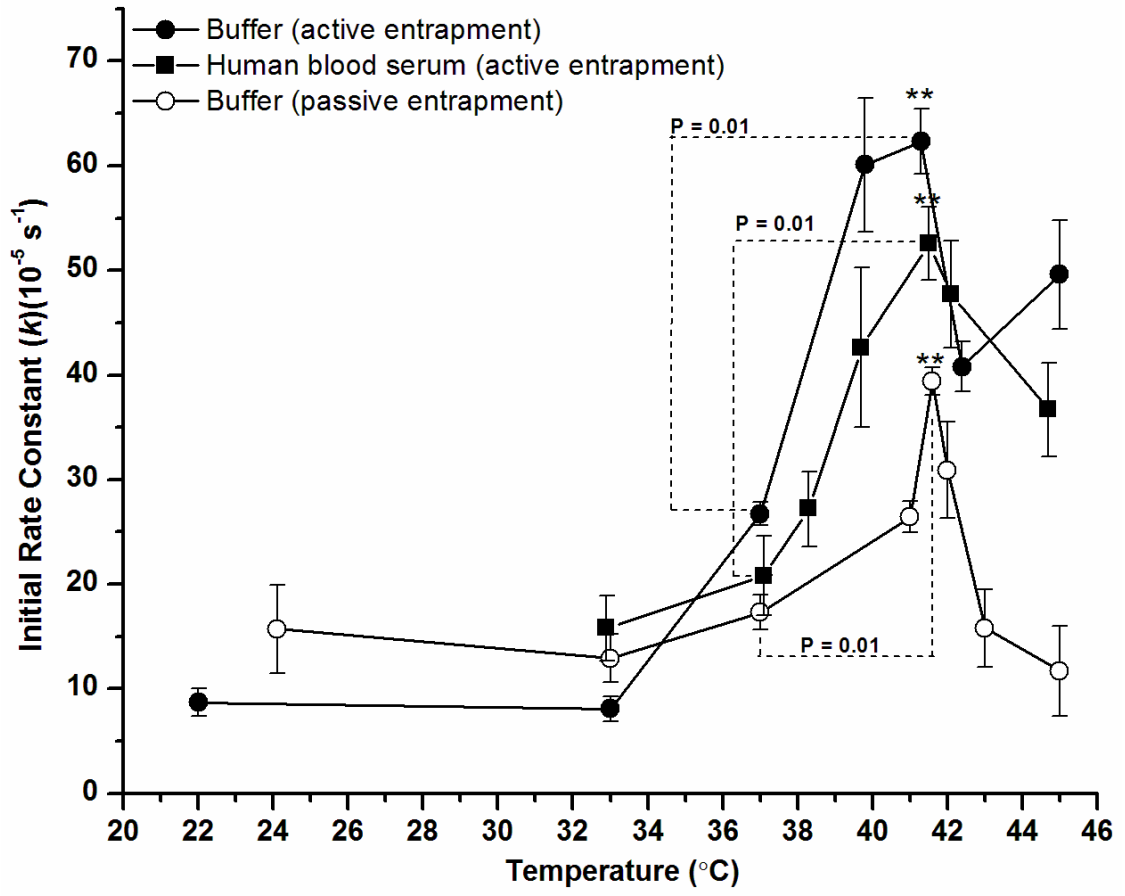

Figure 30: Effect of temperature on the rate constant of doxorubicin(DXO) release from 70 mol% DPPC/30 mol% PLFE liposomes in Tris-HCl buffer (using passive and active entrapment) and in human blood serum

Liposomes containing 200 µM DXO were separated from free drug using a Sephadex G-50 size exclusion column and incubated in cuvette at the desired temperature (between 20-45°C). Drug release was monitored for 1 hour using DXO fluorescence in Tris-HCL buffer or in 50% human blood serum in HBS buffer. Blood plasma was isolated from healthy donors then used after removal of coagulating factors (serum). **$p<0.05$

2.5.3 Observing in-vitro drug release in MCF-7 cells using confocal microscope

In the previous section, it was demonstrated that, at physiological temperature, the drug release *k* is much smaller from 70 mol% DPPC /30 mol% PLFE liposomes than 100 mol% DPPC liposomes (Figure 29). Using confocal microscopy, we have also studied *in-vitro* drug release in MCF-7 cells treated with free DXO and liposomal doxorubicin with 0 and 30 mol% PLFE. Figure 31-1 shows cells treated with free DXO or liposomal DXO for 30min-1 hour after 15 min incubation at 37°C (control) or at 41.6°C (hyperthermia treatment) (Diagram 5). Cells were observed using fluorescence of nuclear dye Hoechst (blue) and doxorubicin (red). Cells without hyperthermia treatment (control, 37°C) display DXO fluorescence in the nucleus after 30 min, and even higher DXO fluorescence is observed after 1 hour. Cells treated with 70mol%DPPC/30mol%PLFE liposomal DXO at 37°C show little drug in the nucleus after 30 min and 1 hour treatment, however, some DXO fluorescence was also observed in the cytoplasm (Figure 31-1). All hyperthermia treated cells display higher DXO fluorescence inside nucleus after 30 min and even more after 1 hour. The biggest difference was observed between hyperthermia treated and control groups after treatment with 70mol%DPPC/30mol%PLFE liposomal DXO. Hyperthermia treatment increases drug release which explains the significantly high DXO fluorescence observed after treatment with 70 mol% DPPC/30 mol% PLFE liposomal DXO. But, when cells were incubated at 37°C with 70 mol% DPPC/30 mol% PLFE, little DXO was released and therefore lower DXO fluorescence was observed in the nucleus (Figure 31-1, 37°C).

PLFE lipids in the liposomal formulation reduce drug release at 37°C by increasing stability of liposomes.

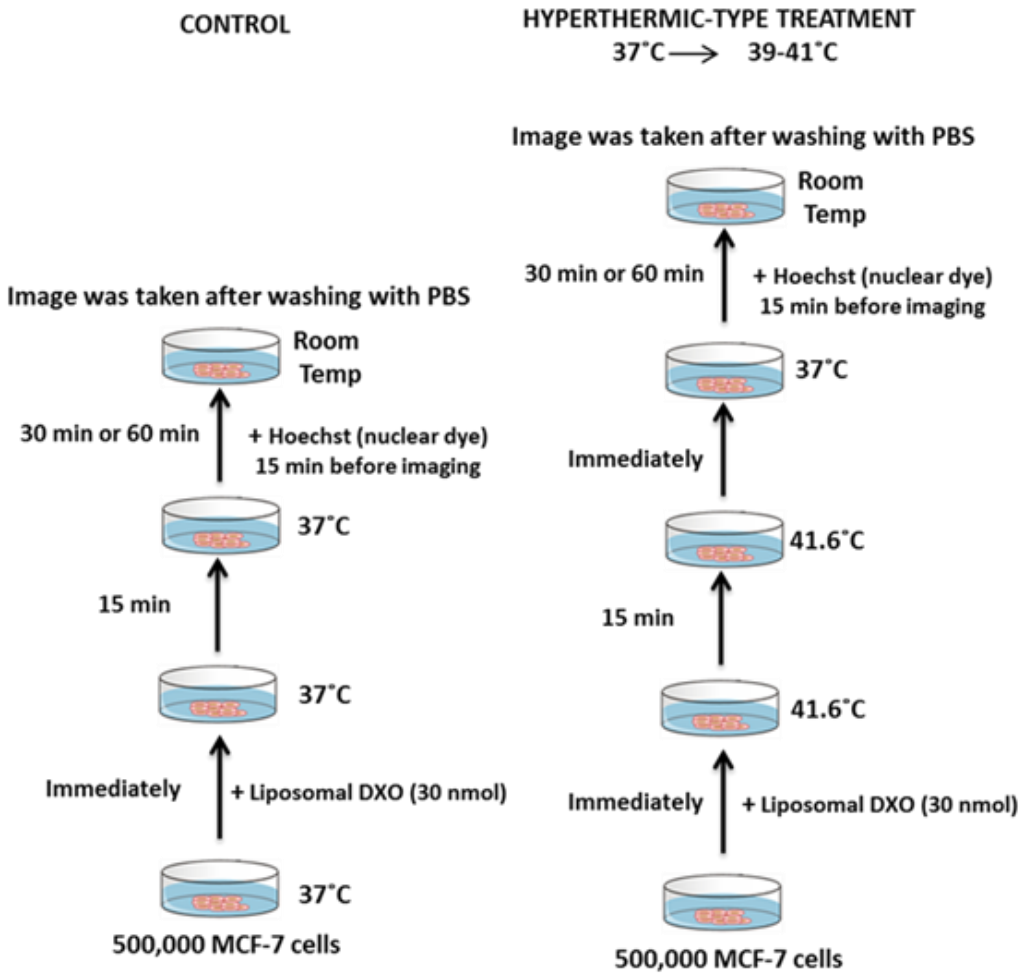

Diagram 5: Experimental setup for imaging MCF-7 cells after treatment with free DXO and liposomal DXO (30 min and 60 min) with or without (control) hypothermic treatment (41.6°C**).**

500,000 MCF-7 cells were plated in a Mat-tak glass bottom dish. Then, cells were treated with 30 nmol of free DXO or liposomal DXO and immediately put into incubator set at either 37°C (control) or 41.6°C (hyperthermia treatment) for 15 minutes. Afterwards, dishes containing cells with drugs were incubated at 37°C for additional 30 or 60 minutes. Nuclear dye, Hoechst, was added to cells 15 minutes prior to imaging. Treated and stained cells were washed with 1x PBS. Images were taken under Zeiss LSM 510 META (Jena, Germany).

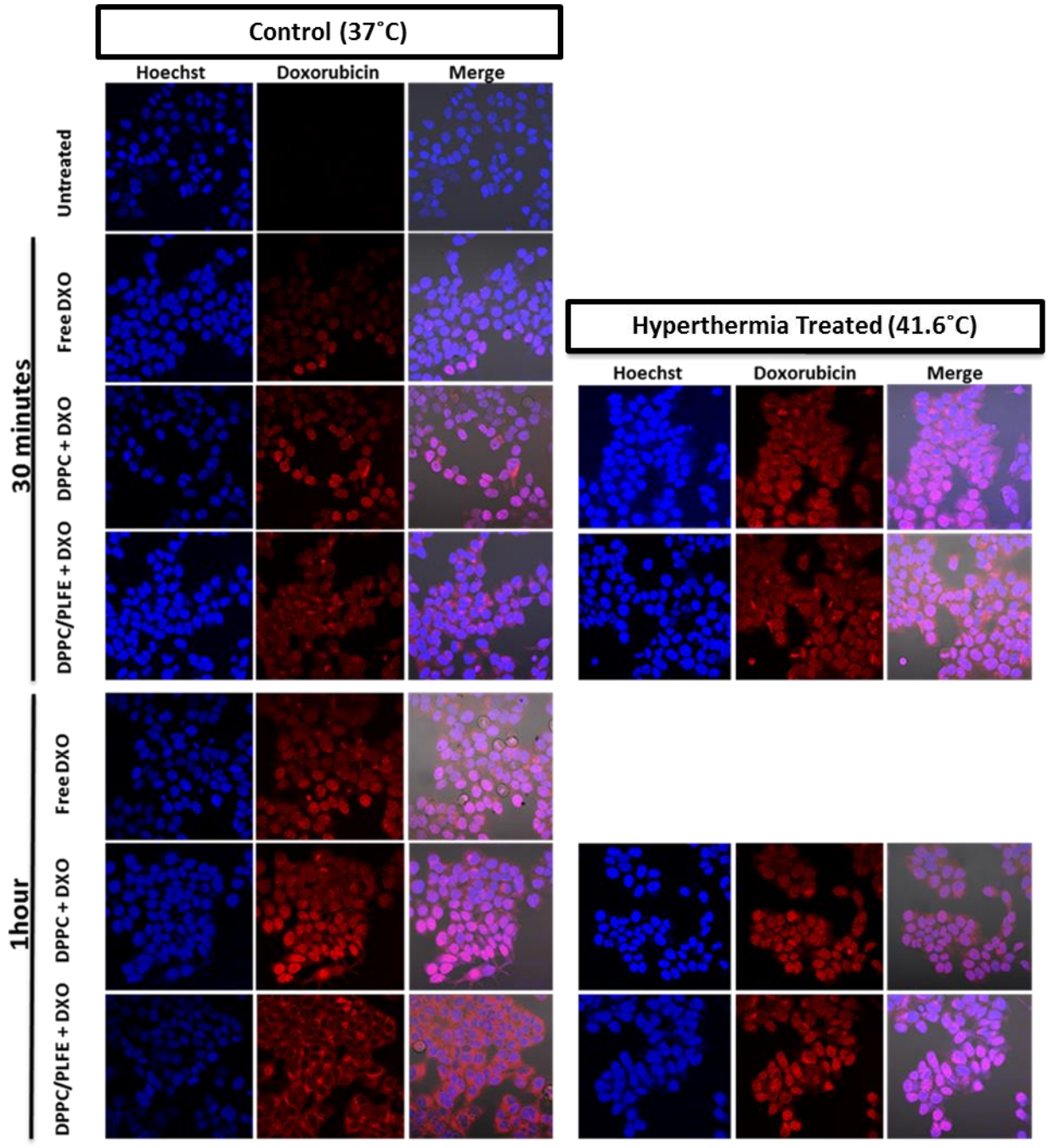

Figure 31-1: MCF-7 cells treated with 10 µM of free DXO, 100 mol% DPPC liposomes , and 70 mol% DPPC /30 mol% PLFE liposomes containing doxorubicin (in buffer) for 30 minutes or 1 hour after 15 min incubation at 37°C (control) or 41.6 °C (hyperthermia treatment).

More notably, cells exhibit higher fluorescence in the nucleus after combination of hyperthermia treatment (41-42°C) and either 100 mol% DPPC or 70 mol% DPPC/30 mol% PLFE liposomal DXO (Figure 31-2B & C). However, cells that were treated with liposomal DXO alone display significantly less DXO fluorescence inside the cell nucleus. The highest DXO fluorescence was observed at 41.6°C when cells were treated with 70 mol% DPPC/30 mol% PLFE liposomal DXO for 1 hour. Cells treated with 70 mol% DPPC/ 30 mol% PLFE liposomes have lower DXO fluorescence in the nucleus at 37°C, but a significantly higher DXO fluorescence at 41.6°C which correlates with the drug release study. This occurrence was not obvious with 100 mol% DPPC DXO treated cells (Figure 31-1, Figure 31-2B), in which DXO fluorescence in the nucleus was almost as equally high at both temperatures. *In vitro* imaging study demonstrates that treatment with 70 mol% DPPC/30 mol% PLFE liposomal DXO and mild hyperthermia (41.6°C) increases intracellular DXO, considerably more than the control (37°C), as a result of slower DXO release at 37°C and faster release at 41.6°C (Figure 30).

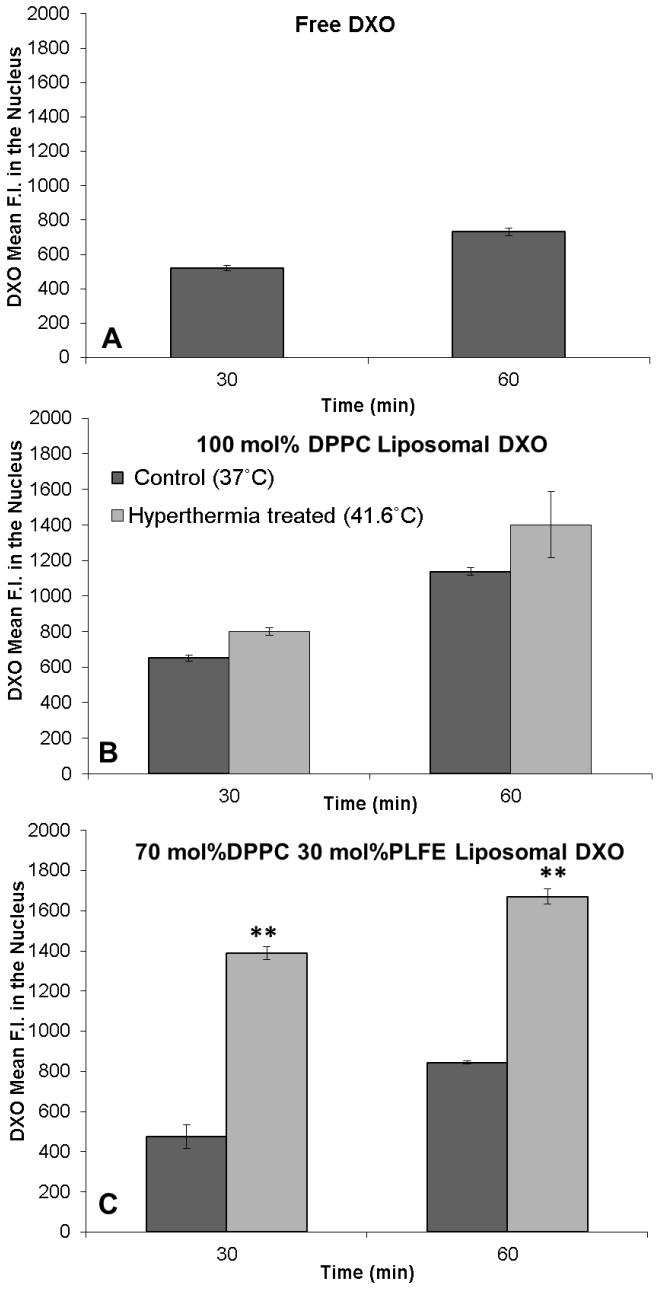

Figure 31-2: DXO Fluorescent intensity (F.I.) in the nucleus after treatment with free doxorubicin, 100 mol % DPPC liposomal doxorubicin and 70 mol% DPPC 30 mol% PLFE liposomal doxorubicin

Fluorescent intensity (F.I.) of DXO in the nucleus was measured after treatment with free doxorubicin (A) 100 mol % DPPC liposomal doxorubicin (B) and 70 mol% DPPC 30 mol% PLFE liposomal doxorubicin (C) was measured and compared between control (37°C) and hyperthermia treated (~41.6°C) cells (see Diagram 5). **$p<0.05$

2.6 DPPC/PLFE Liposomes Induce Toxicity to Cells in Response to Hyperthermia

To test how hyperthermia treatment (from 37°C to ~42°C) affects the cytotoxicity of 70 mol% DPPC/30 mol% PLFE DXO liposome to cells, cells were briefly incubated at 41.6-42 °C with DXO liposomes for 15 minutes, then, continued incubating at 37 °C. Concurrently, a control was set up (without incubation at 42°C) to compare the result of hyperthermia treated cells. Then, cell cytotoxicity assay was performed to determine cell death. Figure 32 reveals that free DXO has a higher killing effect than liposomal DXO. Treatment with 100 mol% DPPC, 70 mol% DPPC 30 mol% PLFE, and 100 mol% PLFE liposomal DXO results in much less toxicity compared to free doxorubicin most likely due to the drug being entrapped inside liposomes (Figure 32). When cells are treated with a higher dose of liposomal drug, the percent of cell death increases to ~40% (Figure 32). This effect is even greater when combination of hyperthermia treatment and liposomal DXO is used, in which case, almost 50% cell death occurs at greater than 20μM liposomal DXO concentrations. Treatment with 100 mol% PLFE liposomes does not show much difference in cell viability with or without applying hyperthermia (i.e. at ~42 °C) there was a slight increase in toxicity with free DXO treated cells after applying hyperthermia (Figure 32). Also, untreated cells did not show significant cell death when hyperthermia treatment was used. From these studies it is evident that utilizing hyperthermia treatment with 70 mol% DPPC/30 mol% PLFE liposomal DXO increases liposome drug release (Figure 30) and increases DXO localization in the nucleus (Figure 31) which results in more cell death.

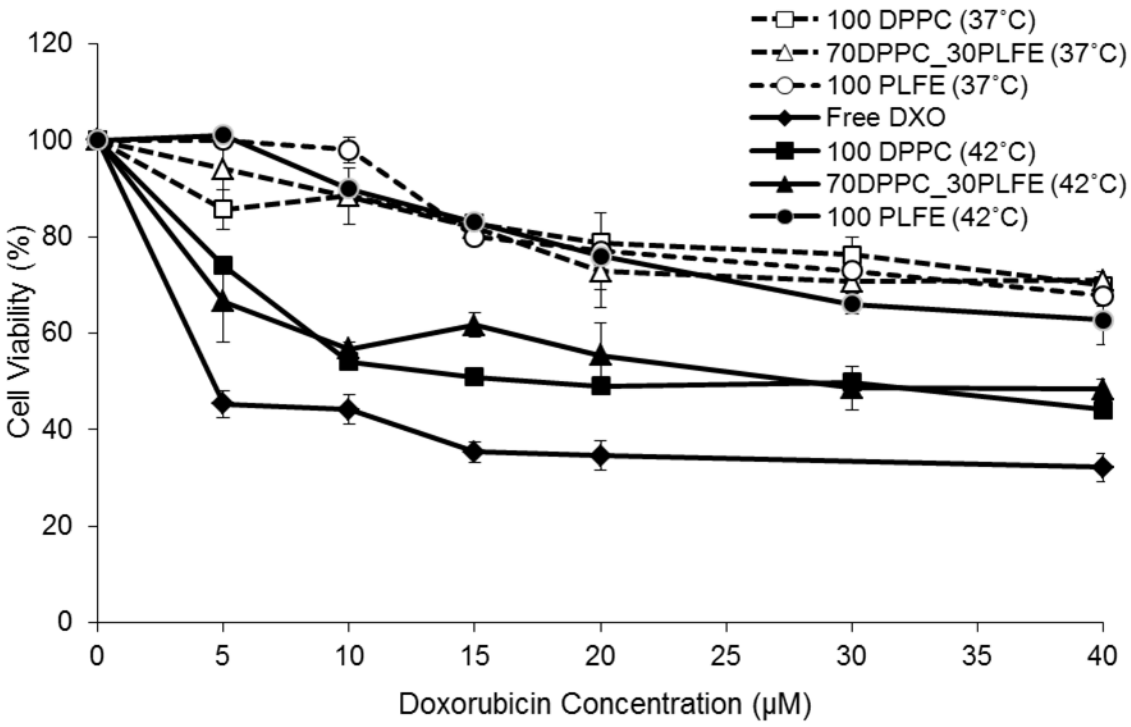

Figure 32: MCF-7 cell cytotoxicity after treatment with 0- 40 μM DXO in the form of free and 100 mol% DPPC, 70 mol% DPPC/30 mol% PLFE, or 100 mol% PLFE liposomal doxorubicin for 24 hours.

CHAPTER 4: DISCUSSION

First Generation of Liposomal Drugs

One hundred years ago, Paul Ehrlich received the Nobel Prize for Physiology and Medicine for discovering chemotherapy and conceptualizing “magic bullets”, personalized medicine which can cure patients by selectively targeting harmful cells. His idea initiated the synthesis of chemical compounds that behave in a specific manner within the physiological environment and generated numerous chemotherapeutics against cancer. Some of his first efforts included the development of small molecular drugs that target the cancer cell’s replicating DNA and mutated proteins to inhibit proliferation, invasion, and metastasis(Strebhardt & Ullrich, 2008). Also, he developed monoclonal antibody drug conjugates, which can recognize specific cell surface markers (Strebhardt & Ullrich, 2008). After Ehrilich’s accomplishments, scientists tried to achieve his vision of the “magic bullets” by focusing on finding an agent that can target diseased cells in a highly specific manner. More than a decade of research generated an interest in nanocarriers which could be used to deliver drugs to a target. One of the firsts to describe liposomes was Alec Bingham and colleagues, and Gregory Gregoriadis was one of the early pioneers to conceptualize liposomes for drug delivery (Allen & Cullis, 2013). After showing success in the laboratory and in clinical trials, the first generation of liposomal drug carriers were subsequently approved by the FDA to be used for treating diseases (H. L. Chang & Yeh, 2012; Tila et al., 2015).

The first generation of liposomal drugs passively delivered drugs to the leaky tumor vasculatures. In tumor blood vessels, gaps between endothelial cells, normally 5-10 nm, widen to 100-780 nm, as a result, liposomes are able to accumulate at the tumor site(H. A. Deshpande, Gettinger, & Sosa, 2008); this is also known as the enhanced permeability and retention or EPR effect. Liposomes are designed to be between 100-200 nm in size, and the composition, size, surface characteristic, fluidity of the bilayer are studied to determine the liposomes' behavior in the biological environment (Pathak & Thassu, 2009). Original liposomal drugs, without much manipulation, improve the therapeutic index of free drugs and lower the toxicity. For example, liposomal doxorubicin, Myocet, increases half-life of free doxorubicin hydrochloride from several hours to 16-50 hours and decreases cardio-toxicity significantly (Pillai, 2014). Furthermore, Caelyx and Lipodox, PEgylated liposomal doxorubicin formulations, improve the half-life to 72 hours (Pillai, 2014). However, there are problems associated with PEGylate liposomes which includes higher toxicity than Myocet (non-PEGylated), hypersensitivity, and skin reaction (Barenholz, 2012; Pillai, 2014). To improve the formulation, researchers concentrated on developing the second generation of liposomal drugs with decreased toxicity, better targeting specificity and more controllable release. Addition of proteins, small molecules, polymers to increase the stability and the opportunity for the liposomes to reach the target as well as developing liposomes with the ability to release drugs using external stimuli are some strategies that have been utilized to design the second generation of liposomal delivery systems.

Second Generation of Liposomal Drug Delivery Systems

Creating multifunctional liposomes for targeting tumor is a promising approach to deliver drugs for cancer treatment. One strategy to improve the formulation of conventional liposome is by incorporating PS recognizing molecules to gain better specificity to diseased tissues. PS is a biomarkers for a wide range of diseases. PS is exposed on the lining of tumor vasculatures (Stafford & Thorpe, 2011; Zhou et al., 2014), and found on the surfaces of lung, ovarian, prostate and other types of cancer cells(Borst & Elferink, 2002; Ran & Thorpe, 2002; Riedl et al., 2011; Zwaal et al., 2005).PS is also exposed in some non-cancer related diseases such as in heart disease, braid injuries and at the site of any injured tissues. (Schutters & Reutelingsperger, 2010; Sipkens et al., 2011) The level of PS exposure between different disease conditions and between different cancer cells varies, but PS is significantly elevated in diseased cells than in normal cell surfaces (Borst & Elferink, 2002; Ran & Thorpe, 2002).

When administered systemically using intravenous injections, PS-targeting liposomes have the potential to target PS-exposed cells, tissues, and endothelial cells of tumor vasculature (Ran et al., 2005; Schutters & Reutelingsperger, 2010; Zhou et al., 2014). Moreover, while use of radiation alone can lead to resistance, local radiation therapy can increase PS exposure in tumor endothelial cells (He, Luster, & Thorpe, 2007), which allows radiation to be used in combination with PS- targeted liposomal drugs for a more effective treatment. Unfortunately, the PS targeting nanoparticles that are currently being studied are developed for imaging and diagnosis purposes (Garnier et al., 2009; Zhang et al., 2014). Therefore, there is a need for PS-targeting drug carriers

because they have the potential to target a broad range of diseases and can be used in combination with radiation therapy.

The lipid-based PS targeted nanoparticles that are discussed in the literature (Qi et al., 2009; Turkyilmaz et al., 2014; Zhang et al., 2014) have to overcome some limitations in order to be used as drug delivery systems. Therefore, an alternative PS-targeting liposomal system is proposed for the purpose of drug delivery. First, most PS targeting liposomes are created with large proteins, antibody and molecules conjugated on the liposome surface (Qi et al., 2009; Zhang et al., 2014). Because of the size of these molecules, maintaining the structural stability and long shelf-life is challenging. Yet, achieving high stability is essential for the use of liposomes for therapy. Protein conjugated liposomes, for example, PS-binding protein annexin V conjugated to PEgylated-malamide lipids containing liposomes, aggregate easily if protein density per liposome is too high (Garnier et al., 2009). Therefore, to avoid structural instability and interaction between the protein and bulky lipid head-groups, very little annexin V is used which can affect the affinity to PS (Garnier et al., 2009; Loughrey et al., 1990). To create a stable PS-targeting liposomal system, we used hydrophobic Zn-DPA called DPA-Cy3[22,22] which spontaneously forms liposomes with POPC lipids. Applying this method, various molar ratios of DPA-Cy3[22,22] to POPC can be used to generate 100-200 nm size liposomes. When DPA-Cy3[22,22] was used in liposomes with POPC, very high level of PS binding molecules (17 mol% DPA-Cy3[22,22] to POPC) can be incorporated to create vesicles. We found that 4.8 mol% or less DPA-Cy3[22,22] in POPC results in liposomes that maintain size stability for at least a few weeks. In

summary, DPA-Cy3[22,22]/POPC liposomes can be prepared easily and have the potential to carry hydrophobic or hydrophilic drugs for delivery.

The second challenge in developing PS targeted liposome for therapy is to ensure that liposomes can bind their target effectively. One major limitation for PS-targeting annexin V-conjugated liposomes is that annexin V binding to PS depends on high Ca^{2+} level which is difficult to control in physiological conditions (Garnier et al., 2009; Niu & Chen, 2010). In contrast, Zn-DPA conjugated liposomes do not need Ca^{2+} to bind PS surfaces (Turkyilmaz et al., 2014). And, the amount of DPA content on the liposome surface can vary, which can alter the affinity to PS (Loughrey et al., 1990). We found that liposomes prepared with hydrophobic DPA-Cy3[22,22] and POPC bind to cells in a Ca^{2+}-independent manner. Also, it was demonstrated that DPA-Cy3[22,22]/POPC liposomes bind to cells *in vitro*, and cell binding increases upon increasing the amount of DPA-Cy3[22,22] in liposomes

Third, for successful intracellular delivery, PS-targeted liposomes must be internalized by cells and escape endosomal degradation. PEGylated lipids, used to incorporate the PS or PE binding proteins and molecules on the liposome surface and to increase longevity in blood, reduce cellular uptake and can result in endosomal degradation (P. Deshpande, Biswas, & Torchilin, 2013). However, DPA-Cy3[22,22]/POPC liposomes do not contain PEGylated lipids and display binding and entry by cells. Also, our microscopy study showed that the internalization of DPA-Cy3[22,22]/POPC liposomes results in nuclear localization perhaps by evading endosomal degradation (Figure 17). When considering PS-targeting liposomes for drug

delivery *in-vivo*, DPA-Cy3[22,22]/POPC liposomes are likely to be stable and are able to carry drugs to the site of interest.

Local hyperthermia treatment also known as thermal therapy or thermotherapy could be used to treat cancer but does not show promising results when used alone (Gasselhuber, Dreher, Rattay, Wood, & Haemmerich, 2012; Kong et al., 2001). It is then of interest to develop thermosensitive liposomal carriers that can be used in conjunction with hyperthermia treatment for controlled drug release. The FDA approved thermosensitive liposomes (TSL) currently available in the market and in clinical trials such as Thermodox and Arikace claim to release entrapped, drugs within 5-10 min upon hyperthermia treatment (Chen et al., 2014; Gaber et al., 1995; Pillai, 2014). The primary component of mentioned and other TSL formulations is DPPC lipid. DPPC lipid with a phase transition of ~41.6°C is advantageous for thermosensitive formulation because it exhibits an increase in the membrane fluidity as a result of transitioning from gel-to-liquid state. The original TSL, containing DPPC and 1,2-Distearoyl-sn-glycero-3-phosphorylcholine (DSPC)(May & Li, 2012), is a thermosensitive drug carrier that can release drug when the temperature is increased from 37°C to 42.5°C-44.5°C. PEGylated TSL, similar to the original TSL formulation, is composed of DPPC and DSPC as well as DSPE-PEG lipids. As discussed previously, PEGylated lipids increase blood circulation time but has some disadvantages such as lower drug loading and cellular uptake (May & Li, 2012). Moreover, some TSL formulations use cholesterol (e.g., DPPC/HSPC/Chol/PEG-PE) to stabilize the liposomes. The addition of cholesterol in TSL can lead to changes in membrane properties in a very complicated manner (Beck et al., 2007; May & Li, 2012; Venegas et al., 2012). Besides, the use of cholesterol can

increase the blood cholesterol level which may result in harming patients with cardiovascular diseases. For these challenges, an alternative formulation such as DPPC/PLFE hybrid system was explored in this study to reduce the possible side effects of liposomal drugs.

Like many other formulations, DPPC/PLFE hybrid archaeosomes consist of DPPC lipids. However, exclusively, this formulation contains archaea BTL PLFE lipids, which makes the liposomal system novel. PLFE lipids in DPPC/PLFE liposomes provides similar advantages as cholesterol without causing toxicity (Daswani, 2015; Z. Li et al., 2010). Liposomes with 20-100 mol% of PLFE yields incredibly stable liposomes. More interestingly, we found that at particular PLFE mole fractions (20-30 mol% PLFE), liposomes behave in temperature-dependent manner. Raising the temperature from the physiological temperature (37°C) to hyperthermic treatment temperature (41-42°C) induces change in membrane surface and packing of 70 mol% DPPC/30 mol% PLFE liposome formulation. At 37°C, 70 mol% DPPC/30 mol% PLFE liposomes have very slow DXO release, and with hyperthermia treatment (41-42°C), liposomes increase DXO release and cytotoxic in cells. Other TSL formulations also show lower drug leakage at physiological temperatures (37°C) and faster drug leakage upon hyperthermia treatment, but TSL liposomes with cholesterol require hyperthermia treatment at or above 43°C for maximum drug release. Unfortunately, using higher temperatures increases the chance of vascular hemorrhage and thermal ablation (Al-Jamal et al., 2012; Kneidl et al., 2014; Kong et al., 2001). PLFE lipids can be a better stabilizing agent because unlike cholesterol, PLFE is not limited by membrane solubility. When cholesterol content exceeds 67 mol%, cholesterol precipitates out of the membrane (Huang, Buboltz, &

Feigenson, 1999). However, PLFE increases stability and membrane order of liposome even at 100 mol% PLFE. Therefore, 70 mol% DPPC/30 mol% PLFE liposomes overcome the limitations of other formulations that contain either cholesterol or PEGylated lipids and can be used in combination with local hyperthermia treatment for maximizing drug release.

Conclusions & Future Directions

In summary, in this study, we utilized characterization techniques to select and optimize the right formulations of liposomal carriers that can be used for drug/DNA/shRNA delivery. We found two liposomal systems with potential to deliver drugs better than first generation liposomal drugs or passive delivery systems. These two delivery liposomal systems can (1) target PS on the diseased surface and (2) release drug in response to local hyperthermia. The *in-vitro* studies show that both liposomal systems are potentially useful. The next step in testing DPA-Cy3[22,22]/POPC liposomes as carrier is to entrap highly potent drugs/siRNA into DPA-Cy3[22,22]/POPC liposomes, study drug release and demonstrate successful delivery of drugs or siRNA in cells and in animals. Also, in order to enhance the specificity of DPA-Cy3[22,22]/POPC liposomes to cancer cells, addition of multiple target molecules into the liposomal formulation should be explored. TSL 70 mol% DPPC/30 mol% PLFE hybrid archaeosomes have great potential for delivering drugs and inducing cytotoxicity *in vitro* when used in combination with hyperthermia treatment. Next, it is important to conduct *in vivo* studies to test the ability of the 70 mol% DPPC/30 mol% PLFE hybrid archaeosomes to deliver drugs and to determine the bio-distribution of liposomes after administration into small

animals. It is also necessary to explore the option of adding target molecules to generate multifunctional drug carriers which have the ability to target diseased cells and to maximize drug release upon hyperthermia treatment.

REFERENCES

Al-Jamal, W. T., Al-Ahmady, Z. S., & Kostarelos, K. (2012). Pharmacokinetics & tissue distribution of temperature-sensitive liposomal doxorubicin in tumor-bearing mice triggered with mild hyperthermia. *Biomaterials, 33*(18), 4608-4617.

Allen, T. M., & Cullis, P. R. (2013). Liposomal drug delivery systems: From concept to clinical applications. *Advanced Drug Delivery Reviews, 65*(1), 36-48.

Amselem, S., Gabizon, A., & Barenholz, Y. (1990). Optimization and upscaling of doxorubicin-containing liposomes for clinical use. *J. Pham. Sci., 79*, 1045-1052.

Anyarambhatla, G., & Needham, D. (1999). Enhancement of the phase transition permeability of DPPC liposomes by incorporation of MPPC: A new temperature-sensitive liposome for use with mild hyperthermia. *Journal of Liposome Research, 9*(4), 491-506.

Bagatolli, L. A., Gratton, E., Khan, T. K., & Chong, P. L. (2000). Two-photon fluorescence microscopy studies of bipolar tetraether giant liposomes from thermoacidophilic archaebacteria *sulfolobus acidocaldarius*. *Biophysical Journal, 79*(1), 416-425.

Banno, B., Ickenstein, L. M., Chiu, G. N., Bally, M. B., Thewalt, J., Brief, E., et al. (2010). The functional roles of poly(ethylene glycol)-lipid and lysolipid in the drug retention and release from lysolipid-containing thermosensitive liposomes in vitro and in vivo. *Journal of Pharmaceutical Sciences, 99*(5), 2295-2308.

Barenholz, Y. (. (2012). Doxil (R) - the first FDA-approved nano-drug: Lessons learned. *Journal of Controlled Release, 160*(2), 117-134.

Batist, G., Ramakrishnan, G., Rao, C. S., Chandrasekharan, A., Gutheil, J., Guthrie, T., et al. (2001). Reduced cardiotoxicity and preserved antitumor efficacy of liposome-encapsulated doxorubicin and cyclophosphamide compared with conventional doxorubicin and cyclophosphamide in a randomized, multicenter trial of metastatic

breast cancer. *Journal of Clinical Oncology : Official Journal of the American Society of Clinical Oncology, 19*(5), 1444-1454.

Beck, J. G., Mathieu, D., Loudet, C., Buchoux, S., & Dufourc, E. J. (2007). Plant sterols in "rafts": A better way to regulate membrane thermal shocks. *FASEB Journal : Official Publication of the Federation of American Societies for Experimental Biology, 21*(8), 1714-1723.

Belhocine, T. Z., & Prato, F. S. (2011). Transbilayer phospholipids molecular imaging. *EJNMMI Research, 1*(1), 17-219X-1-17.

Borst, P., & Elferink, R. O. (2002). Mammalian ABC transporters in health and disease. *Annual Review of Biochemistry, 71*, 537-592.

Brown, D. A., Venegas, B., Cooke, P. H., English, V., & Chong, P. L. (2009). Bipolar tetraether archaeosomes exhibit unusual stability against autoclaving as studied by dynamic light scattering and electron microscopy. *Chemistry and Physics of Lipids, 159*(2), 95-103.

Chang, H. I., & Yeh, M.K. (2012). Clinical development of liposome-based drugs: Formulation, characterization and therapeutic efficacy. *International Journal of Nanomedicine, 7*, 49-60.

Chang, E. L., & Lo, S. L. (1991). Extraction and purification of tetraether lipids from *sulfolobus acidocaldarius*. *Protocols for archaebacterial research* (Fleischmann, E.M.; Place, A.R.; Robb, R.T.; Schreier, H.J. ed., pp. 2.3.1-2.3.14). Baltimore, MD: Maryland Biotechnology Institute.

Chen, J., He, C. Q., Lin, A. H., Gu, W., Chen, Z. P., Li, W., et al. (2014). Thermosensitive liposomes with higher phase transition temperature for targeted drug delivery to tumor. *International Journal of Pharmaceutics, 475*(1-2), 408-415.

Chong, P. L. G., Cossins, A. R., & Weber, G. (1983). A differential polarized phase fluorometric study of the effects of high hydrostatic pressure upon the fluidity of cellular membranes. *Biochemistry (John Wiley & Sons), 22*(2), 409-415.

Chong, P. L., Ravindra, R., Khurana, M., English, V., & Winter, R. (2005). Pressure perturbation and differential scanning calorimetric studies of bipolar tetraether liposomes derived from the thermoacidophilic archaeon *sulfolobus acidocaldarius*. *Biophys.J., 89*, 1841-1849.

Chong, P. L, Sulc, M., & Winter, R. (2010). Compressibilities and volume fluctuations of archaeal tetraether liposomes. *Biophys. J., 99*, 3319-3326.

Chong, P. L.-G., & Weber, G. (1983). Pressure dependence of 1,6-diphenyl-1,3,5-hexatriene fluorescence in single-component phosphatidylcholine liposomes. *Biochemistry, 22*, 5544-5550.

Chu, Z., Abu-Baker, S., Palascak, M. B., Ahmad, S. A., Franco, R. S., & Qi, X. (2013). Targeting and cytotoxicity of SapC-DOPS nanovesicles in pancreatic cancer. *PloS One, 8*(10), e75507.

Daswani, V. P. (2015). *Fluorescence and aggregation properties of the anti-cancer drug CA4P in archaeal liposomes.* Unpublished Ph.D., Temple University School of Medicine, Philadelphia, PA.

Davis, M. E., Chen, Z., & Shin, D. M. (2008). Nanoparticle therapeutics: An emerging treatment modality for cancer. *Nature Reviews Drug Discovery, 7*(9), 771-782.

Deshpande, P., Biswas, S., & Torchilin, V. P. (2013). Current trends in the use of liposomes for tumor targeting. *Nanomedicine, 8*, 1509-1528.

Deshpande, H. A., Gettinger, S. N., & Sosa, J. A. (2008). Novel chemotherapy options for advanced thyroid tumors: Small molecules offer great hope. *Current Opinion in Oncology, 20*(1), 19-24.

DiVittorio, K. M., Leevy, W. M., O'Neil, E. J., Johnson, J. R., Vakulenko, S., Morris, J. D., et al. (2008). Zinc(II) coordination complexes as membrane-active fluorescent probes and antibiotics. *Chembiochem : A European Journal of Chemical Biology, 9*(2), 286-293.

Dreher, M. R., Liu, W., Michelich, C. R., Dewhirst, M. W., Yuan, F., & Chilkoti, A. (2006). Tumor vascular permeability, accumulation, and penetration of macromolecular drug carriers. *Journal of the National Cancer Institute, 98*(5), 335-344.

Duggan, S. T., & Keating, G. M. (2011). Pegylated liposomal doxorubicin A review of its use in metastatic breast cancer, ovarian cancer, multiple myeloma and AIDS-related kaposi's sarcoma. *Drugs, 71*(18), 2531-2558.

Engeland, M., Nieland, L. J. W., Ramaekers, F. C. S., Schutte, B., & Reutelingsperger, C. P. M. (1998). Annexin v affinity assay: A review on an apoptosis detection system based on phosphatidylserine exposure. *Cytometry, 31*, 1-9.

Faiß, S., Kastl, K., Janshoff, A., & Steinem, C. (2008). Formation of irreversibly bound annexin A1 protein domains on POPC/POPS solid supported membranes. *Biochim. Biophys. Acta., 1778*, 1601-1610.

Fiorini, R., Valentino, M., Wang, S., Glaser, M., & Gratton, E. (1987). Fluorescence lifetime distributions of 1,6-diphenyl-1,3,3-hexatriene in phospholipid vesicles. *Biochem, 26*, 3864-3870.

Frasch, S. C., Henson, P. M., Kailey, J. M., Richter, D. A., Janes, M. S., Fadok, V. A., et al. (2000). Regulation of phospholipid scramblase activity during apoptosis and cell activation by protein kinase c delta. *The Journal of Biological Chemistry, 275*(30), 23065-23073.

Gaber, M. H., Hong, K., Huang, S. K., & Papahadjopoulos, D. (1995). Thermosensitive sterically stabilized liposomes: Formulation and in vitro studies on mechanism of doxorubicin release by bovine serum and human plasma. *Pharmaceutical Research, 12*(10), 1407-1416.

Gabizon, A., & Papahadjopoulos, D. (1992). The role of surface charge and hydrophilic groups on liposome clearance in vivo. *Biochimica Et Biophysica Acta, 1103*(1), 94-100.

Gabizon, A., Peretz, T., Sulkes, A., Amselem, S., Ben-Yosef, R., Ben-Baruch, N., et al. (1989). Systemic administration of doxorubicin-containing liposomes in cancer patients: A phase I study. *European Journal of Cancer & Clinical Oncology, 25*(12), 1795-1803.

Gabizon, A., Shmeeda, H., & Barenholz, Y. (2003). Pharmacokinetics of pegylated liposomal doxorubicin: Review of animal and human studies.. *Clinical Pharmacokinetics,* (42), 419-436.

Garnier, B., Bouter, A., Gounou, C., Petry, K. G., & Brisson, A. R. (2009). Annexin A5-functionalized liposomes for targeting phosphatidylserine-exposing membranes. *Bioconjugate Chemistry, 20*(11), 2114-2122.

Gasselhuber, A., Dreher, M. R., Rattay, F., Wood, B. J., & Haemmerich, D. (2012). Comparison of conventional chemotherapy, stealth liposomes and temperature-sensitive liposomes in a mathematical model. *Plos One, 7*(10), e47453.

Goyal, P., Goyal, K., Kumar, S. G. V., Singh, A., Katare, O. P., & Mishra, D. N. (2005). Liposomal drug delivery systems-clinical applications. *Acta Pharm., 55*, 1-25.

Guo, P., You, J. O., Yang, J., Moses, M. A., & Auguste, D. T. (2012). Using breast cancer cell CXCR4 surface expression to predict liposome binding and cytotoxicity. *Biomaterials, 33*(32), 8104-8110.

Hanshaw, R. G., & Smith, B. D. (2005). New reagents for phosphatidylserine recognition and detection of apoptosis. *Bioorganic & Medicinal Chemistry, 13*(17), 5035-5042.

Haran, G., Cohen, R., Bar, L. K., & Barenholz, Y. (1993). Transmembrane ammonium sulfate gradients in liposomes produce efficient and stable entrapment of amphipathic weak bases. *Biochimica Et Biophysica Acta, 1151*(2), 201-215.

Harashima, H., Iida, S., Urakami, Y., Tsuchihashi, M., & Kiwada, H. (1999). Optimization of antitumor effect of liposomally encapsulated doxorubicin based on simulations by pharmacokinetic/pharmacodynamic modeling. *Journal of Controlled Release : Official Journal of the Controlled Release Society, 61*(1-2), 93-106.

Harris, F. M., Best, K. B., & Bell, J. D. (2002). Use of laurdan fluorescence intensity and polarization to distinguish between changes in membrane fluidity and phospholipid order. *Biochimica Et Biophysica Acta, 1565*(1), 123-128.

He, J., Luster, T. A., & Thorpe, P. E. (2007). Radiation-enhanced vascular targeting of human lung cancers in mice with a monoclonal antibody that binds anionic phospholipids. *Clinical Cancer Research : An Official Journal of the American Association for Cancer Research, 13*(17), 5211-5218.

Huang, J., Buboltz, J. T., & Feigenson, G. W. (1999). Maximum solubility of cholesterol in phosphatidylcholine and phosphatidylethanolamine bilayers. *Biochimica Et Biophysica Acta, 1417*(1), 89-100.

Hunter, R. J., Midmore, B. R., & Zhang, H. (2001). Zeta potential of highly charged thin double-layer systems. *Journal of Colloid and Interface Science, 237*(1), 147-149.

Immordino, M. L., Dosio, F., & Cattel, L. (2006). Stealth liposomes: Review of the basic science, rationale, and clinical applications, existing and potential. *International Journal of Nanomedicine, 1*(3), 297-315.

Iwamoto, T. (2013). Clinical application of drug delivery systems in cancer chemotherapy: Review of the efficacy and side effects of approved drugs. *Biological & Pharmaceutical Bulletin, 36*(5), 715-718.

Iyer, A. K., Khaled, G., Fang, J., & Maeda, H. (2006). Exploiting the enhanced permeability and retention effect for tumor targeting. *Drug Discovery Today, 11*(17-18), 812-818.

Jameson, D. M. (2014). *Introduction to fluorescence*. Boca Raton, FL: CRC Press.

Kaimal, V., Chu, Z., Mahller, Y. Y., Papahadjopoulos-Sternberg, B., Cripe, T. P., Holland, S. K., et al. (2011). Saposin C coupled lipid nanovesicles enable cancer-selective optical and magnetic resonance imaging. *Molecular Imaging and Biology : MIB : The Official Publication of the Academy of Molecular Imaging, 13*(5), 886-897.

Kaiser, R. D., & London, E. (1998). Location of diphenylhexatriene (DPH) and its derivatives within membranes: Comparison of different fluorescence quenching analyses of membrane depth. *Biochemistry, 37*(22), 8180-8190.

Kanichay, R., Boni, L. T., Cooke, P. H., Khan, T. K., & Chong, P. L. -. G. (2003). Calcium-induced aggregation of archaeal bipolar tetraether liposomes derived from thermoacidophilic archaeon *sulfolobus acidocaldarius*. *Archaea, 1*, 175-183.

Kao, Y. L., Chong, P. L. -. G., Huang, C. H., & van der Meer, B. W. (1990). Dynamic motions of 1,6-diphenyl-1,3,5-hexatriene in interdigitated C(18):C(10)phosphatidylcholine bilayers. *Biophysical Journal, 58*(4), 947-956.

Khan, T. K., & Chong, P. L. -. (2000). Studies of archaebacterial bipolar tetraether liposomes by perylene fluorescence. *Biophysical Journal, 78*(3), 1390-1399.

Kinosita, K.,Jr, Ikegami, A., & Kawato, S. (1982). On the wobbling-in-cone analysis of fluorescence anisotropy decay. *Biophysical Journal, 37*(2), 461-464.

Kneidl, B., Peller, M., Winter, G., Lindner, L. H., & Hossann, M. (2014). Thermosensitive liposomal drug delivery systems: State of the art review. *International Journal of Nanomedicine, 9*, 4387-4398.

Komatsu, H., & Chong, P. L. -. (1998). Low permeability of liposomal membranes composed of bipolar tetraether lipids from thermoacidophilic archaebacterium *sulfolobus acidocaldarius*. *Biochemistry (John Wiley & Sons), 37*(1), 107-115.

Kong, G., Braun, R. D., & Dewhirst, M. W. (2001). Characterization of the effect of hyperthermia on nanoparticle extravasation from tumor vasculature. *Cancer Research, 61*(7), 3027-3032.

Koulov, A. V., Hanshaw, R. G., Stucker, K. A., Lakshmi, C., & Smith, B. D. (2005). Biophysical studies of a synthetic mimic of the apoptosis-detecting protein annexin V. *Israel. J. Chem., 45*, 373-379.

Koulov, A. V., Stucker, K. A., Lakshmi, C., Robinson, J. P., & Smith, B. D. (2003). Detection of apoptotic cells using a synthetic fluorescent sensor for membrane surfaces that contain phosphatidylserine. *Cell Death and Differentiation, 10*(12), 1357-1359.

Lakowicz, J. R. (1999). *Principles of fluorescence spectroscopy* (second edition ed.). New York: Plenum Publishers.

Lakshmi, C., Hanshaw, R. G., & Smith, B. D. (2004). Fluorophore linked zinc (II) dipicolylamine coordination complexes as sensors for phosphatidylserine containing membrane. *Tetrahedron, 60,* 11307-11315.

Laouini, A., Jaafar-Maalej, C., Limayem-Blouza, I., Sfar, S., Charcosset, C., & Fessi, H. (2012). Preparation, characterization and applications of liposomes: State of the art. *Journal of Colloid Science and Biotechnology, 1*(2), 147-168.

Leevy, W. M., Gammon, S. T., Jiang, H., Johnson, J. R., Maxwell, D. J., Jackson, E. N., et al. (2006). Optical imaging of bacterial infection in living mice using a fluorescent near-infrared molecular probe. *Journal of the American Chemical Society, 128*(51), 16476-16477.

Li, L., ten Hagen, T. L. M., Hossann, M., Suess, R., van Rhoon, G. C., Eggermont, A. M. M., et al. (2013). Mild hyperthermia triggered doxorubicin release from optimized stealth thermosensitive liposomes improves intratumoral drug delivery and efficacy. *Journal of Controlled Release, 168*(2), 142-150.

Li, Z., Chen, J., Sun, W., & Xu, Y. (2010). Investigation of archaeosomes as carriers for oral delivery of peptides. *Biochemical and Biophysical Research Communications, 394*(2), 412-417.

Lim, S. B., Banerjee, A., & Onyuksel, H. (2012). Improvement of drug safety by the use of lipid-based nanocarriers. *Journal of Controlled Release : Official Journal of the Controlled Release Society, 163*(1), 34-45.

Lima, L. G., Chammas, R., Monteiro, R. Q., Moreira, M. E., & Barcinski, M. A. (2009). Tumor-derived microvesicles modulate the establishment of metastatic melanoma in a phosphatidylserine-dependent manner. *Cancer Letters, 283*(2), 168-175.

Liu, L. F., Desai, S. D., Li, T. K., Mao, Y., Sun, M., & Sim, S. P. (2000). Mechanism of action of camptothecin. *Annals of the New York Academy of Sciences, 922*, 1-10.

Lo, S. L., & Chang, E. L. (1990). Purification and characterization of a liposomal-forming tetraether lipid fraction. *Biochemical and Biophysical Research Communications, 167*(1), 238-243.

Lo, S. L., Montague, C. E., & Chang, E. L. (1989). Purification of glycerol dialkyl nonitol tetraether from *sulfolobus acidocaldarius*. *Journal of Lipid Research, 30*(6), 944-949.

Loughrey, H. C., Wong, K. F., Choi, L. S., Cullis, P. R., & Bally, M. B. (1990). Protein-liposome conjugates with defined size distributions. *Biochimica Et Biophysica Acta, 1028*(1), 73-81.

Lyass, O., Hubert, A., & Gabizon, A. A. (2001). Phase I study of doxil-cisplatin combination chemotherapy in patients with advanced malignancies. *Clinical Cancer Research : An Official Journal of the American Association for Cancer Research, 7*(10), 3040-3046.

Mabrey, S., & Sturtevant, J. M. (1976). Investigation of phase transitions of lipids and lipid mixtures by sensitivity differential scanning calorimetry. *Proceedings of the National Academy of Sciences of the United States of America, 73*(11), 3862-3866.

Madni, A., Sarfraz, M., Rehman, M., Ahmad, M., Akhtar, N., Ahmad, S., et al. (2014). Liposomal drug delivery: A versatile platform for challenging clinical applications. *Journal of Pharmacy & Pharmaceutical Sciences : A Publication of the Canadian Society for Pharmaceutical Sciences, Societe Canadienne Des Sciences Pharmaceutiques, 17*(3), 401-426.

Mamot, C., Ritschard, R., Kung, W., Park, J. W., Herrmann, R., & Rochlitz, C. F. (2006). EGFR-targeted immunoliposomes derived from the monoclonal antibody EMD72000 mediate specific and efficient drug delivery to a variety of colorectal cancer cells. *Journal of Drug Targeting, 14*(4), 215-223.

Mamot, C., Ritschard, R., Wicki, A., Kung, W., Schuller, J., Herrmann, R., et al. (2012). Immunoliposomal delivery of doxorubicin can overcome multidrug resistance mechanisms in EGFR-overexpressing tumor cells. *Journal of Drug Targeting, 20*(5), 422-432.

Manzoor, A. A., Lindner, L. H., Landon, C. D., Park, J., Simnick, A. J., Dreher, M. R., et al. (2012). Overcoming limitations in nanoparticle drug delivery: Triggered, intravascular release to improve drug penetration into tumors. *Cancer Research, 72*(21), 5566-5575.

Mariño, G., & Kroemer, G. (2013). Mechanisms of apoptotic phosphatidylserine exposure. *Cell Research, 23*, 1247.

Marquardt, D., Geier, B., & Pabst, G. (2015). Asymmetric lipid membranes: Towards more realistic model systems. *Membranes, 5*(2), 180-196.

May, J. P., & Li, S. -. (2012). Thermosensitive liposomes in cancer therapy. *Recent Patents on Biomedical Engineering, 5*, 148-158.

Mossalam, M., Dixon, A. S., & Lim, C. S. (2010). Controlling subcellular delivery to optimize therapeutic effect. *Therapeutic Delivery, 1*(1), 169-193.

Mufamadi, M. S., Pillay, V., Choonara, Y. E., Du Toit, L. C., Modi, G., Naidoo, D., et al. (2011). A review on composite liposomal technologies for specialized drug delivery. *Journal of Drug Delivery, 2011*, 939851.

Niu, G., & Chen, X. (2010). Apoptosis imaging: Beyond annexin V. *Journal of Nuclear Medicine : Official Publication, Society of Nuclear Medicine, 51*(11), 1659-1662.

O'Neil, E. J., & Smith, B. D. (2006). Anion recognition using dimetallic coordination complexes. *Coordination Chemistry Reviews, 250*(23–24), 3068-3080.

O'Neil, J. E., & Smith, B. D.,. (2006). Anion recognition using dimetallic coordination complexes. *Coordination Chemistry, 250*, 3068.

Parasassi, T. G., Krasnowska, E., & Bagatolli, L. A. (1998). Laurdan and prodan as polarity-sensitive fluorescent membrane probes. *J.Fluorescence, 8*, 365-373.

Parasassi, T., De Stasio, G., d'Ubaldo, A., & Gratton, E. (1990). Phase fluctuation in phospholipid membranes revealed by laurdan fluorescence. *Biophysical Journal, 57*(6), 1179-1186.

Parasassi, T., De Stasio, G., Ravagnan, G., Rusch, R. M., & Gratton, E. (1991). Quantitation of lipid phases in phospholipid vesicles by the generalized polarization of laurdan fluorescence. *Biophysical Journal, 60*(1), 179-189.

Parasassi, T., Di Stefano, M., Loiero, M., Ravagnan, G., & Gratton, E. (1994). Influence of cholesterol on phospholipid bilayers phase domains as detected by laurdan fluorescence. *Biophysical Journal, 66*(1), 120-132.

Patel, G. B., Agnew, B. J., Deschatelets, L. A., Fleming, L. P., & Sprott, G. D. (2000). In vitro assessment of archaeosome stability for developing oral delivery systems. *International Journal of Pharmaceutics, 194*(1), 39-49.

Pathak, Y., & Thassu, D. (2009). *Drug delivery nanoparticles formulation and characterization*. New York, NY: Informa Healthcare USA, Inc.

Picardi, M. V., Cruz, A., Orellana, G., & Perez-Gil, J. (2011). Phospholipid packing and hydration in pulmonary surfactant membranes and films as sensed by LAURDAN. *Biochimica Et Biophysica Acta, 1808*(3), 696-705.

Pillai, G. (2014). Nanomedicines for cancer therapy: An update of FDA approved and those under various stages of development. *SOJ Pharm Pharm Sci, 1*, 13.

Post, A. M., Katsikis, P. D., Tait, J. F., Geaghan, S. M., Strauss, H. W., & Blankenberg, F. G. (2002). Imaging cell death with radiolabeled annexin V in an experimental model of rheumatoid arthritis. *Journal of Nuclear Medicine : Official Publication, Society of Nuclear Medicine, 43*(10), 1359-1365.

Qi, X., Chu, Z., Mahller, Y. Y., Stringer, K. F., Witte, D. P., & Cripe, T. P. (2009). Cancer-selective targeting and cytotoxicity by liposomal-coupled lysosomal saposin C protein. *Clinical Cancer Research : An Official Journal of the American Association for Cancer Research, 15*(18), 5840-5851.

Ran, S., Downes, A., & Thorpe, P. E. (2002). Increased exposure of anionic phospholipids on the surface of tumor blood vessels. *Cancer Research, 62*(21), 6132-6140.

Ran, S., He, J., Huang, X., Soares, M., Scothorn, D., & Thorpe, P. E. (2005). Antitumor effects of a monoclonal antibody that binds anionic phospholipids on the surface of tumor blood vessels in mice. *Clinical Cancer Research : An Official Journal of the American Association for Cancer Research, 11*(4), 1551-1562.

Ran, S., & Thorpe, P. E. (2002). Phosphatidylserine is a marker of tumor vasculature and a potential target for cancer imaging and therapy. *International Journal of Radiation Oncology, Biology, Physics, 54*(5), 1479-1484.

Ren, X., Liu, K., Zhang, Q., Noh, H. M., Kumbur, E. C., Yuan, W. W., et al. (2014). Design, fabrication and characterization of archaeal tetraether free-standing planar membranes in a PDMS- and PCB-based fluidic platform. *ACS Applied Materials & Interfaces, 6*, 12618-12628.

Repakova, J., Holopainen, J. M., Morrow, M. R., McDonald, M. C., Capkova, P., & Vattulainen, I. (2005). Influence of DPH on the structure and dynamics of a DPPC bilayer. *Biophysical Journal, 88*(5), 3398-3410.

Riedl, S., Rinner, B., Asslaber, M., Schaider, H., Walzer, S., Novak, A., et al. (2011). In search of a novel target - phosphatidylserine exposed by non-apoptotic tumor cells

and metastases of malignancies with poor treatment efficacy. *Biochimica Et Biophysica Acta, 1808*(11), 2638-2645.

Riedl, S., Zweytick, D., & Lohner, K. (2011). Membrane-active host defense peptides-challenges and perspectives for the development of novel anticancer drugs. *Chemistry and Physics of Lipids, 164*(8), 766-781.

Sanchez, S. A., Tricerri, M. A., & Gratton, E. (2012). Laurdan generalized polarization fluctuations measures membrane packing micro-heterogeneity in vivo. *Proc. Natl. Acad. Sci. U.S.A., 109*, 7314-7319.

Sandstrom, M. C., Ickenstein, L. M., Mayer, L. D., & Edwards, K. (2005). Effects of lipid segregation and lysolipid dissociation on drug release from thermosensitive liposomes. *Journal of Controlled Release : Official Journal of the Controlled Release Society, 107*(1), 131-142.

Schutters, K., & Reutelingsperger, C. (2010). Phosphatidylserine targeting for diagnosis and treatment of human diseases. *Apoptosis : An International Journal on Programmed Cell Death, 15*(9), 1072-1082.

Segawa, K., Suzuki, J., & Nagata, S. (2011). Constitutive exposure of phosphatidylserine on viable cells. *Proceedings of the National Academy of Sciences of the United States of America, 108*(48), 19246-19251.

Sheela, A. (2005). The liposomal formulation of doxorubicin. *Methods in Enzymology, 391*, 71-97.

Sipkens, J. A., Hahn, N. E., van Nieuw-Amerongen, G. P., Stehouwer, C. D. A., Rauwerda, J. A., van Hinsbergh, V. W. M., et al. (2011). Homocysteine induces phosphatidylserine exposure in cardiomyocytes through inhibition of rho kinase and flippase activity. *Cellular Physiology and Biochemistry, 28*, 53-62.

Smith, B. A., Akers, W. J., Leevy, W. M., Lampkins, A. J., Xiao, S., Wolter, W., et al. (2010). Optical imaging of mammary and prostate tumors in living animals using a

synthetic near infrared zinc(II)-dipicolylamine probe for anionic cell surfaces. *Journal of the American Chemical Society, 132*(1), 67-69.

Smoluchowski, M. V. (1903). Contribution à la théorie de l'endosmose électrique et de quelques phénomènes corrélatifs. *Bull. Int. Acad. Sci. Cracovie, 184*

Stafford, J. H., & Thorpe, P. E. (2011). Increased exposure of phosphatidylethanolamine on the surface of tumor vascular endothelium. *Neoplasia (New York, N.Y.), 13*(4), 299-308.

Strebhardt, K., & Ullrich, A. (2008). Paul ehrlich's magic bullet concept: 100 years of progress. *Nature Reviews. Cancer, 8*(6), 473-480.

Suzuki, J., Denning, D. P., Imanishi, E., Horvitz, H. R., & Nagata, S. (2013). Xk-related protein 8 and CED-8 promote phosphatidylserine exposure in apoptotic cells. *Science (New York, N.Y.), 341*(6144), 403-406.

Ta, T., & Porter, T. M. (2013). Thermosensitive liposomes for localized delivery and triggered release of chemotherapy. *Journal of Controlled Release : Official Journal of the Controlled Release Society, 169*(1-2), 112-125.

Tacar, O., Sriamornsak, P., & Dass, C. R. (2013). Doxorubicin: An update on anticancer molecular action, toxicity and novel drug delivery systems. *Journal of Pharmacy and Pharmacology, 65*(2), 157-170.

Tejera-Garcia, R., Connell, L., Shaw, W. A., & Kinnunen, P. K. (2012). Gravimetric determination of phospholipid concentration. *Chemistry and Physics of Lipids, 165*(6), 689-695.

Thorn, C. F., Oshiro, C., Marsh, S., Hernandez-Boussard, T., McLeod, H., Klein, T. E., et al. (2011). Doxorubicin pathways: Pharmacodynamics and adverse effects. *Pharmacogenetics and Genomics, 21*(7), 440-446.

Thorpe, P. E. (2010). Targeting anionic phospholipids on tumor blood vessels and tumor cells. *Thrombosis Research, 125 Suppl 2*, S134-7.

Tila, D., Ghasemi, S., Yazdani-Arazi, S. N., & Ghanbarzadeh, S. (2015). Functional liposomes in the cancer-targeted drug delivery. *Journal of Biomaterials Applications, 30*(1), 3-16.

Todor, I. N., Lukyanova, N. Y., & Chekhun, V. F. (2012). The lipid content of cisplatin- and doxorubicin-resistant MCF-7 human breast cancer cells. *Experimental Oncology, 34*(2), 97-100.

Toxnet. (2010). *Doxorubicin. http://toxnet.nlm.nih.gov/cgibin/sis/search2/r?dbs+hsdb:@term+@rn+@rel+23214-92-8*

Turkyilmaz, S., Rice, D. R., Palumbo, R., & Smith, B. D. (2014). Selective recognition of anionic cell membranes using targeted liposomes coated with zinc(II)-bis(dipicolylamine) affinity units. *Organic & Biomolecular Chemistry, 12*(30), 5645-5655.

Uster, P. S., Working, P. K., & Vaage, J. (1998). Pegylated liposomal doxorubicin (DOXIL, CAELYX) distribution in tumor models observed with confocal laser scanning microscopy. *International Journal of Pharmaceutics, 162*, 77-86.

Utsugi, T., Schroit, A. J., Connor, J., Bucana, C. D., & Fidler, I. J. (1991). Elevated expression of phosphatidylserine in the outer membrane leaflet of human tumor cells and recognition by activated human blood monocytes. *Cancer Research, 51*(11), 3062-3066.

Vaage, J., Working, P., & Uster, P. (1998). Inhibition of mouse mammary carcinoma development with doxorubicin in liposomes. *International Journal of Cancer.Journal International Du Cancer*, 75(1), 158-159.

van Meer, G. (2011). Dynamic transbilayer lipid asymmetry. Cold Spring Harbor *Perspectives in Biology*, 3(5), 10.1101/cshperspect.a004671.

Venegas, B., Zhu, W., Haloupek, N. B., Lee, J., Zellhart, E., Sugar, I. P., et al. (2012). Cholesterol supelattice modulates combretastatin A4 disodium phosphate (CA4P)

release from liposomes and CA4P cytotoxicity on mammary cancer cells *Biophys. J.*, *102*, 2086-2094.

Woehlecke, H., Pohl, A., Alder-Baerens, N., Lage, H., & Herrmann, A. (2003). Enhanced exposure of phosphatidylserine in human gastric carcinoma cells overexpressing the half-size ABC transporter BCRP (ABCG2). *The Biochemical Journal*, 376(Pt 2), 489-495.

Xingong, L., Hirsh, D. J., Cabral-Lily, D., Zirkel, A., Gruner, S. M., Janoff, A. S., et al. (1998). Doxorubicin physical state in a solution and inside liposomes loaded via a pH gradient. *Biochimica Et Biophysica Acta, 1415*, 23-40.

Zhang, L., Zhou, H., Belzile, O., Thorpe, P., & Zhao, D. (2014). Phosphatidylserine-targeted bimodal liposomal nanoparticles for in vivo imaging of breast cancer in mice. *Journal of Controlled Release : Official Journal of the Controlled Release Society, 183*, 114-123.

Zhou, H., Stafford, J. H., Hallac, R. R., Zhang, L., Huang, G., Mason, R. P., et al. (2014). Phosphatidylserine-targeted molecular imaging of tumor vasculature by magnetic resonance imaging. *Journal of Biomedical Nanotechnology, 10*(5), 846-855.

Zhu, X., Migrino, R. Q., Hellman, R. S., Brahmbhatt, T., & Zhao, M. (2008). Early uptake of 99mTc-C2A in the acute phase of myocardial infarction as a prognostic indicator for follow-up cardiac dysfunction. *Nuclear Medicine Communications, 29*(9), 764-769.

Zwaal, R. F. A., Comfurius, P., & Bevers, E. M. (2005). Surface exposure of phosphatidylserine in pathological cells. Cell. *Mol. Life Sci, 62*, 971-988.